BASAL GANGLIA FUNCTION IN GENETIC MOUSE MODELS OF HUNTINGTON'S DISEASE: A CIRCUIT-LEVEL APPROACH

By Joshua W. Callahan

A Dissertation submitted to the

Graduate School-Newark

Rutgers, The State University of New Jersey

in partial fulfillment of the requirements

for the degree of

Doctor of Philosophy

Graduate Program in Behavioral and Neural Sciences

written under the direction of

Dr. Elizabeth Abercrombie

and approved by

_____

_____

_____

_____

_____

Newark, New Jersey

October 2013

ABSTRACT

Basal Ganglia Function in Genetic Mouse Models of Huntington's Disease: A Circuit-Level Approach

By Joshua W. Callahan

Thesis Advisor: Dr. Elizabeth D. Abercrombie

Huntington's disease (HD) is an autosomal dominant neurodegenerative disorder that results in motor, cognitive and psychiatric abnormalities. Impairments in the processing of information between the cortex and basal ganglia are fundamental to the onset and progression of the HD phenotype. The corticosubthalamic hyperdirect pathway plays a crucial role in motor selection and blockade of neuronal activity in the STN results in a hyperkinetic movement syndrome, similar to the HD phenotype. The aim of the present study was to examine whether changes in the fidelity of information transmission between the cortex and STN emerge as a function of phenotype severity in R6/2 and YAC128 transgenic mouse models of HD. We performed in vivo extracellular recordings in the STN of anesthetized mice and measured concomitant cortical activity with electrocorticogram (ECoG) recordings during brain states that represented global cortical network synchronization or desynchronization. Dopamine (DA) can have profound effects on network synchronization between the cortex and basal ganglia and disturbances in DA transmission have been reported in HD. To monitor whether differences existed in DAergic tone in the basal ganglia we used in vivo microdialysis to measure extracellular striatal DA levels. We found in symptomatic HD transgenic mice that cortically patterned STN neuronal discharge was progressively disrupted as a function of phenotypic severity. In addition, the spontaneous activity of STN neurons

was reduced in symptomatic HD transgenic mice. Stimulation of the ipsilateral cortex leads to a short latency monosynaptic excitatory response in STN neurons. Concomitant to the dissipation of STN entrainment, there was a reduction in the proportion of responsive STN neurons to cortical stimulation as a function of age. These results indicate dysfunction in the flow of information within the corticosubthalamic circuit and demonstrate progressive disconnection of the hyperdirect pathway in transgenic HD mice. Glutamatergic STN neurons provide the major excitatory drive to the output nuclei of the basal ganglia and altered discharge patterns could lead to aberrant basal ganglia output and disordered motor control.

ACKNOWLEDGEMENTS

I would like to give my sincerest thanks to everyone that I have had the honor of working with during my tenure in the Abercrombie lab. I want to thank the members of my thesis committee, Dr. Ian Creese, Dr. Peter Magill, Dr. James Tepper, and Dr. Laszlo Zaborszky. I want to thank Dr. James Tepper and members of his lab for their assistance and invaluable advice. Thank you to my friends and colleagues, Anna Chavez, Dr. Andy Farrar, and Nupur Jain for always lending a helping hand. Thank you to my mentor, Dr. Elizabeth Abercrombie, for always instilling confidence in me and giving me the support to achieve my goals.

TABLE OF CONTENTS

CHAPTER 1: INTRODUCTION

1.1 HUNTINGTON'S DISEASE

1.1.1 Human Neuropathology

Huntington's disease (HD) is a debilitating neurodegenerative disorder that affects approximately 3 in every 100,000 individuals worldwide (Pringsheim et al., 2012). HD is inherited as an autosomal dominant condition and results from a polyglutamine (CAG) repeat expansion in the 5' end of the IT15 gene ("interesting transcript 15") on chromosome 4 (4p16.3) (Huntington's Disease Collaborative Research Group, 1993). The disease occurs when a critical threshold of 37 (median 44) polyglutamine repeats is exceeded (Kremer et al., 1994) and the length of the CAG repeat expansion is directly correlated with the severity of symptoms (Ghiglieri et al., 2012). The illness is inexorably progressive with death occurring on average within 15 to 20 years from the time of symptom onset (Vonsattel, 2008). To date there is no cure and therapeutic options are minimal.

While affected individuals are born with the mutated Huntingtin (HTT) gene, HD is considered a progressive disorder as symptoms do not usually manifest until 30-50 years of age (Nguyen et al., 2010). Symptoms are diverse and include motor, cognitive and psychiatric disabilities (Huntington's Disease Collaborative Research Group, 1993). Motor dysfunction encompasses disturbances that affect both involuntary and voluntary aspects of movement. Chorea, defined by the occurrence of irregular and uncontrollable movements, is the primary involuntary motor disturbance in HD (Mink, 1996). This is represented in electromyography (EMG) recordings which show variable and random patterns of muscle activation throughout the body in HD patients (Thompson et al., 1988).

Involuntary, sustained muscle contractions (dystonia) also manifest in HD and lead to impaired gait and posture (Vonsattel, 2008). Chorea and dystonia are often referred to as hyperkinetic aspects of HD. Muscle rigidity (hypertonia), inability to initiate movement (akinesia), slowness in intentional motion (bradykinesia) and difficulty in swallowing (dysphagia) are common deficits in voluntary motor control in HD patients (Vonsattel, 2008). These set of symptoms are often referred to as hypokinetic aspects of HD. Hyperkinetic abnormalities usually emerge earliest while hypokinetic deficits worsen with disease progression, however, both hyperkinetic and hypokinetic symptoms can manifest simultaneously (Berardelli et al., 1999). Cognitive impairments, albeit most difficult to detect, are thought to manifest before the onset of classical motor symptoms. The most severe cognitive symptoms include deficits in executive function, memory decline, behavioral inflexibility and difficulty in spatial perception (Mohr et al., 1991; Foroud et al., 1995; Lange et al., 1995; Paulsen, 2011; Brooks and Dunnett, 2013; Dumas et al., 2013). The prevalence of psychiatric disturbances is the most variable between HD patients and includes depression, anxiety, aggression, apathy and compulsive behavior (Adam and Jankovic, 2008; Vonsattel, 2008). While less common (> 10%), symptoms can emerge during infantile or juvenile ages and progress at a much more accelerated pace (Levy et al., 1999). This aggressive variant results from a larger CAG repeat expansion (> 60 repeats) and is classified as juvenile or Westphal variant HD (Levy et al., 1999). In juvenile HD, hypokinetic impairments are the most dominant clinical symptoms, with hyperkinetic syndromes rarely being expressed or for only very brief stints (Robitaille et al., 1997). Severe cognitive decline and epileptic seizures are also common symptoms in juvenile HD (Brackenridge, 1980).

The HTT gene encodes the highly conserved, ubiquitously expressed protein, huntingtin (htt) (Huntington's Disease Collaborative Research Group, 1993). The function of the htt protein is unclear, however, examination of the pathogenesis caused by the mutated variant (mHtt) has given clues into the diverse role that it plays throughout the nervous system. The expression of the mHtt protein leads to both gain of function as well as loss of function effects including transcriptional dysregulation, mitochondrial deficits, proteosomal dysfunction, impairments in endocytosis and exocytosis, axonal transport deficits, neuronal degeneration and synaptic dysfunction (Zoghbi and Orr, 2000; Zuccato et al., 2001; Dunah et al., 2002; Panov et al., 2002; Zeron et al., 2002; Gunawardena et al., 2003; Luthi-Carter et al., 2003; Steffan et al., 2004). The deletion of the HTT gene in mice results in embryonic lethality (Duyao et al., 1995) indicating the critical role that it plays in embryogenesis and normal development.

The precise mechanisms in which mHtt protein expression leads to such deleterious effects are undetermined in HD. Traditional views posit that the proteolysis of the mHtt protein into toxic N-terminal fragments is an early and critical pathogenic event (Davies et al., 1997). It is thought that the exaggerated expression of glutamine residues on these fragmented mHtt molecules promote abnormal interactions that leads to the formation of aggregate bodies (Vonsattel, 2008). Accumulations of these aggregate bodies are termed inclusions and they manifest in intranuclear or cytoplasmic compartments (Davies et al., 1997). The formation of inclusion bodies in the brain in HD is one of the earliest pathological events and can be detected long before the onset of symptoms (Davies et al., 1997; Gomez-Tortosa et al., 2001). As the severity of symptoms progress, the appearance of inclusion bodies is followed by the selective

degeneration of principal neurons within the striatum and cortex. While the pronounced existence of inclusion bodies is undeniably present throughout the nervous system in human HD and experimental animal models of HD (DiFiglia et al., 1997; Becher et al., 1998; Gourfinkel-An et al., 1998), recent evidence has indicated that these inclusions cannot be the only pathogenic factor in HD and that non-cell-autonomous deficits may be more detrimental. In accordance, studies have failed to find a correlation between mHtt protein expression and neuronal vulnerability (Fusco et al., 1999). Expression of the mHtt protein exhibits relative enrichment in cortical pyramidal neurons projecting to the striatum but relatively low levels in medium spiny neurons of the striatum, which are the most vulnerable cell type in HD (Fusco et al., 1999; Sapp et al., 1999). Interestingly, restricting mHtt expression to cortical pyramidal neurons is sufficient to produce mHtt intranuclear and cytoplasmic aggregation but insufficient to produce motor deficits in experimental animal models of HD (Gu et al., 2005). Thus, these results suggest that the HD phenotype is induced by the interactions between cells.

1.1.2 Transgenic Mouse Models of HD

The generation of genetically engineered mouse models has helped to elucidate impairments underlying HD by allowing the direct examination of the mechanisms that lead to disease pathogenesis. Transgenic models display unique phenotypes depending on the size, location and number of copies of the CAG repeat as well as the identity of the promoter driving transgene expression. Transgenic HD mouse lines traditionally differ based upon whether they express only the truncated N-terminal fragment containing the

CAG repeat sequence of the mutant HTT gene (fragment model) or whether they possess the complete mutant HTT gene (full-length model). Transgenic mice expressing only N-terminal fragments display neuropathological changes earlier than mice expressing the full-length HTT gene (Vonsattel, 2008). This is thought to occur because fragments of the mHtt protein are more toxic (Vonsattel, 2008). The most commonly used fragment model in HD research is the R6/2 strain and the most commonly used full-length model is the YAC128 strain.

The transgenic R6/2 line was generated by Mangiarini et al. (1996). These mice express exon 1 of the N-terminal portion of the human HTT gene containing approximately 160 CAG repeats under the control of the human HTT gene promoter (Mangiarini et al., 1996). R6/2 mice display a distinct temporal sequence of neuropathological changes that are similar to those seen in human HD patients and include N-terminal mHtt protein aggregation, followed by the appearance of inclusion bodies and the subsequent manifestation of behavioral symptoms (Davies et al., 1997; Davies et al., 1999; Turmaine et al., 2000). Inclusion bodies are present throughout the whole R6/2 brain as early as 3 weeks of age (Morton et al., 2000). The extent and distribution of inclusion bodies is much more widespread in R6/2 mice than that found in human HD brains (Vonsattel, 2008). As in the human disease, R62 mice display significant reductions in brain weight that can be detected as early as 4-5 weeks of age with regional decreases in volume of striatal and cortical areas at 13 weeks of age (Turmaine et al., 2000; Stack et al., 2005). Interestingly, there exists little, if any, cell death in R6/2 mice and brain weight reductions are instead more likely the result of reduced somatic size and loss or thinning of dendrites and spines (Klapstein et al., 2001).

Cognitive dysfunction also becomes apparent as early as 4 weeks of age as demonstrated by spatial learning deficits in the Morris water maze task (Lione et al., 1999). Involuntary movement disturbances are apparent at 6-7 weeks of age and manifest as dystonic posturing in the hind limbs, which consists of wide splay or limb clasping (Stack et al., 2005). Age related increases in dystonic posturing have been reported in human HD patients (Myers et al., 1988; Mahant et al., 2003). In addition, 7-week-old R6/2 mice spend more time in grooming bouts and less time in quiet wakefulness, indicative of hyperkinetic disturbances (Hong et al., 2012). At 7-8 weeks of age, R6/2 mice display deficits in voluntary motor control on the rotarod task (Ferrante et al., 2000; Hickey et al., 2002). Rotarod deficits have been associated with impairments in both gait timing and postural instability observed in human HD patients (Tian et al., 1992; Bilney et al., 2005). Reduced grip strength is also observed in 7-week-old R6/2 mice (Stack et al., 2005) consistent with deficits seen in human HD patients (Gordon et al., 2000). At 8 weeks of age, weight loss is observed in R6/2 mice (Higgins et al., 1999; Stack et al., 2005), similar to the weight loss reported in human HD patients (Djousse et al., 2002; Mahant et al., 2003). R6/2 mice also develop seizures at variable intervals throughout the course of the disease. Survival time in R6/2 mice is approximately 13-15 weeks (Ferrante et al., 2000; Stack et al., 2005). While the R6/2 model recapitulates key features of HD and serves as an excellent paradigm for rapid screening, a major flaw is that unlike the human disorder these mice do not develop neuronal loss. This has hindered the ability to examine the progressive nature of disease pathogenesis in relation to neuronal degeneration and led to the development of the YAC128 transgenic mouse line.

The YAC128 line was generated by Slow et al. (2003). These mice express the full-length human HTT gene with approximately 128 CAG repeats under the control of the human HTT gene promoter. Phenotype onset is much slower and progressive in YAC128 mice compared to R6/2 mice. Cognitive dysfunction is apparent at 1-2 months of age as demonstrated by set-shifting impairments in the T-Maze paradigm (Van Raamsdonk et al., 2005). Hyperkinetic movement disturbances have been described as early as 2 months of age as demonstrated by increased spontaneous ambulation in the open field task (Slow et al., 2003). Unexpectedly, YAC128 mice demonstrate a progressive increase in body weight at 2 months of age (Van Raamsdonk et al., 2007), contrary to that seen in R6/2 mice or human HD patients. Hyperkinetic movement disturbances are followed by deficits in volitional movement at 6 months of age as demonstrated by impairments on the rotarod task and reduced grip strength (Van Raamsdonk et al., 2005). At 9 months of age, YAC128 mice display decreased spontaneous locomotor activity in the open field task indicating the presence of hypokinetic deficits (Slow et al., 2003). Nuclear and cytoplasmic inclusion bodies are detectable in the brain at 12 months of age but are much less abundant than that observed in R6/2 mice (Slow et al., 2003). Similar to human HD patients, YAC128 mice exhibit progressive neuronal degeneration in the cortex and striatum (Slow et al., 2003). Regional decreases in striatal volume develop at 9 month of age in YAC128 mice and are followed by neuronal loss in the cortex and striatum by 12 months of age (Slow et al., 2003; Van Raamsdonk et al., 2005).

1.2 OVERVIEW OF THE BASAL GANGLIA IN HD

1.2.1 Basal Ganglia Anatomy and Physiology

The basal ganglia are an ensemble of subcortical nuclei that are anatomically and functionally connected and together form a biological neural network. The basal ganglia are involved in a variety of motor, associative and limbic functions (Alexander et al., 1990). The basal ganglia are comprised of the striatum (caudate and putamen), the globus pallidus (internal and external segments), the subthalamic nucleus (STN) and the substantia nigra (pars compacta and pars reticulata) (Albin et al., 1989; Alexander et al., 1990; DeLong, 1990). Excitatory glutamatergic projections from the cortex and thalamus make up the largest inputs into the basal ganglia and project to the striatum and STN.

Cortical projection neurons to the basal ganglia are categorized into two main types, intratelencephalic (IT) and pyramidal tract (PT) neurons (Jinnai and Matsuda, 1979; Landry et al., 1984; Wilson, 1987; Cowan and Wilson, 1994; Levesque et al., 1996; Levesque and Parent, 1998; Wright et al., 1999; Wright et al., 2001; Zheng and Wilson, 2002; Reiner et al., 2003). Corticostriatal projections arise from IT or PT neurons in layer III or V of monkeys, dogs, cats and rodents, and although not exclusively, densely target the principal cell type of the striatum, medium spiny neurons (MSNs) (Kemp and Powell, 1970; Kitai et al., 1976; Oka, 1980; Royce, 1982; McGeorge and Faull, 1989). While corticostriatal innervation is dense, each axon makes few synaptic contacts (Kincaid et al., 1998) and thus shared input among striatal MSNs is minimal (Kincaid et al., 1998; Zheng and Wilson, 2002). Corticosubthalamic projections originate from PT neurons in layer V of rats and monkeys that also emit collaterals which

innervate multiple other brain areas, including striatum, thalamus, lower brainstem and spinal cord (Rouzaire-Dubois and Scarnati, 1985; Canteras et al., 1990; Nambu et al., 1996; Mathai and Smith, 2011; Kita and Kita, 2012). The cortex transmits information to the output nuclei of the basal ganglia nuclei through the STN with the shortest latency and thus this circuit has been termed the hyperdirect pathway (Nambu et al., 2000). Evidence indicates that more convergence occurs within corticosubthalamic projections compared to corticostriatal projections (Haynes and Haber, 2013).

Inputs to the basal ganglia, through the striatum and STN, are integrated and processed via multiple pathways until reaching the output nuclei, the internal segment of the globus pallidus (GPi) and the substantia nigra pars reticulata (SNr) (Albin et al., 1989; Alexander et al., 1990; DeLong, 1990). Traditional basal ganglia models posit that this is completed through three partially overlapping pathways (Alexander and Crutcher, 1990; Nambu, 2011): (1) Direct pathway – Comprised of GABAergic MSNs in the striatum that express D1 dopamine receptors, substance P and dynorphin and provide monosynaptic inhibition to the GABAergic output nuclei. (2) Indirect pathway – Comprised of GABAergic MSNs in the striatum that express D2 dopamine receptors and proenkephalin/enkephalin (PENK/ENK) and provide polysynaptic disinhibition, through GPe and STN, to the GABAergic output nuclei. (3) Hyperdirect pathway – Comprised of monosynaptic cortical afferents to glutamatergic STN neurons that provide excitation to the GABAergic output nuclei. Models suggest that activity in the direct pathway sends a "go" signal to facilitate the execution of an appropriate command by disinhibiting basal ganglia targets such as the thalamus and brainstem (Bronfeld and Bar-Gad, 2011). In contrast, activity in the indirect pathway or hyperdirect pathway sends a "no go" signal to

suppress the execution of competing responses by increasing inhibition on basal ganglia targets (Alexander et al., 1990; Mink, 1996; Frank, 2006; Schmidt et al., 2013). In addition, neurons from the SNc send diffuse dopaminergic (DA) projections to the striatum, as well as other basal ganglia nuclei, and modulate the relative balance of these pathways by exciting direct pathway MSNs via D1 receptors while inhibiting indirect pathway MSNs via D2 receptors (Gerfen, 1992).

1.2.2 Anatomical Disturbances in HD

The most prominent morphological change in HD is the selective degeneration of the striatum which is associated with pronounced loss of MSNs (Vonsattel et al., 1985; Vonsattel and DiFiglia, 1998). Specifically, loss of indirect pathway MSNs occurs earliest while loss of direct pathway MSNs occurs later in the disease progression (Albin et al., 1989; Albin et al., 1990; Richfield et al., 1991; Richfield and Herkenham, 1994; Hedreen and Folstein, 1995; Sapp et al., 1995; Sapp et al., 1999). Early animal models of HD utilized excitotoxins to selectively destroy MSNs and recapitulate the striatal loss associated with the disease (Coyle and Schwarcz, 1976; Coyle et al., 1977). Concomitant to striatal degeneration, the cortex also undergoes dramatic structural alterations. Thinning of the cerebral cortex is widespread and develops progressively throughout the disorder (Rosas et al., 2002; Rosas et al., 2006; Rosas et al., 2008a; Rosas et al., 2008b; Rosas et al., 2011). Reductions in cortical volume can be measured early and followed by the selective degeneration of pyramidal neurons (Halliday et al., 1998; Vonsattel and DiFiglia, 1998). Cell loss is greatest in the motor, prefrontal and sensorimotor cortex

although atrophy takes place across the entire cortical mantle (Jernigan et al., 1991; Aylward et al., 1998; Halliday et al., 1998; Kassubek et al., 2004; Selemon et al., 2004).

While neuronal loss is a pronounced feature of HD, transgenic mouse models have demonstrated that the disease phenotype emerges prior to cell loss (Raymond et al., 2011). In R6/2 mice, neuronal loss is absent, yet motor impairments are evident as early as 6 weeks of age (Davies et al., 1997; Turmaine et al., 2000). Similarly, in YAC128 mice, behavioral symptoms manifest before neuronal death in the striatum and cortex (Slow et al., 2003). Recent evidence in transgenic mouse models of HD suggests that neuronal dysfunction precedes neuronal loss and that such alterations contribute dramatically to the HD phenotype (Levine et al., 2004; Cepeda et al., 2007; Miller et al., 2011; Raymond et al., 2011).

1.2.3 Circuit Dysfunction in HD

Synaptic dysfunction in cortico-basal ganglia circuits is an early and dynamic event in HD transgenic mouse models. Multiple studies have reported signs of early increased excitability of cortical pyramidal neurons in R6/2 and YAC128 mice (Walker et al., 2008; Cummings et al., 2009; Joshi et al., 2009; Andre et al., 2011b). Pyramidal neurons in the prefrontal cortex spontaneously discharge at higher rates in 7-week-old R6/2 mice (Walker et al., 2008). Spontaneous IPSP currents in cortical pyramidal neurons are diminished early in HD transgenic mice and suggest that GABAergic neurotransmission is reduced which could lead to disinihibition (Gu et al., 2005). In addition, changes in the intrinsic membrane properties of cortical pyramidal neurons take

place in R6/2 mice and include increased input resistance and lower rectification (Stern, 2011). Collectively, these changes are thought to lead to increased excitatory synaptic transmission into the basal ganglia at early ages in transgenic mouse models of HD. In accordance, in presymptomatic YAC128 mice, corticostriatal glutamate release is augmented (Joshi et al., 2009; Andre et al., 2011b) and glutamate mediated postsynaptic currents evoked by cortical stimulation are increased in striatal MSNs (Graham et al., 2009; Joshi et al., 2009).

Strikingly, early increased excitability in the cortex is followed by a progressive reduction in excitatory drive (Cepeda et al., 2007). In contrast to early age points, glutamate release is decreased from cortical terminals at late stages in YAC128 mice (Joshi et al., 2009; Andre et al., 2011a). The frequency of spontaneous EPSP currents in striatal MSNs is reduced in symptomatic transgenic HD mice and becomes more evident as the disease phenotype advances (Cepeda et al., 2003; Milnerwood and Raymond, 2007; Cummings et al., 2010). In addition, glutamate mediated postsynaptic currents evoked by cortical stimulation are significantly reduced in striatal MSNs and higher stimulus intensity is necessary to elicit synaptic currents in R6/2 and YAC128 mice (Klapstein et al., 2001; Laforet et al., 2001; Graham et al., 2009; Joshi et al., 2009). Thus, biphasic alterations in cortical excitatory drive on basal ganglia targets manifest as a function of disease progression in transgenic HD mouse models.

The cortex and thalamus are the main providers of entrant excitatory glutamatergic inputs into the basal ganglia via two structures, the striatum and the subthalamic nucleus (STN). While corticostriatal transmission has been examined extensively in HD, neural transmission within the corticosubthalamic pathway remains

uninvestigated thus far. Glutamatergic STN neurons control the activity of the same target neurons as the striatum and provide a major excitatory drive on the output nuclei of the basal ganglia that counteracts the inhibitory influence exerted by GABAergic striatal MSNs. Studies point to a critical role of the cortex and STN in modulating basal ganglia neuronal activity through the hyperdirect pathway (Fujimoto and Kita, 1993; Maurice et al., 1998; Nambu et al., 2000; Magill et al., 2001; Magill et al., 2004; Sharott et al., 2005; Mathai and Smith, 2011; Nambu, 2011). Specifically, the hyperdirect pathway has been implicated in action suppression (Aron and Poldrack, 2006; Frank, 2006; Jahfari et al., 2011) and blockade of STN neuronal activity through discrete lesions or pharmacological inactivation (Carpenter et al., 1950; Hamada and DeLong, 1992) produces hyperkinetic movement disorders which mimic Huntington's chorea. Based on the importance of control exerted by the STN on motor commands, elucidating alterations in processing between the cortex and STN could have valuable implications for understanding HD pathogenesis.

1.3 THE SUBTHALAMIC NUCLEUS (STN) AND BASAL GANGLIA CIRCUIT FUNCTION

1.3.1 Intrinsic Properties of STN neurons

STN neurons possess intrinsic membrane properties that lead to autonomous tonic firing in the absence of synaptic input (Overton and Greenfield, 1995; Beurrier et al., 1999; Bevan and Wilson, 1999; Beurrier et al., 2000; Song et al., 2000). This autonomous pacemaking activity is generated primarily from persistent and resurgent

voltage-dependent sodium currents (Beurrier et al., 1999; Bevan and Wilson, 1999; Beurrier et al., 2000; Do and Bean, 2003). The persistent sodium current exhibits slow inactivation kinetics and is the principal pacemaker for autonomous activity in STN neurons (Bevan and Wilson, 1999). The resurgent sodium current activates immediately following a spike and leads to an inward current during afterhyperpolarization that depolarizes the membrane back towards spike threshold (Do and Bean, 2003). These channels allow STN neurons to fire with tonic regularity at rest in a self sustained single spike discharge. In addition, two potassium channels contribute to the rate and regularity of spiking in STN neurons. Voltage-gated potassium channels (KV3) facilitate high-frequency firing by reducing sodium channel inactivation (Rudy and McBain, 2001). Small conductance calcium-activated potassium channels (SKCa) open briefly during each action potential and hyperpolarize STN neurons back to steady state membrane potential, helping to promote firing regularity (Bevan and Wilson, 1999; Rudy and McBain, 2001; Hallworth et al., 2003). Cooperatively, these currents engender the ability of STN neurons to spontaneously discharge at high rates.

STN neurons also have intrinsic characteristics that allow them to switch from single spike to burst firing modes of discharge (Bevan et al., 2000; Kass and Mintz, 2006). While still under investigation, it is postulated that burst firing is induced by the activation of voltage-dependent calcium channels that are normally inactive at resting membrane potentials. Specifically, it is thought that hyperpolarization leads to the activation of low-threshold T/R calcium currents that depolarize STN neurons to the threshold potential of L-type calcium currents and then inactivate. L-type calcium currents are slowly inactivating and depolarize the membrane to a plateau phase during

which bursts of spikes are evoked. The precipitant increase in intracellular calcium activates calcium-activated potassium channels and together with L-type channel inactivation leads to a gradual decline of the burst plateau. This results in hyperpolarization of the membrane, deinactivation of low-threshold T/R calcium currents and renewal of the cycle. Interestingly, while the mechanisms are unresolved, STN neurons can exhibit prolonged plateau periods after a burst that lack spike activity. These "silent plateaus" represent a depolarization block that could be important for modulating the responses to synaptic inputs (Kass and Mintz, 2006). It is currently unknown whether all STN neurons have the intrinsic characteristics needed to generate plateau potentials or whether such neurons only represent a fraction of the total STN population. During normal conditions, external synaptic inputs will be exerted within the context of this intrinsic activity to shape STN neuronal discharge.

1.3.2 Excitatory Input Signals to the STN

STN neurons receives excitatory glutamatergic afferents from extensive areas of the cortex, the parafasicular nucleus of the thalamus and the pedunculopontine nucleus (Kitai and Deniau, 1981; Jackson and Crossman, 1983; Sugimoto et al., 1983; Afsharpour, 1985; Rouzaire-Dubois and Scarnati, 1985; Canteras et al., 1988; Fujimoto and Kita, 1993; Feger et al., 1994; Lavoie and Parent, 1994; Bevan et al., 1995; Mouroux et al., 1995; Parent and Hazrati, 1995). The STN can be topographically divided into functional territories based upon connections with segregated regions. Dorsolateral and dorsomedial STN neurons receive motor-related projections, ventrolateral STN neurons

receive associative-related inputs and ventromedial STN neurons receive limbic input (Monakow et al., 1978; Nambu et al., 1996; Shink et al., 1996; Karachi et al., 2005). The most extensive input to the STN originates from motor regions and the anterior cingulate cortex (Monakow et al., 1978; Kitai and Deniau, 1981; Afsharpour, 1985; Canteras et al., 1988; Bevan et al., 1995; Parent and Hazrati, 1995). Interestingly, the dendrites of individual STN neurons extend across multiple functional regions which suggest high levels of functional convergence (Mathai and Smith, 2011; Haynes and Haber, 2013). In rats, corticosubthalamic projections from functionally distinct cortical regions have been shown to converge onto single STN neurons (Kolomiets et al., 2001).

STN neurons are enriched with ionotropic glutamate receptors, NMDAR and AMPAR, as well as group I metabotropic glutamate receptors, mGluR1 and mGluR5, located along the plasma membrane near asymmetric glutamatergic synapses (Bevan et al., 1995; Clarke and Bolam, 1998; Kuwajima et al., 2004). Due to the high input resistance and short refractory period in STN neurons, excitatory inputs can trigger action potentials with minimal delays and produce strong excitation even when small EPSPs are evoked (Nakanishi et al., 1987; Beurrier et al., 1999; Bevan and Wilson, 1999; Beurrier et al., 2000). As such, STN neurons represent a potent substrate for cortical entrainment and multiple studies have demonstrated that the cortex can powerfully pattern rhythmic activity in the STN (Magill et al., 2000, 2001; Magill et al., 2004; Mallet et al., 2008).

1.3.3 Inhibitory Input Signals to the STN

The primary source of synaptic innervation to the STN arises from the GPe, which provides an extensive GABAergic input that is spread across the entire structure (Van der Kooy and Kolb, 1985; Smith et al., 1990; Moriizumi and Hattori, 1992). The GPe exerts a tonic inhibitory influence over the STN that is mediated through GABA-A receptors and has a powerful effect on patterning STN neuronal discharge (Moriizumi and Hattori, 1992; Bevan et al., 1997; Bevan et al., 2002; Bevan et al., 2007). While GPe neurons fire persistently, their inputs are subject to synaptic depression (Atherton et al., 2013). This leads to weak background inhibition and nonsynchronized patterns of discharge under resting states (Atherton et al., 2013). The STN and GP are also reciprocally connected and under certain conditions the two nuclei can form a powerful pacemaker (Plenz and Kital, 1999). Large or multiple GABA-A receptor-mediated IPSPs can produce sufficient hyperpolarization in STN neurons to activate low-threshold calcium currents which generate rebound bursts of action potentials (Nakanishi et al., 1987; Beurrier et al., 1999; Bevan and Wilson, 1999; Beurrier et al., 2000; Bevan et al., 2000; Song et al., 2000). In turn, burst firing in STN neurons leads to excitation of GPe neurons and the cycle is renewed leading to synchronized burst patterns. The level of polarization of STN neurons is critical in determining the impact of GPe synaptic input and the patterns of response.

1.3.4 Neuromodulatory Input to the STN

The STN receives monoaminergic inputs from the SNc and the dorsal raphe nucleus as well as acetylcholinergic inputs from the pedunculopontine nucleus (Brown et

al., 1979; Jackson and Crossman, 1983; Mori et al., 1985; Lavoie et al., 1989; Canteras et al., 1990; Lavoie and Parent, 1990, 1994; Bevan et al., 1995; Hassani et al., 1997; Cossette et al., 1999; Hedreen, 1999; Francois et al., 2000). Both D1 and D2 receptors are present in the STN and thought to exert excitatory effects on neuronal activity in the structure (Johnson et al., 1994; Francois et al., 2000; Ni et al., 2001a; Ni et al., 2001b). Locally infused DA agonists cause an increase in the frequency of firing of STN neurons thought to occur directly through the activation of postsynaptic D1 receptors (Kreiss et al., 1996; Kreiss et al., 1997). In addition, D2 receptors are expressed on GPe axon terminals and through presynaptic inhibition, can reduce the magnitude of evoked GABA-A IPSPs in STN neurons and increase the frequency of autonomous single spiking (Shen and Johnson, 2000; Cragg et al., 2004). Serotonin and acetylcholine are both involved in the regulation of the sleep-wake cycle and may effectively modulate STN neuronal excitability during these periods (Canteras et al., 1990; Lavoie and Parent, 1990; Xiang et al., 2005).

1.3.5 STN Output Signals

Decreases or increases in the discharge of inhibitory output neurons facilitates or suppresses the activity of basal ganglia targets, such as thalamocortical circuits, which is thought to lead to the execution of an appropriate command (Albin et al., 1989; Alexander et al., 1990; DeLong, 1990). Dendrites of GABAergic output nuclei neurons are densely covered with excitatory terminals from STN neurons as well as inhibitory terminals from striatal and GPe neurons (Francois et al., 1984). STN neurons project

diffusely and synapse on the proximal dendrites of output nuclei neurons whereas striatal and GPe inputs are more spatially focused (Difiglia et al., 1982; Hazrati and Parent, 1992a, b; Shink and Smith, 1995). It is posited by models of action selection that the combined effects of spatially focused inhibitory projections from the striatum and spatially diffuse excitatory projections from the STN enable selective movement related patterns (Mink, 1996; Nambu et al., 2002; Frank, 2006). Specifically, during the initial stages of a response, activation of the hyperdirect pathway elicits rapid excitation of STN neurons. In turn, STN neuronal activation produces widespread, divergent excitation of GABAergic output nuclei neurons, promoting inhibition of basal ganglia targets and suppressing unintended motor commands. Through more slowly conducting circuits, cortical excitation of direct pathway MSNs leads to focused suppression of select subpopulations of output nuclei neurons. This disinhibition actively releases appropriate basal ganglia targets from normal inhibitory control and facilitates the execution of a proper movement. Subsequently, activation of indirect pathway striatal MSNs disinhibits neuronal activity in the STN, further increasing the excitatory drive on inhibitory output nuclei neurons and terminating the selected command in favor of subsequent motor sequences. Thus, STN neurons effectively act as a brake on basal ganglia mediated behavioral action through their excitatory output signals. (Nambu et al., 2000; Nambu et al., 2002; Aron and Poldrack, 2006; Frank, 2006; Nambu, 2011; Schmidt et al., 2013).

In addition to traditional basal ganglia output targets, STN neurons send sparse projections to the striatum (Nauta and Cole, 1978; Beckstead, 1983; Royce and Laine, 1983; Kitai and Kita, 1987; Parent and Smith, 1987), the thalamus (Nauta and Cole, 1978) and the cerebral cortex (Kitai and Kita, 1987; Degos et al., 2008). STN neurons

also send excitatory projections to the SNc (Lee and Tepper, 2009; Pazo et al., 2010). The STN exerts a tonic excitatory influence over the activity of this structure and alterations within the STN, or indirectly cortex, can modulate DAergic discharge patterns (Shimo and Wichmann, 2009; Pazo et al., 2010). Through local bicuculline infusions it was shown that STN activation could lead to increased bursting of SNc DA neurons (Smith and Grace, 1992; Chergui et al., 1994). Alternatively, STN lesions result in reductions in the burst discharge of DA neurons (Smith and Grace, 1992).

1.4 DOPAMINERGIC INFLUENCE ON BASAL GANGLIA PROCESSING

1.4.1 Modulation of Basal Ganglia

DA is crucial for the execution of movements and goal-directed behavior (Bradbury et al., 1985; Hollerman and Schultz, 1998; Missale et al., 1998; Fiorillo et al., 2003; Schultz, 2007; Joshua et al., 2009). DA neurons in the SNc innervate all nuclei of the basal ganglia, with the densest projection terminating in the striatum (Schultz, 2007; Joshua et al., 2009). DA is thought to induce dynamic changes throughout the basal ganglia network by weakening or strengthening synaptic connections and in turn acts as a reward prediction error signal (Hollerman and Schultz, 1998; Schultz, 1998a, b, 2007; Joshua et al., 2009). Phasic DA release during error feedback leads to transient excitation of direct pathway MSNs and transient inhibition of indirect pathway MSNs to selectively strengthen responses that result in positive feedback. In turn, DA plays a pivotal role in overall network excitability and the response selection of motor commands.

1.4.2 Role of Dopamine in HD

Disturbances in DA transmission have been reported in HD, however, the trajectory of these changes is unresolved. Kish et al. (1987) described a reduction in DA content in the striatum of HD patients but separate groups have found no change in striatal DA concentrations (Reynolds and Garrett, 1986) and others have even reported elevated amounts (Spokes, 1980). These studies were based on postmortem tissue assays, which are limited because they cannot delineate intracellular versus extracellular concentrations and as a result are not a sensitive index of synaptic change. In HD animal models, evidence indicates that extracellular striatal DA transmission may be compromised even in the absence of tissue depletion. Johnson et al. (2006) used fast-scan cyclic voltammetry to demonstrate that evoked DA release is attenuated *in vitro* in 6-week-old R6/2 mice. Similarly, Hickey et al. (2002) reported that motor activity is depressed in response to AMPH beginning at 6 weeks of age. While these results suggest that DA release is diminished in transgenic mouse models of HD, exactly how DAergic transmission is affected as a function of disease progression is largely unresolved.

CHAPTER 2: RELATIONSHIP BETWEEN SUBTHALAMIC NUCLEUS (STN) NEURONAL ACTIVITY AND ELECTROCORTICOGRAM (ECoG) IS ALTERED IN THE R6/2 MOUSE MODEL OF HUNTINGTON'S DISEASE

Authors: Joshua W. Callahan and Elizabeth D. Abercrombie

Journal: Journal of Neuroscience (Submitted)

2.1 ABSTRACT

Huntington's disease (HD) is an autosomal dominant neurodegenerative disorder in which impairments in the processing of information between the cortex and basal ganglia are fundamental to the onset and progression of the HD phenotype. Excitatory cortical inputs into the basal ganglia through the subthalamic nucleus (STN) play a pivotal role in motor selection and blockade of neuronal activity in the STN results in a hyperkinetic movement syndrome, similar to the HD phenotype. The aim of the present study was to examine the relationship between neuronal activity in the STN and cortex in an animal model of HD. We performed extracellular recordings in the STN to measure unit activity and local-field potentials (LFPs) in the R6/2 transgenic mouse model of HD. These recordings were obtained during epochs of simultaneously acquired electrocorticographic (ECoG) in extreme brain states representative of global cortical network synchronization or desynchronization. Cortically patterned STN neuronal discharge was less phase-locked in R6/2 mice which is likely to result in less efficient coding of cortical inputs by the basal ganglia. In R6/2 mice, the power of the ECoG concentrated in lower frequencies (0.5-4 Hz) was diminished and the power expressed in higher frequencies (30-100 Hz) was increased. In addition, the spontaneous activity of STN neurons in R6/2 mice was characterized by reduced firing rates and less tonic discharge patterns. Glutamatergic STN neurons provide the major excitatory drive to the output nuclei of the basal ganglia and altered discharge patterns could lead to aberrant basal ganglia output and disordered motor control.

2.2 INTRODUCTION

Huntington's disease (HD) is an autosomal dominant neurodegenerative disorder that results in motor, cognitive and psychiatric abnormalities. Evidence indicates that dysfunction across the cerebral cortex is fundamental to the onset and progression of the HD phenotype in humans and animal models of the disease (DiFiglia et al., 1997; Rosas et al., 2002; Cepeda et al., 2003). Dynamic changes occur specifically within cortico-basal ganglia circuitry and result in structural and functional alterations that lead to pathological behavioral output (Sapp et al., 1999; Cepeda et al., 2007; Miller et al., 2011). The consequences of altered cortical drive on the flow of information within cortico-basal ganglia loops are not fully understood and elucidating such alterations could have valuable implications for understanding the precise pathological changes that drive HD disease progression.

The cortex is the main provider of entrant excitatory glutmatergic inputs into the basal ganglia via two structures, the striatum and the subthalamic nucleus (STN). The cortex recruits STN neurons at much shorter latencies than striatal projection neurons (Magill et al., 2004) and studies point to a critical role of the cortex and STN in sculpting basal ganglia network activity (Fujimoto and Kita, 1993; Maurice et al., 1998; Nambu et al., 2000; Magill et al., 2001; Litvak et al., 2011). These signals play an important function in movement selection, procedural learning, habit formation and motivational processes (Hamada and DeLong, 1992; Mink, 1996; Baunez and Robbins, 1997; Barnes et al., 2005). In turn, glutamatergic neurons of the STN provide the major excitatory drive to the output structures of the basal ganglia (Smith and Parent, 1988; Bevan and

Wilson, 1999). Blockade of neuronal activity in the STN produces hyperkinetic movement disorders, which mimic chorea, the most common symptom of HD. In animal models, unilateral electrolytic lesions (Whittier and Mettler, 1949), transient pharmacological inactivation (Carpenter et al., 1950) and toxic lesions (Hamada and DeLong, 1992) restricted to the STN result in excessive, involuntary movements of the contralateral limbs reflecting the importance of control exerted by the STN on motor commands. Presently, it is unknown how neural activity between the cortex and STN is affected as a function of the expression of the mutant huntingtin (mHtt) protein.

The generation of genetic mouse models has helped to elucidate network alterations underlying HD by allowing the direct examination of mechanisms that lead to disease pathogenesis (Raymond et al., 2011). In order to examine neural processing between the cortex and STN we utilized the R6/2 transgenic mouse model of HD (see Experimental Procedures). We tested the hypothesis that synchronous neural activity between the STN and cortex, as previously described in rats (Magill et al., 2000, 2001), would be disrupted as a function of the mHtt protein. We performed in vivo extracellular unit recordings in the STN and measured concomitant cortical activity via electrocorticogram (ECoG) in R6/2 mice to assess changes in the complex coding of information between these two regions in HD.

2.3 EXPERIMENTAL PROCEDURES

Animals. Male R6/2 transgenic mice (n = 6) and male control mice (n = 9) were studied in the present experiments. All mice were purchased from Jackson Laboratories (Bar

Harbor, ME, USA) at 6 weeks of age. Animal orders were timed such that studies for each cohort began approximately 2 weeks after arrival at the animal colony (8–9 weeks of age). The transgenic R6/2 mouse strain (B6CBA-Tg(HDexon1)62Gpb/1J) was created by Mangiarini and colleagues (1996) and is a fragment model of HD that carries a random insertion of exon 1 of the human Huntingtin (HTT) gene with approximately 160 ± 5 polyglutamine repeats (Jackson Laboratories). The resultant expression of the CAG expansion region of the HTT gene produces animals that recapitulate behavioral and neuropathological aspects of human HD with notably early onset and rapid progression of the phenotype (Mangiarini et al., 1996). The wild-type (WT) control mouse strain (strain B6CBAF1/J) is the parent strain from which the R6/2 line was developed (Mangiarini et al., 1996).

Mice were housed individually in plastic microisolator cages with food and water available ad libitum. The mice were maintained under conditions of constant temperature (21°C) and humidity (40%) with a 12-hour light/dark cycle (0700 h on/1900 h off). The R6/2 transgenic mice are of generally poor overall health, therefore measures to assist in the maintenance of their vitality were included in the animal husbandry procedures. Moistened food pellets and HydroGel wells (ClearH20, Portland, ME) were placed on the floor of the home cage to facilitate caloric intake and hydration. Nesting pads, composed of compressed cotton fibers, also were provided. All reasonable effort was made in order to minimize animal suffering and to limit the number of animals utilized for these experiments. Animal procedures were conducted in accordance with the National Institutes of Health Guide for the Care and Use of Laboratory Animals and were approved by Rutgers University Institutional Animal Care and Use Committee.

Rotarod testing. Potential phenotypic impairment of motor performance was examined using the rotarod task (Economex; Columbus Instruments, Columbus, OH). This task is the most widely used paradigm for assessment of motor function in HD animal models and is a sensitive measure for detecting the progressive gait and balance abnormalities that are characteristic of R6/2 mice (Pallier et al., 2009). R6/2 and WT mice were trained on the rotarod treadmill task at 10 rpm for three consecutive trials (60 s maximum duration) one day prior to testing. On the test day, motor performance at five fixed speeds (5, 10, 15, 20, and 25 rpm) was measured (60 s interspeed interval) for two separate trials (5 min intertrial interval). Fall latencies (60 s cutoff) at each speed were averaged across trials for each subject. One WT subject was excluded from this component of the experimental protocol due to the presence of a hindpaw laceration that interfered with task performance.

Electrophysiological Studies

Surgical protocol. Extracellular recording of STN neuronal activity along with simultaneous acquisition of ECoG signal was carried out in the same mice that participated in the rotarod testing. Anesthesia was initiated by administration of urethane (1.25 g/kg, i.p.; Sigma-Aldrich Corporation, St. Louis, MO). Following the loss of righting reflexes, an appropriate surgical level of anesthesia was achieved by administration of a solution containing ketamine (80-100 mg/kg, i.p.; Phoenix Pharmaceutical Inc., St. Joseph, MO) combined with xylazine (10 mg/kg, i.p.; Sigma-Aldrich Corporation, St. Louis, MO). Supplemental doses of ketamine (30 mg/kg, i.p.)

plus xylazine (3 mg/kg, i.p.) were used for the remainder of the experiment as needed (Magill et al., 2000; Mallet et al., 2008). Sterile saline (0.9% w/v) served as the vehicle for all drug solutions. Throughout the experiment, the effectiveness of this anesthetic technique was verified by subjective observation of the ECoG signal, the respiration rate, and by testing for the presence of reflex withdrawal to cutaneous paw pinch and corneal stimulation (Whelan and Flecknell, 1992). Subsequent to anesthetization of the mouse, local anesthetic (bupivacaine hydrochloride solution, 0.5%, APP Pharmaceuticals, Schaumburg, IL) was injected beneath the scalp (0.1 ml, s.c.) and the animal was placed into a stereotaxic frame (David Kopf Instruments, Tujunga, CA). With the skull flat, a craniotomy was performed directly above the STN at the following coordinates: AP: -2.1 mm, ML: ±1.6 mm relative to bregma (Franklin and Paxinos, 2008) and the underlying dura mater was carefully resected. A second craniotomy was performed directly above the ipsilateral primary motor cortex (M1) at the following coordinates: AP: +2.1 mm, ML: ±2.0 mm relative to bregma (Franklin and Paxinos, 2008). Body temperature was maintained at 37 ± 0.5°C using a heating pad. Lactated ringer's solution (Fisher Scientific, Suwanee, GA) was administered (1.0-2.0 ml/30 g, s.c.) approximately every 2-3 h to prevent dehydration.

The sensitivity of R6/2 mice to anesthesia has been noted previously (Stern, 2011). Despite extensive empirical work aimed at optimizing the present protocol, the morbidity rate was ~40% in R6/2 mice *versus* 0% for WT mice. For the benefit of other investigators wishing to utilize R6/2 mice under anesthetized conditions, we report here that preliminary attempts with the anesthetic agents isoflurane (0.5-3.0 % vol concentration) and Avertin (2, 2, 2-Tribromoethanol) (400 mg/kg, i.p.) provided

unacceptable outcomes. While neither of these agents was problematic in terms of morbidity, both were associated with effects upon ECoG activity that precluded their use in the examination of the dependent measures of interest in the present studies. Isoflurane induces a burst-suppression pattern in the ECoG that ultimately leads to a continuous isoelectric ECoG signal characteristic of comatose states (Brenner, 1985; Ferron et al., 2009). We found that Avertin produced ECoG signals consisting of an unusual pattern of low frequency oscillations entirely lacking in higher frequency components. To our knowledge, this is the first report of this unusual action of Avertin upon cortical activity. Thus, we determined that in mice, as in rats (Magill et al., 2000; Mallet et al., 2008), a combination of urethane followed by supplemental doses of ketamine plus xylazine gave the best outcome in terms of preparation viability for the dependent measures of interest as well as overall survival.

STN activity. Extracellular action potentials generated by single STN neurons and local field potentials (LFP) in STN were recorded from single 10–25 MΩ glass recording pipettes (tip diameter ~1.0-2.0 μm) filled with a 0.5 M NaCl solution containing 2% pontamine sky blue (Sigma-Aldrich Corporation, St. Louis, MO). The electrode was lowered to a point ~500 μm above STN and then slowly was advanced in 1.0-10 μm increments using a micropositioner (Model 2660, David Kopf Instruments, Tujunga, CA) until a well-isolated single unit recording was obtained. Units characteristic of STN neurons recorded in rats such as ~10 Hz firing rates with biphasic waveforms (Magill et al., 2000) were encountered 4.0-4.5 mm below dura (see Figure 1). For all analyses, recordings were used if they were obtained when the electrode track was between AP -

1.82 mm to -2.30 mm (relative to bregma). Recordings typically lasted for 2-10 min. The amplified neuronal signals were band-pass filtered between 300 and 20 kHz (Model 1800, A-M Systems Microelectrode Amplifier, Sequim, WA). Amplified LFP signals were band-pass filtered between 0.1 and 20 kHz (A-M Systems Microelectrode Amplifier, Sequim, WA) and digitized on-line using a PC and a Micro1401 interface (Cambridge Electronic Design, Cambridge, UK) using Spike2 data acquisition and analysis software (Cambridge Electronic Design, Cambridge, UK). Single unit activity was sampled at 21 kHz and the LFP signal was down-sampled to 500 Hz and low-pass filtered at 100 Hz (Butterworth filter). Data from all recording sessions were visually inspected off-line and epochs with breathing or electrical artifacts were discarded.

ECoG activity. A bipolar nylon coated stainless steel electrode (outer diameter 100 μm, contact separation < 100 μm) used for ECoG recording was stereotaxically implanted and fixed to the skull using dental cement (Orthodontic Acrylic Resin, Lang Dental Manufacturing Co, Wheeling, IL). A steel screw was fixed into place over the ipsilateral cerebellum to serve as a reference electrode. Raw ECoG was band-pass filtered between 0.1 and 100 Hz (Grass P5 Series Preamplifier; West Warwick, RI). The resulting amplified ECoG signal was sampled at 500 Hz and digitized on-line with Spike2 data acquisition and analysis software (Cambridge Electronic Design, Cambridge, UK).

The ECoG was monitored continuously throughout all recording sessions. Global cortical network activity was observed to transition in distinct stages between a high-voltage, slow activity pattern (synchronized) and low-voltage periods containing a heterogeneous pattern (desynchronized). Epochs of synchronized activity are characterized by recurring large amplitude, low-frequency (0.5-4 Hz) oscillations in the

ECoG. The transition to epochs of desynchronized ECoG occurred spontaneously. Importantly, during these desynchronized epochs, the animal did not show any signs of reflexive responses or marked changes in respiration, indicating anesthesia levels were sufficient throughout the recordings.

Data Analysis

STN single-unit activity. In order to assess the discharge properties of STN neurons, 30 sec epochs of ECoG composed of easily discernable synchronized or desynchronized patterns were identified by visual inspection offline and a portion of the coincident STN spike train consisting of 500 spikes was isolated and further analyzed. The mean firing rate (spikes per second; Hz) for each STN neuron was calculated. Spike train regularity was determined by calculating the coefficient of variation (CV) of the interspike interval (ISI) distribution (ISI standard deviation/ISI mean). A more detailed analysis of the STN spike train patterns was conducted using an automatic burst detection algorithm implemented with custom-derived scripts for use with Spike2 (Cambridge Electronic Design, Cambridge, UK). Specifically, individual ISI histograms were constructed using a bin size determined by dividing the longest ISI in the spike train into 1000 bins. Bursts were defined as an epoch containing a sequence of two or more spikes beginning with an ISI 40 bins larger than the mode of the ISI distribution and ending with an ISI 80 bins larger than the mode. These parameters were empirically defined and upon comparison with alternative burst detection algorithms (such as fixed parameter settings and Poisson Surprise) we determined that this script was most accurate for our dataset. Further, the criteria chosen were specifically designed to identify events of clustered spiking that occur in response to cortical synchronization and are different than that which would be

classically used to define the bursting of STN neurons or other neuronal subtypes during desynchronized states. Thus, the burst detection algorithm was only used for the analysis of spike trains recorded during synchronized conditions. For each epoch of STN activity, the number of bursts, percentage of spikes per burst, mean spikes per burst, ISI within bursts, burst duration and interburst duration was compared. Lomb periodograms were estimated from the autocorrelograms of spike trains to quantify the significance of any patterns of periodic, oscillatory activity that might be present (Kaneoke and Vitek, 1996). Autocorrelograms were constructed with 20 ms bins and 4 s of lag time for each epoch of STN activity analyzed. The frequency bin that contained the highest power within the Lomb periodogram was used as a measure of the dominant oscillatory frequency in a given spike train. We considered oscillations significant if spectral power within these peaks was significantly greater than expected in comparison with independent Guassian random variables ($p < 0.05$). Those neurons that displayed significant peaks in the periodogram spectra between 0.5-4 Hz were classified as exhibiting significant low-frequency oscillations and termed LFO in the subsequent text.

Cortical ECoG activity. In order to assess the spectral composition of ECoG we performed Fast Fourier transform (FFT) analysis. Estimates of the spectral power density were extracted via Welch's periodogram method using a Hanning window with 50% overlap and a resolution frequency of 0.242 Hz. Estimates were summed within the following frequency bins to obtain the power densities of low frequency and higher frequency bandwidths: 0.5-4 Hz, 4-7 Hz, 7-13 Hz, 13-30 Hz and 30-100 Hz.

Coherence between STN activity and ECoG. Coherence measures the amount of linear

correlation between two time series as a function of frequency and is an absolute value that varies between 0, no systematic phase relationship between two signals, and 1, indicating a perfect phase relationship (i.e. phase-locked). The coherence between STN activity (unit firing or LFP) with coincident ECoG was calculated using the multitaper method implemented in the Chronux 2.0 data analysis toolbox (Bokil et al., 2010) for Matlab (MathWorks). Coherence spectra were estimated for the frequency range from 0.5-100 Hz. We extracted the peak coherence value for statistical comparison.

Histology. To identify the location of recorded sites, at the end of each experiment the electrode placement of the last recorded neuron was marked with an iontophoretic deposit of pontamine sky blue (15-20 min, -20 μA, constant current injection). Upon completion of each experiment, animals were administered a lethal dose of sodium pentobarbital and were perfused intracardially with 0.9% saline followed by 10% formaldehyde. Brains were extracted and post-fixed in fresh fixative overnight at 4°C and transferred to 30% sucrose in phosphate buffer solution at 4°C for cryoprotection. Coronal sections of 60 μm thickness were obtained and stained with Neutral Red (Sigma-Aldrich Corporation, St. Louis, MO) to verify the recording site in the STN (Fig. 1).

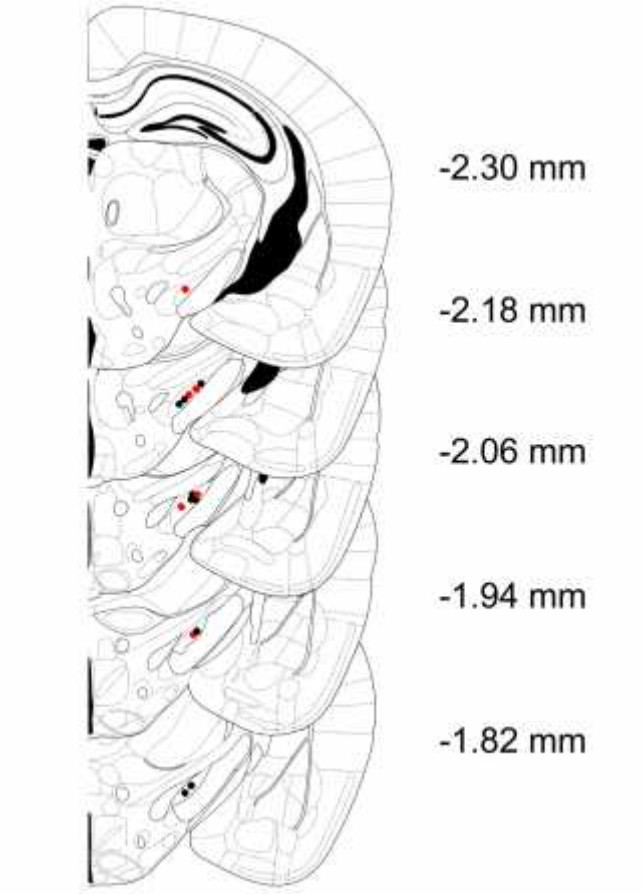

Figure 1: Schematic coronal diagrams of the mouse brain indicating the location of electrode tracks in the STN (modified from Franklin and Paxinos, 2008) of WT (black) and R6/2 (red) mice. Numbers indicate distance (mm) posterior to bregma.

Statistical analysis. All data are presented as mean ± SEM. Data were analyzed with a t-test for unpaired comparisons and by using a Mann-Whitney U-test in the case of non-normal distributions. Between-group differences for paired comparisons were assessed using two-way ANOVA. When appropriate, two-way ANOVA determinations were followed by Bonferroni's post-hoc test. For the analysis of within-group effects for paired comparisons, one-way ANOVA was used coupled to Bonferroni's post-hoc test. Between-group differences for three comparisons were assessed using one-way ANOVA coupled to Bonferroni's post-hoc test when appropriate. For the analysis of group

differences for three comparisons with non-normal distributions, a Kruskal-Wallis test was used together with Dunn's post-hoc test. Differences were considered statistically significant when $p < 0.05$.

2.4 RESULTS

Experimental overview. As summarized in Table 1, a total of nine WT (n = 65 STN neurons) and six R6/2 mice (n = 45 STN neurons) were included in the present experiments. The number of epochs of single unit STN activity acquired for each animal during simultaneously recorded synchronized or desycnchronized ECoG is provided. The number of epochs acquired varied across animals and, in some cases, recording conditions permitted STN activity to be acquired from a single neuron during both ECoG states in WT (n = 7 neurons) and R6/2 mice (n = 8 neurons), although this was not the norm. The total number of epochs analyzed for each condition in each group is specified in Table 1. For the R6/2 group, ~20% of STN recordings (6/28) obtained during the synchronized ECoG state did not exhibit significant periodicity in their spike trains according to the Lomb analysis and termed tonic in the subsequent text. Data collected from tonic neurons were therefore analyzed separately. Also provided in Table 1 is the fall latency for the fastest speed on the rotarod task (25 rpm) for each animal.

Table 1. Overview of STN single unit data collected during synchronized and desynchronized ECoG states.

WT	Rotarod 25 rpm (sec)	Synch Epochs	Desynch Epochs	R6/2	Rotarod 25 rpm (sec)	Synch Epochs	Desynch Epochs
1	60	4	1	1	2	-	8
2	60	1	1	2	17	7 (3) *	1
3	60	5	2	3	4.5	8 (1) *	2
4	60	9	5	4	10.5	(1) *	3
5	60	3	3	5	10	2	1
6	57	12 (1) *	-	6	52	10 (1) *	10
7	59	-	9				
8	N/A	-	5				
9	56	5	7				
TOTAL (N=9)		39 (1) *	33	TOTAL (N=6)		28 (6) *	25

Table 1: * Indicates STN recordings (500 spikes) obtained during synchronized ECoG epochs (30 sec) with non-significant Lomb periodicity value for STN unit. For the R6/2 group (referred to as 'tonic'), these data were analyzed separately (n = 6). The single case for the WT group was excluded from analysis.

Motor performance on the rotarod task. Fall latencies were significantly reduced as a function of speed [$F(4, 48) = 15.55$; $p < 0.01$] and genotype [$F(1, 48) = 18.55$; $p < 0.01$]. Furthermore, there was a significant speed x genotype interaction [$F(4, 48) = 10.93$; $p < 0.01$]. Planned comparisons indicated that fall latencies in R6/2 mice were significantly reduced relative to WT mice at 15, 20, and 25 rpm (Fig. 2).

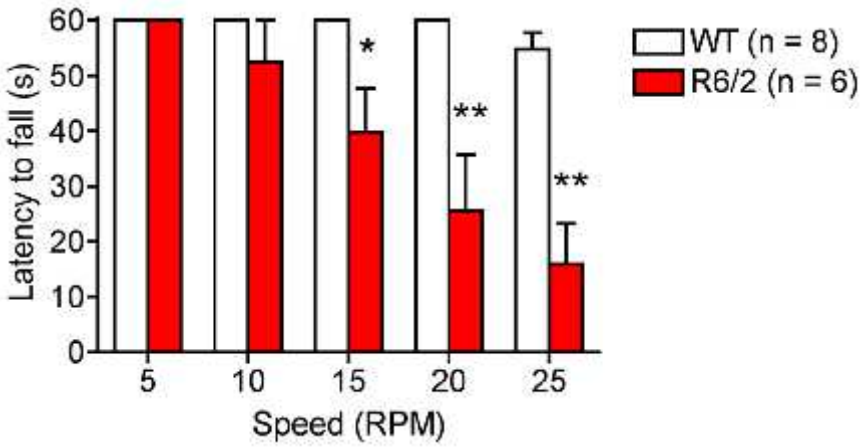

Figure 2: Rotarod performance comparison of WT and R6/2 mice as a function of rotation speed. All data are mean ± SEM. * indicates significantly different from WT, $p < 0.05$; ** indicates significantly different from WT, $p < 0.01$.

Firing properties of STN neurons are dependent on ECoG state. Figure 3 shows a representative example depicting the patterns of activity of STN units during synchronized and desynchronized ECoG epochs. STN neurons preferentially fire bursts of action potentials that are phase-locked to cortical up states during synchronized ECoG epochs. In contrast, STN neurons fire with more tonic regularity during desynchronized ECoG epochs.

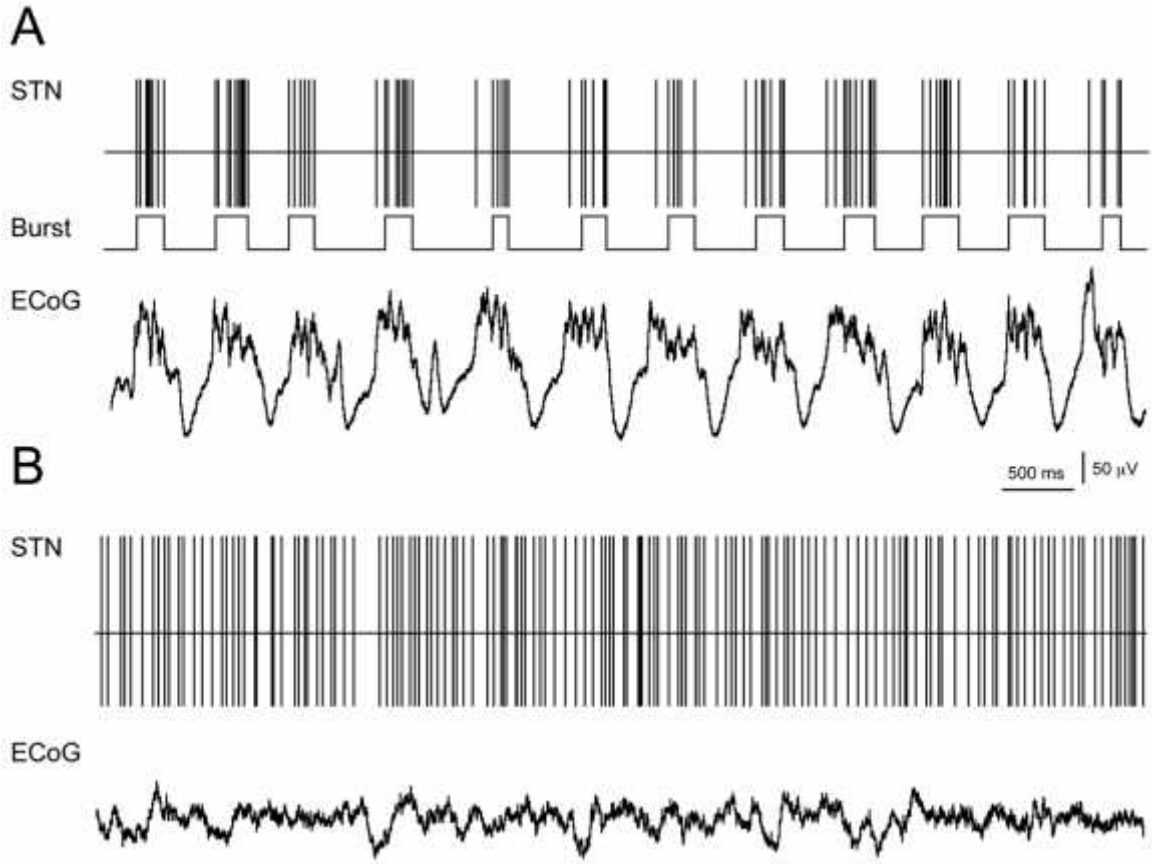

Figure 3: Representative neuronal activity in the STN and concomitant ECoG collected from WT mice. (*A*) LFO STN neuron (firing rate = 8.34 Hz; CV = 1.36; lomb frequency = 1.45 Hz) recorded during synchronized ECoG epoch (total power = 734.50 µV; 0.5-4 Hz power = 628.80 µV; 4-7 Hz power = 62.95 µV; 7-13 Hz power = 29.60; 13-30 Hz power = 11.00; and 30-100 Hz power = 2.18 µV; dominant frequency = 1.45 Hz). (*B*) Tonically firing STN neuron (firing rate = 17.23 Hz; CV = 0.59) recorded during desynchronized ECoG epoch (total power = 53.97 µV; 0.5-4 Hz power = 36.55 µV; 4-7 Hz power = 7.14 µV; 7-13 Hz power = 4.28; 13-30 Hz power = 3.43; and 30-100 Hz power = 2.58 µV).

STN spike train activity in the synchronized ECoG state in R6/2 mice. In R6/2 mice, tonic neurons discharged with significantly reduced spike rates (8.97 ± 2.26 Hz) relative to LFO neurons recorded from the STN (15.13 ± 0.78 Hz) [$H = 8.64$, d.f.= 2, $p < 0.05$] (Table 2). Moreover, the CV of tonic neurons (0.69 ± 0.12) was significantly less than that of LFO neurons recorded from the STN in both R6/2 (1.36 ± 0.05) and WT mice (1.40 ± 0.08) [$H = 12.26$, d.f.= 2, $p < 0.01$] (Table 2). The number of burst events in LFO

neurons recorded from R6/2 mice (54.18 ± 2.92) was significantly less than that in LFO neurons recorded from WT mice (63.95 ± 4.07) [U (58) = 299.0; $p < 0.05$] (Table 2). However, the number of action potentials per burst in LFO neurons recorded from R6/2 mice (8.03 ± 0.79) was significantly greater that that in LFO neurons recorded from WT mice (8.18 ± 0.55) [U (58) = 301.0; $p < 0.05$] (Table 2). In addition, the duration between burst events was significantly shorter in LFO neurons recorded from R6/2 mice (446.2 ± 19.38 ms) relative to LFO neurons recorded from WT mice (601.1 ± 29.97 ms) [U (58) = 167.0; $p < 0.01$] (Table 2). There was no significant difference between genotypes in the percentage of spikes within bursts [t (58) = 0.02; $p = 0.49$], the ISI of spikes within bursts [U (58) = 362.5; $p = 0.20$] or the burst duration [t (58) = 0.01; $p = 0.49$] in LFO neurons. In addition, there was no significant difference between genotypes in the peak oscillating frequency of the spike train in LFO neurons [U (58) = 343.5; $p = 0.13$] (Table 2).

STN spike train activity in the desynchronized ECoG state in R6/2 mice. Neurons recorded from the STN in R6/2 mice (10.71 ± 0.97 Hz) discharged with significantly slower firing rates compared to units recorded in WT mice (17.23 ± 1.40 Hz) [U (56) = 197.0; $p < 0.01$] (Table 2). In addition, the CV of the ISI distribution was significantly larger in STN neurons recorded from R6/2 mice (0.96 ± 0.12) in comparison to WT mice (0.59 ± 0.03) [U (56) = 240.0; $p < 0.01$] (Table 2).

Table 2. Firing properties of STN neurons.

	Synchronized Epochs			Desynchronized Epochs	
	WT	R6/2 LFO	R6/2 tonic	WT	R6/2
Firing rate (Hz)	12.52 ± 1.23	15.13 ± 0.78	8.97 ± 2.26 #	17.23 ± 1.40	10.71 ± 0.97 **
CV	1.40 ± 0.08	1.36 ± 0.05	0.69 ± 0.12 ** ##	0.59 ± 0.03	0.96 ± 0.12 **
Number of bursts	63.95 ± 4.07	54.18 ± 2.92 *	-	-	-
Spikes per burst	8.03 ± 0.79	8.18 ± 0.55 *	-	-	-
Interburst duration (ms)	601.1 ± 29.9	446.2 ± 19.4 **	-	-	-
Lomb freq (Hz)	1.37 ± 0.05	1.48 ± 0.12	-	-	-

Table 2: All data are mean ± SEM. * indicates significantly different from WT, $p < 0.05$; ** indicates significantly different from WT, $p < 0.01$; # indicates significantly different from R6/2 LFO, $p < 0.05$; ## indicates significantly different from R6/2 LFO, $p < 0.01$.

Spectral composition of ECoG in the synchronized state. The dominant frequency of the ECoG was significantly higher during recording epochs in both LFO (1.78 ± 0.18 Hz) and tonic STN neurons (1.68 ± 0.05 Hz) in R6/2 mice in comparison to those collected from LFO neurons in WT mice (1.42 ± 0.04 Hz) [$F(2, 63) = 8.63$; $p < 0.01$]. The total power of the ECoG within the lowest frequency bandwidth (0.5-4 Hz) was significantly diminished during recording epochs in both LFO and tonic neurons in R6/2 mice in comparison to those collected from LFO neurons in WT mice [$H = 18.52$, d.f.= 2, $p < 0.01$] (Figure 4A). The total power of the ECoG in higher frequencies (4-100 Hz) was significantly skewed as a function of genotype [$F(2, 63) = 5.13$; $p < 0.01$] and bandwidth [$F(3, 63) = 62.20$; $p < 0.01$] and there was a significant genotype x bandwidth interaction [$F(6, 63) = 12.20$; $p < 0.01$]. Planned comparisons indicated that the power within 13-30 Hz and 30-100 Hz was greater during recording epochs in LFO neurons in R6/2 mice relative to those collected from LFO neurons in WT mice (Fig. 4B). Furthermore, the power within 4-7 Hz was less during recording epochs in tonic neurons in R6/2 mice in comparison to those collected from LFO neurons in WT mice (Fig. 4B). In addition, the

power within 4-7 Hz and 7-13 Hz was lower during recording epochs in tonic neurons relative to those collected from LFO neurons recorded in R6/2 mice (Fig. 4B).

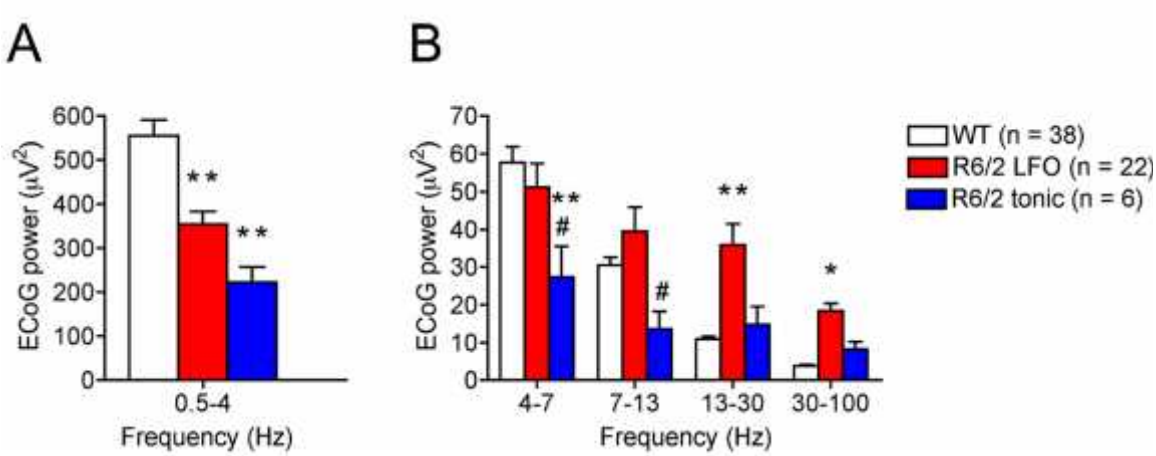

Figure 4: ECoG spectral power acquired in synchronized epochs concomitant to the recording of WT STN neurons (ECoG dominant frequency = 1.42 Hz), R6/2 LFO STN neurons (ECoG dominant frequency = 1.68 Hz) and R6/2 tonic STN neurons (ECoG dominant frequency = 1.78 Hz). (*A*) Total power spectral density of ECoG within low frequency components. (*B*) Total power spectral density of ECoG within high frequency components. All data are mean ± SEM. * indicates significantly different from WT, $p < 0.05$; ** indicates significantly different from WT, $p < 0.01$; # indicates significantly different from R6/2 LFO, $p < 0.05$.

Coherence between STN activity and ECoG in the synchronized state. The magnitude of the coherence between STN unit spiking and ECoG specifically within the lowest frequency bandwidth (0.5-4 Hz) was significantly reduced in both LFO neurons (0.63 ± 0.04) and tonic neurons (0.56 ± 0.06) in R6/2 mice compared to WT mice (0.81 ± 0.02) [H = 19.77, d.f.= 2, p < 0.01] (Fig. 5C). Likewise, the magnitude of the coherence between STN LFP activity and ECoG specifically within the lowest frequency bandwidth was significantly reduced in R6/2 mice (0.69 ± 0.2) relative to WT mice (0.83 ± 0.02) [t (7) = 4.91; p < 0.01; n = 6 WT, n = 3 R6/2].

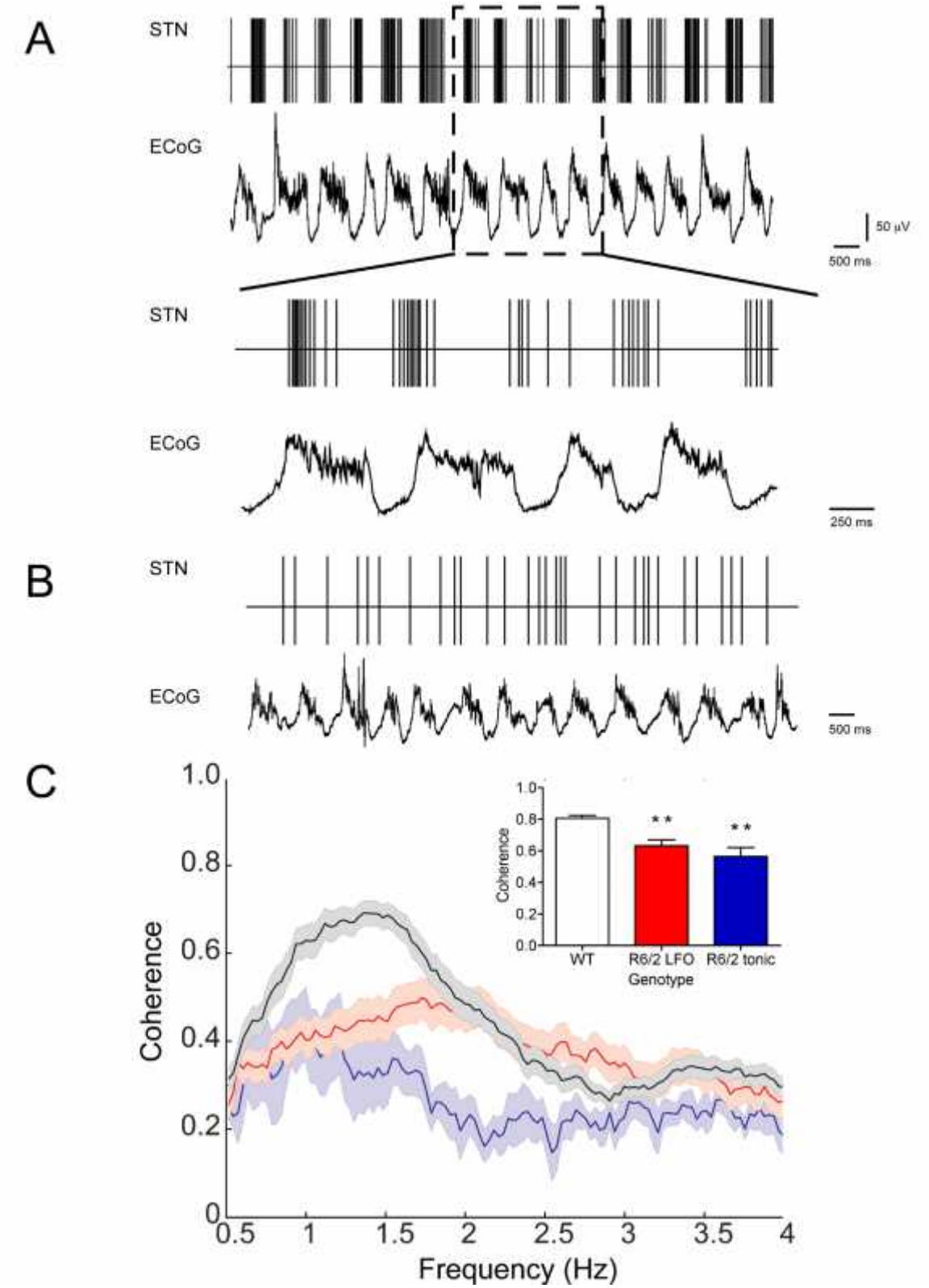

Figure 5: Oscillatory entrainment of STN neuronal activity during synchronized ECoG epochs in WT and R6/2 mice. (*A*) R6/2 LFO STN neuron (firing rate = 17.68 Hz; CV =

1.82; lomb frequency = 1.48 Hz) recorded during synchronized ECoG epoch (total power = 662.1 μV; 0.5-4 Hz power = 561.0 μV; 4-7 Hz power = 50.59 μV; 7-13 Hz power = 22.17; 13-30 Hz power = 15.27; and 30-100 Hz power = 13.00 μV; dominant frequency = 1.21 Hz). (*Bottom panel*) Magnified demonstration of phase synchronization of neuronal discharge to coincident ECoG LFO. (*B*) R6/2 tonic STN neuron (firing rate = 4.31 Hz; CV = 0.56; lomb frequency = N/A Hz) recorded during synchronized ECoG epoch (total power = 286.8 μV; 0.5-4 Hz power = 222.9 μV; 4-7 Hz power = 27.41 μV; 7-13 Hz power = 13.56; 13-30 Hz power = 14.75; and 30-100 Hz power = 8.20 μV; dominant frequency = 1.78 Hz). (*C*) Coherence between STN neuronal spike discharge and coincident ECoG activity as a function of frequency. All data are mean ± SEM. ** indicates significantly different from WT, $p < 0.01$.

Spectral composition of ECoG in the desynchronized state. The total power of the ECoG within the lowest frequency bandwidth (0.5-4 Hz) was significantly attenuated during recording epochs in STN neurons in R6/2 mice in comparison to WT mice [$t(56) = 5.18$; $p < 0.01$] (Figure 6A). The total power of the ECoG in higher frequencies (4-100 Hz) was significantly altered as a function of genotype [$F(1, 56) = 8.49$; $p < 0.01$] and bandwidth [$F(3, 56) = 14.12$; $p < 0.01$] and there was a significant genotype x bandwidth interaction [$F(3, 56) = 33.14$; $p < 0.01$]. Planned comparisons indicated that the power within 13-30 Hz and 30-100 Hz was higher during recording epochs in STN neurons in R6/2 mice in comparison to those collected from STN neurons in WT mice (Fig. 6B). In addition, the power within 4-7 Hz was diminished during recording epochs in STN neurons in R6/2 mice in comparison to those collected from STN neurons in WT mice (Fig. 6B).

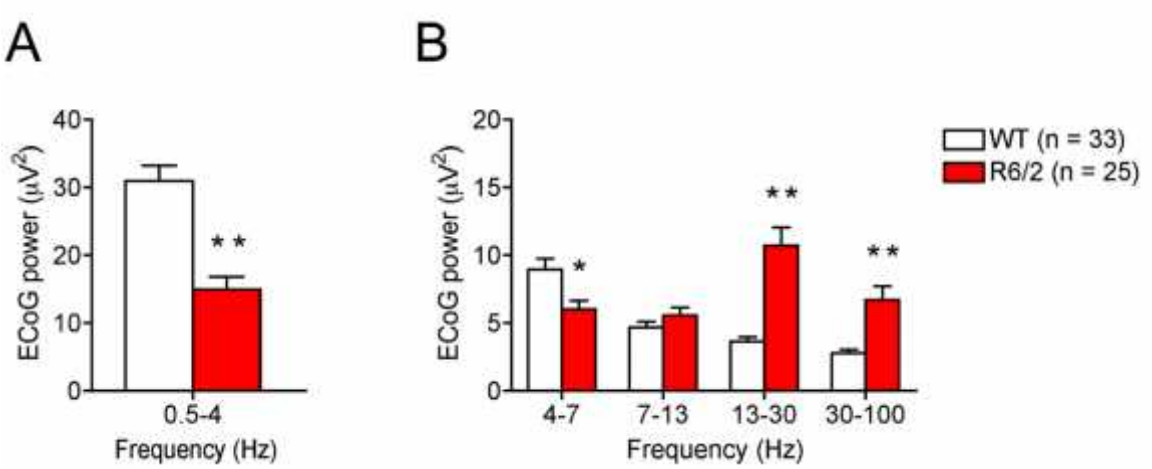

Figure 6: ECoG spectral power acquired in desynchronized epochs concomitant to the recording of WT and R6/2 STN neurons. (*A*) Total power spectral density of ECoG within low frequency components. (*B*) Total power spectral density of ECoG within high frequency components. ** indicates significantly different from WT, $p < 0.01$.

Coherence between STN activity and ECoG in the desynchronized state. We found no significant difference in the magnitude of the coherence between STN unit spiking and ECoG within the lowest frequency bandwidth (0.5-4 Hz) in R6/2 (0.32 ± 0.02) as compared to WT mice (0.31 ± 0.01) [U (56) = 412.0; p = 0.50] (Fig. 7B). Likewise, we report no significant difference in the magnitude of the coherence between STN LFP activity and ECoG within the lowest frequency bandwidth across genotypes [t (2) = 0.88; p = 0.24; n = 2 WT, n = 2 R6/2].

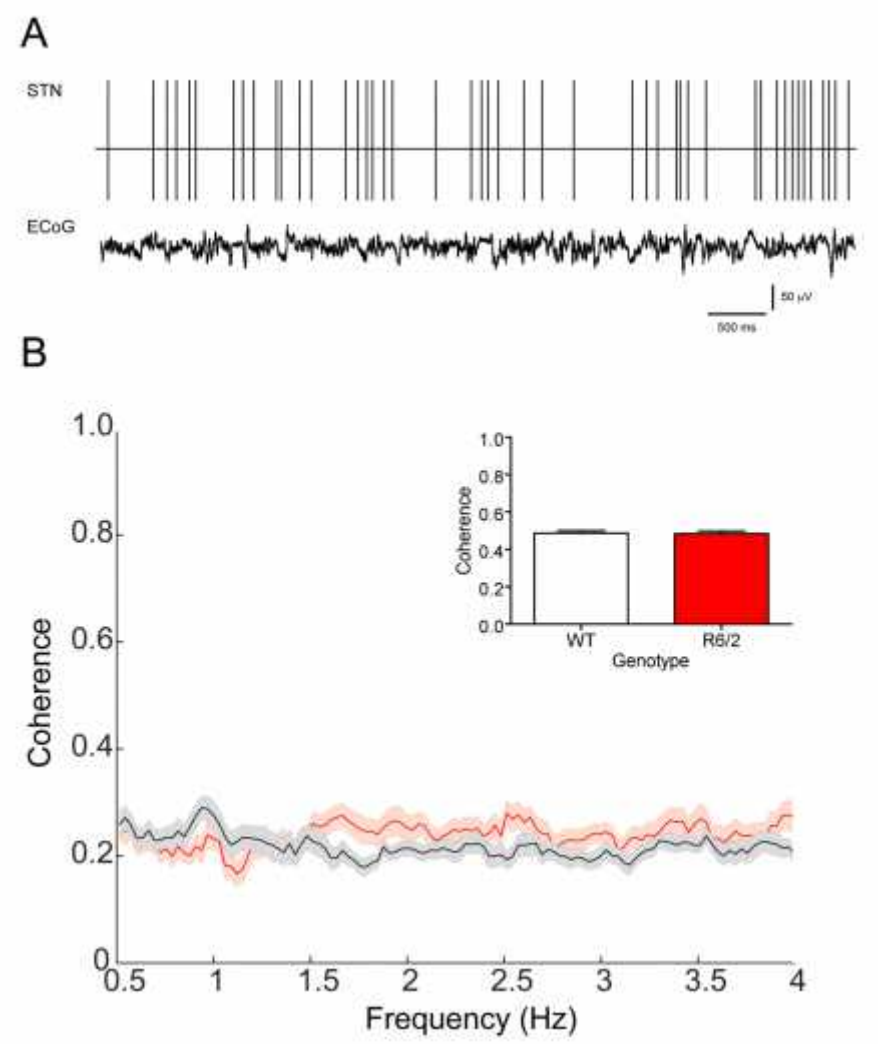

Figure 7: Spontaneous neuronal activity in the STN during desynchronized ECoG epochs in WT and R6/2 mice. (*A*) Representative neuronal activity in the STN (firing rate = 7.35 Hz; CV = 1.16) and concomitant ECoG (total power = 30.89 μV; 0.5-4 Hz power = 12.11 μV; 4-7 Hz power = 3.58 μV; 7-13 Hz power = 3.48; 13-30 Hz power = 8.78; and 30-100 Hz power = 2.94 μV) collected from R6/2 mouse during desynchronized ECoG epoch. (*B*) Coherence between STN neuronal spike discharge and coincident ECoG activity as a function of frequency. All data are mean ± SEM.

2.5 DISCUSSION

The present study was undertaken to investigate how the flow of information between the cerebral cortex and the STN is altered as a function of the expression of the

mHtt protein in the R6/2 transgenic mouse model of HD. Our results demonstrate that cortically patterned STN neuronal discharge is markedly less synchronized in R6/2 mice. In addition, the spontaneous activity of STN neurons in the absence of synchronized cortical input is diminished in R6/2 mice.

Under urethane anesthesia cortical activity alternates between two principal patterns, synchronized and desynchronized states, which have differential effects on shaping the neuronal activity in the STN (Magill et al., 2000, 2001; Mallet et al., 2008). During synchronized ECoG states, large ensembles of cortical neurons coherently oscillate between a depolarized up state and a silent hyperpolarized down state (Steriade, 2001). This pattern of rhythmic activity is expressed in the ECoG as recurring large amplitude oscillations in the low-frequency (~1 Hz) range (Steriade et al., 1993; Amzica and Steriade, 1998). Such rhythmic cortical discharge has a powerful synchronizing effect on STN activity and leads to the entrainment of neuronal firing in the STN (Magill et al., 2000, 2001; Bevan et al., 2002). Similar to that reported in rats during synchronized ECoG conditions (Magill et al., 2000, 2001), we observed significant LFO discharge characteristics in the spike trains of all STN neurons recorded from WT mice. STN unit and LFP activity were phase-locked to cortical up states and highly synchronized with concomitant LFO cortical activity. Thus, the urethane-anesthetized animal enables control over ECoG organization and serves as an effective model for assessing the functional connectivity between the cortex and the STN (Magill et al., 2000, 2001; Mallet et al., 2008). In contrast to epochs of cortical synchronization, desynchronization is related to a persistently depolarized state and associated with a reduction of power in low frequency ranges and increases of power in higher frequency

ranges in the ECoG (Steriade, 2001). Hence, desynchronization rapidly restructures the spectral composition of cortical activity and as a result the powerful synchronizing drive of the cortex on the STN is obliterated. During desynchronized ECoG states, STN neurons discharge with higher firing rates and tonic regularity and this autonomous activity is largely a result of intrinsic mechanisms, such as persistent sodium currents (Bevan and Wilson, 1999). To our knowledge this is the first study to perform *in vivo* electrophysiological recordings of the extracellular activity in the STN of mice and our results are similar to that reported previously in rats (Magill et al., 2000, 2001).

During synchronized ECoG states, powerful cortical LFO transmission is propagated to the STN and in contrast to the homogenous patterns of phase locked spiking that we reported in WT mice, strikingly, ~20% of STN neurons recorded from R6/2 mice failed to discharge with LFO patterns. The firing rate and pattern of activity in these tonic STN neurons resembled that observed in the desynchronized ECoG state, when cortical entrainment is less prominent and spiking is more autonomous (Bevan et al., 2002), and thus it is tempting to speculate that this segment of neurons is disconnected from cortical input. Cortical entrainment of STN neuronal activity during synchronized ECoG conditions is believed to occur via monosynaptic connections in the hyperdirect pathway (Magill et al., 2001). Specifically these connections are thought to arise from long range pyramidal tract neurons (PT) (Kita and Kita, 2012). Interestingly, at the 9-week age point that we investigated in R6/2 mice there is no significant cortical neuronal loss. However, Rosas et al. (2006) demonstrated using diffusion tensor imaging that white matter alterations in PT axons occurred early in HD and were independent of neuronal atrophy. Thus, anatomical changes in the connectivity within the

cortiosubthalamic tract could disturb the flow of information between these two nodes even in the absence of neuronal atrophy in the cortex of R6/2 mice.

While the remainder of neurons (~80%) from the STN population in R6/2 mice fired with expected LFO discharge during synchronized ECoG states, there was a marked change in the nature of the relationship between oscillatory activity in the STN and the cortex. R6/2 STN LFO neurons fired with significantly fewer bursts and the degree of phase locking between STN spiking and concomitant cortical LFO activity was significantly reduced. Of note, the firing rate in R6/2 STN LFO neurons was slightly higher and these neurons discharged with increased incidence of spikes per burst in comparison to WT mice, further suggesting that synaptic drive is altered in the STN of R6/2 mice. Loss of entrainment of STN activity was also seen at the network level as the coherence between the STN LFP and cortical LFO activity was attenuated. Thus, these results suggest that cortical rhythms are less effectively transmitted to the STN in R6/2 mice.

The overall spectral composition of cortical activity during synchronized states was altered in R6/2 mice which could lead to altered drive in the STN. Specifically, the density of power concentrated in low frequencies was reduced and the power expressed in higher frequencies was increased in R6/2 mice. Optical stimulation experiments have suggested that the locus of the LFO genesis originates from the synchronization of excitatory pyramidal neurons in deep cortical layers (mainly layer V) (Hughes and Crunelli, 2013; Kuki et al., 2013). Walker et al. (2008) demonstrated that the correlated firing among putative pyramidal neurons is reduced in the prefrontal cortex of R6/2 mice indicating impairments in synchrony. Morphological changes also can occur in

pyramidal neurons in R6/2 mice and include diminished dendritic area, reduced number of dendritic spines and impaired glutamate receptor function (Andre et al., 2006; Cummings et al., 2009). These factors could further contribute to the loss in correlated activity between pyramidal neurons in R6/2 mice and subsequent reductions in cortical LFO activity. In contrast to the reductions in power of oscillations in the low frequency range in R6/2 mice, oscillations in higher frequency ranges were increased. The firing rates of cortical neurons are increased in R6/2 mice (Walker et al., 2008) and several groups have demonstrated that cortical neurons in R6/2 mice are hyperexcitable (Cepeda et al., 2007; Cummings et al., 2009). In accordance, Stern (2011) demonstrated that cortical neurons can transition from down states to up states more easily, which could also account for the increase in the dominant frequency of the cortical LFO in R6/2 mice. These influences could contribute to the increased expression of higher frequencies in R6/2 mice. In addition, the STN receives afferents from a variety of other sources that are in a position to modulate STN neuronal activity and we cannot rule out these influences. These include projections from the parafasicular nucleus of the thalamus (Bevan et al., 1995), dorsal raphe nuclei (Lavoie and Parent, 1990), substantia nigra pars compacta (Hassani et al., 1997), and the pedunculopontine nucleus (Jackson and Crossman, 1983).

While investigating neural patterns of activity in the STN during synchronized ECoG states is invaluable for determining the fidelity of transmission in corticosubthalamic pathways, activity measured during desynchronized conditions is advantageous in that it more closely resembles activity patterns seen during wakefulness (Steriade, 2001). This is especially important in lieu of the fact that chorea manifests

during waking and is absent during states resembling synchronized ECoG conditions, such as sleep (Morton, 2013). During desynchronized ECoG conditions the density of power concentrated in low frequencies was diminished and the power expressed in higher frequencies was increased in R6/2 mice. Similar spectral differences have been reported by other groups in R6/2 mice (Hong et al., 2012; Fisher et al., 2013; Kantor et al., 2013) and seem to be a pathological signature of global cortical activity in R6/2 mice. During desynchronized ECoG epochs, we found significant reductions in the firing rates of STN neurons recorded from R6/2 mice as compared to WT mice. In addition, the discharge patterns of STN neurons in R6/2 mice were significantly less regular as compared to WT mice. Hence, the highly conserved fast spiking, tonic discharge during desynchronized ECoG conditions in STN neurons (Bevan et al., 2002) is disrupted as a function of the mHtt protein. The importance of continuous persistent discharge by STN neurons is exemplified by the fact that experimental or pathological disruption of repetitive firing in the STN is associated with hyperkinetic symptoms (Crossman, 1989; Hamada and DeLong, 1992) similar to that seen in HD. There are several mechanisms that could drive the abnormally patterned discharge of STN neurons during desynchronized states that will need to be addressed in future studies. As striatal degeneration is a cardinal pathology in HD, disinhibition of neurons in the globus pallidus external segment (GPe) could result in an augmented GABAergic tone in the STN in HD. The GPe exerts a powerful GABAergic control over the STN (Smith et al., 1990; Bevan et al., 2007) and neuronal network simulations have indicated that irregular activity can arise in the STN when GPe inhibition is strong and striatal inhibition is weak (Terman et al., 2002). In

addition, we cannot rule out the possibility that intrinsic membrane properties of STN neurons are altered as function of the expression of the mHtt protein in R6/2 mice.

The present results show profound reductions in the response of STN neurons to coordinated cortical inputs, as well as overall reductions in spontaneous discharge. The dramatic reductions in the activity of STN neurons could lead to diminished fidelity of information transmission in the basal ganglia and disordered motor control in HD.

2.5 ACKNOWLEDGEMENTS

This research was supported by NIH grant NS059921 (EDA) and Rutgers, the State University of New Jersey. The authors wish to thank Anna Chavez and Nupur Jain for technical assistance. We thank Dr. Andrew Farrar, Dr. James Tepper and Dr. Peter Magill for their helpful discussions. We declare no competing financial interests.

CHAPTER 3: CONTRIBUTION OF HYPERDIRECT PATHWAY ALTERATIONS TO SUBTHALAMIC NUCLEUS DYSFUNTION IN THE YAC128 MOUSE MODEL OF HUNTINGTON'S DISEASE

Authors: Joshua W. Callahan and Elizabeth D. Abercrombie

Journal: Journal of Neuroscience (Submitted)

3.1 ABSTRACT

Huntington's disease (HD) is an autosomal dominant neurodegenerative disorder that results in motor, cognitive and psychiatric abnormalities. Dysfunction in neuronal processing between the cortex and the basal ganglia is fundamental to the onset and progression of the HD phenotype. The corticosubthalamic hyperdirect pathway plays a crucial role in motor selection and blockade of neuronal activity in the STN results in hyperkinetic movement abnormalities, similar to the HD phenotype. The aim of the present study was to examine whether changes in the fidelity of information transmission between the cortex and STN emerge as a function of phenotypic severity in the YAC128 mouse model of HD. We performed in vivo extracellular recordings in the STN and measured concomitant cortical activity via electrocorticogram (ECoG) during brain states that represented global cortical network synchronization or desynchronization. At early ages in YAC128 mice, cortical and STN neuronal activity exhibited patterns of hyperexcitability. However, cortical entrainment of STN neuronal activity was progressively disrupted and spontaneous firing rates were reduced. Stimulation of the ipsilateral cortex leads to a short latency excitatory response in STN neurons that is generated by excitation of monosynaptic terminals in the hyperdirect pathway. Concomitant to the dissipation of STN entrainment, there was a reduction in the proportion of responsive STN neurons to cortical stimulation as a function of age. These results indicate dysfunction in the flow of information within the corticosubthalamic circuit and demonstrate progressive disconnection of the hyperdirect pathway in a transgenic mouse model of HD.

3.2 INTRODUCTION

Huntington's disease (HD) is a genetically inherited neurodegenerative disorder that results in progressive motor, cognitive and psychiatric abnormalities. Anatomical and functional alterations take place within the connections between the cortex and basal ganglia that seem to be fundamental to HD onset and progression (DiFiglia et al., 1997; Rosas et al., 2002; Cepeda et al., 2003; Raymond et al., 2011). These changes are dynamic and complex as they progress over time and it remains unresolved how cortical targets in the basal ganglia network are affected and contribute to disease pathogenesis.

The cortex is the main provider of entrant excitatory glutamaterigic inputs into the basal ganglia via two structures, the striatum and the subthalamic nucleus (STN). The cortex transmits information to the output nuclei of the basal ganglia nuclei through the STN with the shortest latency and thus this circuit has been termed the hyperdirect pathway (Nambu et al., 2000). Studies point to a critical role of the cortex and STN in modulating basal ganglia neuronal activity through the hyperdirect pathway (Fujimoto and Kita, 1993; Maurice et al., 1998; Magill et al., 2000; Nambu et al., 2000; Magill et al., 2001; Magill et al., 2004; Sharott et al., 2005). Specifically, the hyperdirect pathway has been implicated in action suppression (Aron and Poldrack, 2006; Frank, 2006; Jahfari et al., 2011) and blockade of STN neuronal activity through discrete lesions or pharmacological inactivation (Whittier and Mettler, 1949; Carpenter et al., 1950; Hamada and DeLong, 1992) produces hyperkinetic movement disorders which mimic chorea, the most common symptom of HD. Progressive synaptic disconnection of cortical input at the level of the striatum has been reported in HD (Cepeda et al., 2007; Miller et al., 2011;

Unschuld et al., 2012), however, neural transmission within the corticosubthalamic pathway remains relatively uninvestigated thus far. Based on the importance of control exerted by the STN on motor commands, elucidating alterations in processing between the cortex and STN could have valuable implications for understanding the pathophysiology of HD.

The generation of genetic mouse models has helped to reveal network alterations underlying HD by allowing the direct investigation of pathogenic mechanisms (Raymond et al., 2011). In order to examine the fidelity of neuronal processing between the cortex and STN we utilized the YAC128 transgenic mouse model of HD. YAC128 mice exhibit a progressive neurological phenotype and develop HD-like symptoms as a function of age (Slow et al., 2003; Van Raamsdonk et al., 2005). We performed *in vivo* extracellular single unit recordings in the STN and measured concomitant cortical activity via electrocorticogram (ECoG) across three different age points in YAC128 mice in order to examine the progressive nature of corticosubthalamic alterations in relation to phenotypic severity. Furthermore, we investigated the short latency excitatory responses of STN neurons to focal cortical stimulation to assess the impact of evoked hyperdirect pathway activation in YAC128 mice.

3.3 EXPERIMENTAL PROCEDURES

Animals. Male YAC128 transgenic mice and male control mice were studied in the present experiments. All mice were shipped from the Hayden colony at University of British Columbia or purchased from Jackson Laboratories (Bar Harbor, ME, USA). The transgenic YAC128 mouse strain (FVB-Tg(YAC128)53Hay/J) carries a random insertion of the human Huntingtin (HTT) gene with approximately 128 polyglutamine (CAG) repeats (Jackson Laboratories). The resultant expression of the CAG expansion region of the HTT gene produces animals that recapitulate behavioral and neuropathological aspects of human HD with a progressive disease phenotype (Slow et al., 2003). The wild-type (WT) control mouse strain (strain FVB/NJ) is the parent strain from which the YAC128 line was developed (Slow et al., 2003). Studies for each cohort began at approximately 2, 8, and 12 months in YAC128 mice and their respective WT controls.

Mice were housed individually in plastic microisolator cages with food and water available ad libitum. The mice were maintained under conditions of constant temperature (21°C) and humidity (40%) with a 12-hour light/dark cycle (0700 h on/1900 h off). All reasonable effort was made in order to minimize animal suffering and to limit the number of animals utilized for these experiments. Animal procedures were conducted in accordance with the National Institutes of Health Guide for the Care and Use of Laboratory Animals and were approved by Rutgers University Institutional Animal Care and Use Committee.

Rotarod testing. Potential phenotypic impairment of motor performance was examined using the rotarod treadmill task (Economex; Columbus Instruments, Columbus, OH). This task is the most widely used paradigm for assessment of motor function in HD animal models and is a sensitive measure for detecting the progressive gait and balance abnormalities that are characteristic of transgenic HD mice (Pallier et al., 2009). YAC128 and WT mice were trained on the rotarod task at 10 rpm for five consecutive trials (60 s maximum duration) one day prior to testing. On the test day, motor performance at five fixed speeds (5, 10, 15, 20, and 25 rpm) was measured (60 s interspeed interval) for two separate trials (5 min intertrial interval). Fall latencies (60 s cutoff) at each speed were averaged across trials for each subject.

Open field testing. Quantitative analysis of locomotor activity was examined using the open field test. Spontaneous locomotor activity of YAC128 and WT mice was monitored for 60 min via automated activity chambers (51 cm × 32 cm × 20 cm) equipped with infrared photobeams (Flexfield, San Diego Instruments, Inc., San Diego, CA, USA).

Electrophysiological Studies

Surgical protocol. Extracellular recording of STN neuronal activity along with simultaneous acquisition of ECoG signal was carried out in the same mice that participated in the rotarod and open field testing. Anesthesia was initiated by administration of urethane (1.25 g/kg, i.p.; Sigma-Aldrich Corporation, St. Louis, MO). Following the loss of righting reflexes, an appropriate surgical level of anesthesia was achieved by administration of a solution containing ketamine (80-100 mg/kg, i.p.;

Phoenix Pharmaceutical Inc., St. Joseph, MO) combined with xylazine (10 mg/kg, i.p.; Sigma-Aldrich Corporation, St. Louis, MO). Supplemental doses of ketamine (30 mg/kg, i.p.) plus xylazine (3 mg/kg, i.p.) were used for the remainder of the experiment as needed (Magill et al., 2000; Mallet et al., 2008). Sterile saline (0.9% w/v) served as the vehicle for all drug solutions. Throughout the experiment, the effectiveness of this anesthetic technique was verified by subjective observation of the ECoG signal, the respiration rate, and by testing for the presence of reflex withdrawal to cutaneous paw pinch and corneal stimulation (Whelan and Flecknell, 1992). Subsequent to anesthetization of the mouse, local anesthetic (bupivacaine hydrochloride solution, 0.5%, APP Pharmaceuticals, Schaumburg, IL) was injected beneath the scalp (0.1 ml, s.c.) and the animal was placed into a stereotaxic frame (David Kopf Instruments, Tujunga, CA). With the skull flat, a craniotomy was performed directly above the STN at the following coordinates: AP: -2.1 mm, ML: ±1.6 mm relative to bregma (Franklin and Paxinos, 2008) and the underlying dura mater was carefully resected. A second and third craniotomy was performed directly above the ipsilateral and contralateral primary motor cortex (M1) at the following coordinates: AP: +2.1 mm, ML: ±2.0 mm relative to bregma (Franklin and Paxinos, 2008). Body temperature was maintained at 37 ± 0.5°C using a heating pad. Lactated ringer's solution (Fisher Scientific, Suwanee, GA) was administered (1.0-2.0 ml/30 g, s.c.) approximately every 2-3 h to prevent dehydration.

STN activity. Extracellular action potentials generated by single STN neurons and local field potentials (LFP) in STN were recorded from single 10–25 MΩ glass recording pipettes (tip diameter ~1.0-2.0 μm) filled with a 0.5 M NaCl solution containing 2%

pontamine sky blue (Sigma-Aldrich Corporation, St. Louis, MO). The electrode was lowered to a point ~500 μm above STN and then slowly was advanced in 1.0-10 μm increments using a micropositioner (Model 2660, David Kopf Instruments, Tujunga, CA) until a well-isolated single unit recording was obtained. Units characteristic of STN neurons recorded in rats such as ~10 Hz firing rates with biphasic waveforms (Magill et al., 2000) were encountered 4.0-4.5 mm below dura (see Figure 1). For all analyses, recordings were used if they were obtained when the electrode track was between AP -1.94 mm to -2.30 mm (relative to bregma). Recordings typically lasted for 2-10 min. The amplified neuronal signals were band-pass filtered between 300 and 20 kHz (Model 1800, A-M Systems Microelectrode Amplifier, Sequim, WA). Amplified LFP signals were band-pass filtered between 0.1 and 20 kHz (A-M Systems Microelectrode Amplifier, Sequim, WA) and digitized on-line using a PC and a Micro1401 interface (Cambridge Electronic Design, Cambridge, UK) using Spike2 data acquisition and analysis software (Cambridge Electronic Design, Cambridge, UK). Single unit activity was sampled at 21 kHz and the LFP signal was down-sampled to 500 Hz and low-pass filtered at 100 Hz (Butterworth filter). Data from all recording sessions were visually inspected off-line and epochs with breathing or electrical artifacts were discarded.

ECoG activity. A stainless steel screw used for ECoG recording was secured into the skull and positioned in contact with the dura matter directly above the contralateral M1. Another stainless steel screw was secured into the skull and positioned in contact with the dura matter over the contralateral cerebellum to serve as a reference electrode. Raw ECoG was band-pass filtered between 0.1 and 100 Hz (Grass P5 Series Preamplifier; West Warwick, RI). The resulting amplified ECoG signal was sampled at 500 Hz and

digitized on-line with Spike2 data acquisition and analysis software (Cambridge Electronic Design, Cambridge, UK).

The ECoG was monitored continuously throughout all recording sessions. Global cortical network activity was observed to transition in distinct stages between a high-voltage, slow activity pattern (synchronized) and low-voltage periods containing a heterogeneous pattern (desynchronized). Epochs of synchronized activity are characterized by recurring large amplitude, low-frequency (0.5-4 Hz) oscillations in the ECoG. The transition to epochs of desynchronized ECoG occurred spontaneously. Importantly, during these desynchronized epochs, the animal did not show any signs of reflexive responses or marked changes in respiration, indicating anesthesia levels were sufficient throughout the recordings.

Cortical stimulation. A bipolar nylon coated stainless steel electrode (outer diameter 100 μm, contact separation < 100 μm) used for focal electrical stimulation was stereotaxically implanted in the ipsilateral M1 and fixed to the skull using dental cement (Orthodontic Acrylic Resin, Lang Dental Manufacturing Co, Wheeling, IL). Electrical stimuli consisting of single square wave pulses of 0.3 ms duration and 0.6 mA amplitude were delivered at a frequency of 0.67 Hz using a constant current (Model 2100, A-M Systems Isolated Pulse Stimulator, Sequim, WA).

Data Analysis

STN single-unit activity. In order to assess the discharge properties of STN neurons, 30 sec epochs of ECoG composed of easily discernable synchronized or desynchronized patterns were identified by visual inspection offline and a portion of the coincident STN

spike train consisting of 500 spikes was isolated and further analyzed. The mean firing rate (spikes per second; Hz) for each STN neuron was calculated. Spike train regularity was determined by calculating the coefficient of variation (CV) of the interspike interval (ISI) distribution (ISI standard deviation/ISI mean). A more detailed analysis of the STN spike train patterns was conducted using an automatic burst detection algorithm implemented with custom-derived scripts for use with Spike2 (Cambridge Electronic Design, Cambridge, UK). Specifically, individual ISI histograms were constructed using a bin size determined by dividing the longest ISI in the spike train into 1000 bins. Bursts were defined as an epoch containing a sequence of two or more spikes beginning with an ISI 40 bins larger than the mode of the ISI distribution and ending with an ISI 80 bins larger than the mode. These parameters were empirically defined and upon comparison with alternative burst detection algorithms (such as fixed parameter settings and Poisson Surprise) we determined that this script was most accurate for our dataset. Further, the criteria chosen were specifically designed to identify events of clustered spiking that occur in response to cortical synchronization and are different than that which would be classically used to define the bursting of STN neurons or other neuronal subtypes during desynchronized states. Thus, the burst detection algorithm was only used for the analysis of spike trains recorded during synchronized conditions. For each epoch of STN activity, the number of bursts, percentage of spikes per burst, mean spikes per burst, ISI within bursts, burst duration and interburst duration was compared. Lomb periodograms were estimated from the autocorrelograms of spike trains to quantify the significance of any patterns of periodic, oscillatory activity that might be present (Kaneoke and Vitek, 1996). Autocorrelograms were constructed with 20 ms bins and 4 s of lag time for each epoch of

STN activity analyzed. The frequency bin that contained the highest power within the Lomb periodogram was used as a measure of the dominant oscillatory frequency in a given spike train. We considered oscillations significant if spectral power within these peaks was significantly greater than expected in comparison with independent Guassian random variables ($p < 0.05$). Those neurons that displayed significant peaks in the periodogram spectra between 0.5-4 Hz were classified as exhibiting significant low-frequency oscillations and termed LFO in the subsequent text.

Cortical ECoG activity. In order to assess the spectral composition of ECoG we performed Fast Fourier transform (FFT) analysis. Estimates of the spectral power density were extracted via Welch's periodogram method using a Hanning window with 50% overlap and a resolution frequency of 0.242 Hz. Estimates were summed within the following frequency bins to obtain the power densities of low frequency and higher frequency bandwidths: 0.5-4 Hz, 4-7 Hz, 7-13 Hz, 13-30 Hz and 30-100 Hz.

Coherence between STN activity and ECoG. Coherence measures the amount of linear correlation between two time series as a function of frequency and is an absolute value that varies between 0, no systematic phase relationship between two signals, and 1, indicating a perfect phase relationship (i.e. phase-locked). The coherence between STN activity (unit firing or LFP) with coincident ECoG was calculated using the multitaper method implemented in the Chronux 2.0 data analysis toolbox (Bokil et al., 2010) for Matlab (MathWorks). Coherence spectra were estimated for the frequency range from 0.5-100 Hz. We extracted the peak coherence value for statistical comparison.

Cortical stimulation. Cortically evoked fast excitatory responses (< 4 ms) of STN

neurons were elicited by focal electrical stimulation of the ipsilateral M1. Peristimulus time histograms (PSTHs) of spike trains were constructed using a bin size of 0.1 ms from 50-100 consecutive stimulation trials. Excitatory responses were considered significant if the number of spikes within at least 3 consecutive bins was 2 or more standard deviations above the mean prestimulus frequency during the 50 ms prior to stimulation. The first bin in which a response reached significance was used for the estimation of latency.

Histology. To identify the location of recorded sites, at the end of each experiment the electrode placement of the last recorded neuron was marked with an iontophoretic deposit of pontamine sky blue (15-20 min, -20 μA, constant current injection). Upon completion of each experiment, animals were administered a lethal dose of sodium pentobarbital and were perfused intracardially with 0.9% saline followed by 10% formaldehyde. Brains were extracted and post-fixed in fresh fixative overnight at 4°C and transferred to 30% sucrose in phosphate buffer solution at 4°C for cryoprotection. Coronal sections of 60 μm thickness were obtained and stained with Neutral Red (Sigma-Aldrich Corporation, St. Louis, MO) to verify the recording site in the STN (Fig. 1).

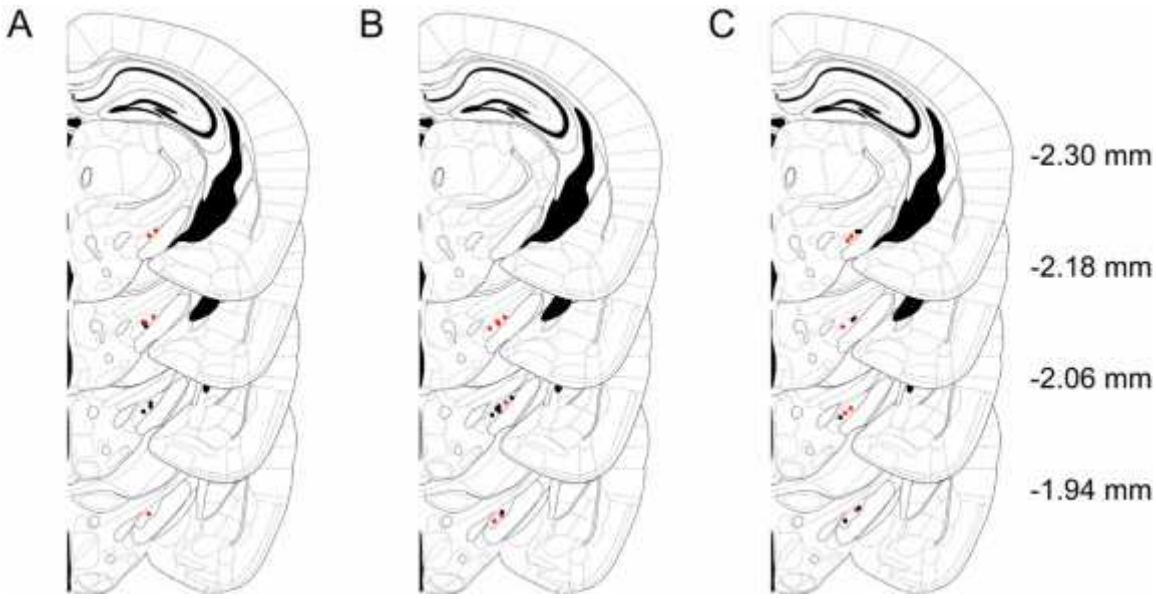

Figure 1: Schematic coronal diagrams of the mouse brain indicating the location of electrode tracks in the STN (modified from Franklin and Paxinos, 2008) of (*A*) 2-month-old (*B*) 8-month-old and (*C*) 12-month-old WT (black) and YAC128 (red) mice. Numbers indicate distance (mm) posterior to bregma.

Statistical analysis. All data are presented as mean ± SEM. Data were analyzed with a t-test for unpaired comparisons and by using a Mann-Whitney U-test in the case of non-normal distributions. Between-group differences for paired comparisons were assessed using two-way ANOVA. When appropriate, two-way ANOVA determinations were followed by Bonferroni's post-hoc test. For the analysis of within-group effects for paired comparisons, one-way ANOVA was used coupled to Bonferroni's post-hoc test. Between-group differences for three comparisons were assessed using one-way ANOVA coupled to Bonferroni's post-hoc test when appropriate. For the analysis of group differences for three comparisons with non-normal distributions, a Kruskal-Wallis test was used together with Dunn's post-hoc test. Differences were considered statistically significant when $p < 0.05$.

3.4 RESULTS

Experimental overview. A total of five 2-month-old YAC128 mice (n = 40 STN neurons) and five age-matched WT mice (n = 41 STN neurons); seven 8-month-old YAC128 mice (n = 61 STN neurons) and six age-matched WT mice (n = 38 STN neurons); seven 12-month-old YAC128 mice (n = 50 STN neurons) and six age-matched WT mice (n = 38 STN neurons) were included in the present experiments. The number of epochs acquired varied across animals and, in some cases, recording conditions permitted STN activity to be acquired from a single neuron during both ECoG states in YAC128 and WT mice, although this was not the norm. For the YAC128 group, STN neurons obtained during synchronized ECoG epochs that did not exhibit significant periodicity in their spike trains, as measured via Lomb periodogram, are termed tonic in the subsequent text. A total of two tonic neurons were found in the WT group and excluded from analysis.

Motor performance on the rotarod task. There was no significant difference in the latency to fall off the rotarod treadmill as a function of genotype in 2-month-old YAC128 and WT mice [$F(1, 32) = 1.68$; $p = 0.23$]. In 8-month-old YAC128 and WT mice, fall latencies were significantly reduced as a function of speed [$F(4, 44) = 3.17$; $p < 0.05$] and genotype [$F(1, 44) = 6.24$; $p < 0.05$]. Planned comparisons indicated that fall latencies in YAC128 mice were significantly reduced relative to WT mice at 20 rpm. Likewise, in 12-month-old YAC128 and WT mice, fall latencies were significantly reduced as a function of speed [$F(4, 44) = 8.61$; $p < 0.01$] and genotype [$F(1, 44) = 22.61$; $p < 0.01$]. Planned comparisons indicated that fall latencies in YAC128 mice were

significantly reduced compared to WT mice at 5, 10, 15, 20, and 25 rpm. Data are presented in graphical form for 20 rpm as this speed is most representative of overall performance in both genotypes across ages (Fig. 2A)

Locomotor activity in the open field test. Spontaneous activity was significantly reduced as a function of age in both YAC128 and WT mice [$F(2, 30) = 13.61$; $p < 0.01$] (Fig. 2B). There was no significant difference in the spontaneous activity between genotypes at any age that was sampled [$F(1, 30) = 0.01$; $p = 0.91$] (Fig. 2B). However, spontaneous activity counts were decreased in both 8-month-old YAC128 mice and 12-month-old YAC128 mice compared to 2-month-old YAC128 mice [$F(2, 18) = 14.36$; $p < 0.01$] (Fig. 2B).

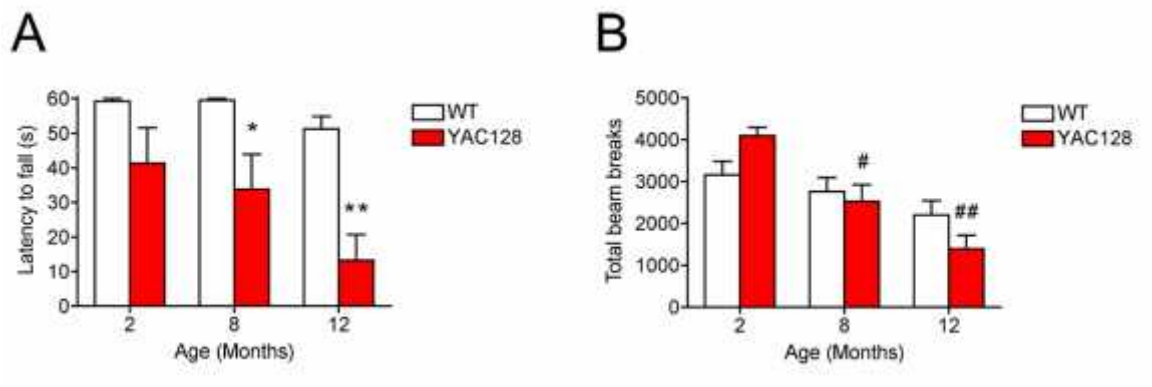

Figure 2: Motor phenotype of WT and YAC128 mice as a function of age. (*A*) Rotarod performance comparison of WT and YAC128 mice at 20 rpm fixed speed. (*B*) Open field activity comparison of WT and YAC128 mice. All data are mean ± SEM. * indicates significantly different from WT, $p < 0.05$; ** indicates significantly different from WT, $p < 0.01$. # indicates significantly different from 2-month-old YAC128, $p < 0.05$; ## indicates significantly different from 2-month-old YAC128, $p < 0.01$.

Firing properties of STN neurons are dependent on ECoG state. Figure 3 shows a representative example depicting the patterns of activity of STN units during

synchronized and desynchronized ECoG epochs in WT mice. STN neurons preferentially fire bursts of action potentials that are phase-locked to cortical up states during synchronized ECoG epochs. In contrast, STN neurons fire with more tonic regularity during desynchronized ECoG epochs.

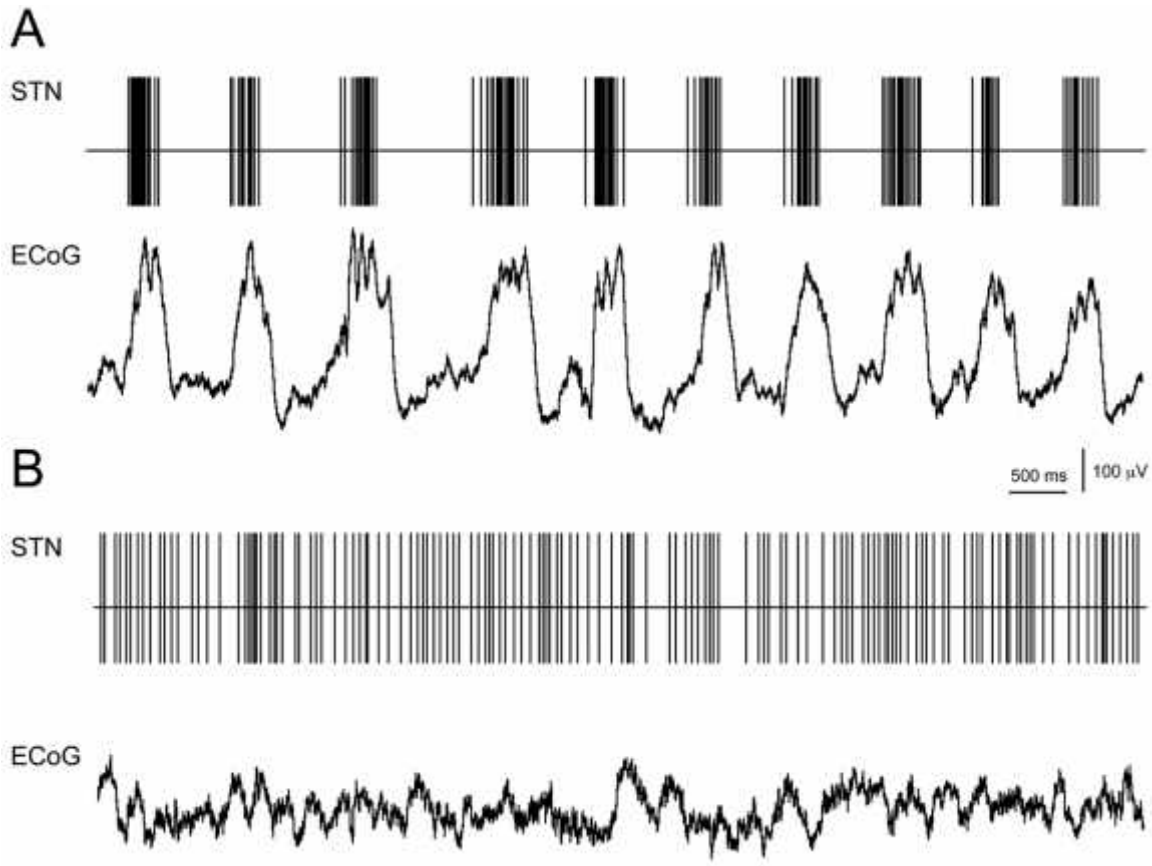

Figure 3: Representative neuronal activity in the STN and concomitant ECoG collected from 12-month-old WT mice. (*A*) LFO STN neuron (firing rate = 12.56 Hz; CV = 1.92; lomb frequency = 1.26 Hz) recorded during synchronized ECoG epoch (total power = 1282.24 µV; 0.5-4 Hz power = 1225.25 µV; 4-7 Hz power = 32.33 µV; 7-13 Hz power = 14.19 µV; 13-30 Hz power = 7.85 µV; and 30-100 Hz power = 2.61 µV; dominant frequency = 1.21 Hz). (*B*) Tonically firing STN neuron (firing rate = 14.40 Hz; CV = 0.67) recorded during desynchronized ECoG epoch (total power = 161.17 µV; 0.5-4 Hz power = 104.37 µV; 4-7 Hz power = 34.74 µV; 7-13 Hz power = 7.06 µV; 13-30 Hz power = 8.08 µV; and 30-100 Hz power = 6.90 µV).

STN spike train activity in the synchronized ECoG state in YAC128 mice. There was no significant difference in the firing rate of STN neurons between genotypes at any age that was sampled (Table 1). In 2-month-old YAC128 mice, the CV of LFO neurons (1.43 ± 0.05) was significantly larger than that of LFO neurons recorded from age-matched WT mice (1.30 ± 0.09) [$U(63) = 370.0$; $p < 0.05$] (Table 1). In addition, the peak oscillating frequency of the spike train in LFO neurons was significantly lower in 2-month-old YAC128 mice (1.03 ± 0.04 Hz) than that of LFO neurons recorded from age-matched WT mice (1.15 ± 0.04 Hz) [$U(63) = 2.18$; $p < 0.05$]. In 2-month-old YAC128 mice, the percentage of action potentials per burst in LFO neurons (81.28 ± 1.79) was significantly greater than that of LFO neurons recorded from age-matched WT mice (74.49 ± 2.97) [$t(63) = 2.04$; $p < 0.05$]. Also, in 2-month-old YAC128 mice, the duration of burst events in LFO neurons (299.9 ± 36.76 ms) was significantly longer than that of LFO neurons recorded from age-matched WT mice (198.2 ± 15.13 ms) [$t(63) = 2.04$; $p < 0.05$]. In 8-month-old YAC128 mice, the CV of tonic neurons (0.63 ± 0.08) was significantly less than that of LFO neurons recorded from both age-matched YAC128 (1.44 ± 0.07) and WT mice (1.52 ± 0.08) [$F(2, 73) = 12.43$; $p < 0.01$] (Table 1). There was no significant difference between 8-month-old YAC128 mice (1.04 ± 0.03 Hz) and age-matched WT mice (1.03 ± 0.05 Hz) in the peak oscillating frequency of the spike train recorded from LFO neurons [$t(66) = 0.27$; $p = 0.39$]. Furthermore, there were no significant differences in the burst characteristics of STN neurons between genotypes recorded at 8 months of age. In 12-month-old YAC128 mice, the CV of tonic neurons (0.79 ± 0.22) was significantly less than that of LFO neurons recorded from both age-matched YAC128 (1.27 ± 0.08) and WT mice (1.56 ± 0.10) [$F(2, 66) = 7.87$; $p < 0.01$] (Table 1). There

was no significant difference between 12-month-old YAC128 mice (1.09 ± 0.05 Hz) and age-matched WT mice (1.08 ± 0.05 Hz) in the peak oscillating frequency of the spike train recorded from LFO neurons [t (56) = 0.23; p = 0.41]. In 12-month-old YAC128 mice, the ISI of spikes within bursts in LFO neurons (44.79 ± 4.62 ms) was significantly greater than that of LFO neurons recorded from age-matched WT mice (33.83 ± 3.63 ms) [t (56) = 1.80; p < 0.05]. For the YAC128 group, in contrast to WT mice, the proportion of STN neurons tonic neurons increased linearly as a function of age (Fig. 4C).

Table 1. Firing properties of STN neurons during synchronized ECoG epochs.

	Genotype	2 Month	8 Month	12 Month
Number of cells	WT	29	26	26
	YAC128 LFO	36	42	32
	YAC128 Tonic	1	6	9
Firing rate (Hz)	WT	10.91 ± 1.28	9.80 ± 1.03	11.05 ± 1.43
	YAC128 LFO	11.87 ± 1.30	10.56 ± 0.81	9.59 ± 1.04
	YAC128 Tonic	7.28	9.62 ± 1.95	11.70 ± 2.49
CV	WT	1.30 ± 0.09	1.52 ± 0.08	1.56 ± 0.10
	YAC128 LFO	1.43 ± 0.05 *	1.44 ± 0.07	1.27 ± 0.08
	YAC128 Tonic	0.65	0.63 ± 0.08 ** ##	0.79 ± 0.22 ** #

Table 1: All data are mean ± SEM. * indicates significantly different from WT, $p < 0.05$; ** indicates significantly different from WT, $p < 0.01$; # indicates significantly different from YAC128 LFO, $p < 0.05$; ## indicates significantly different from YAC128 LFO, $p < 0.01$.

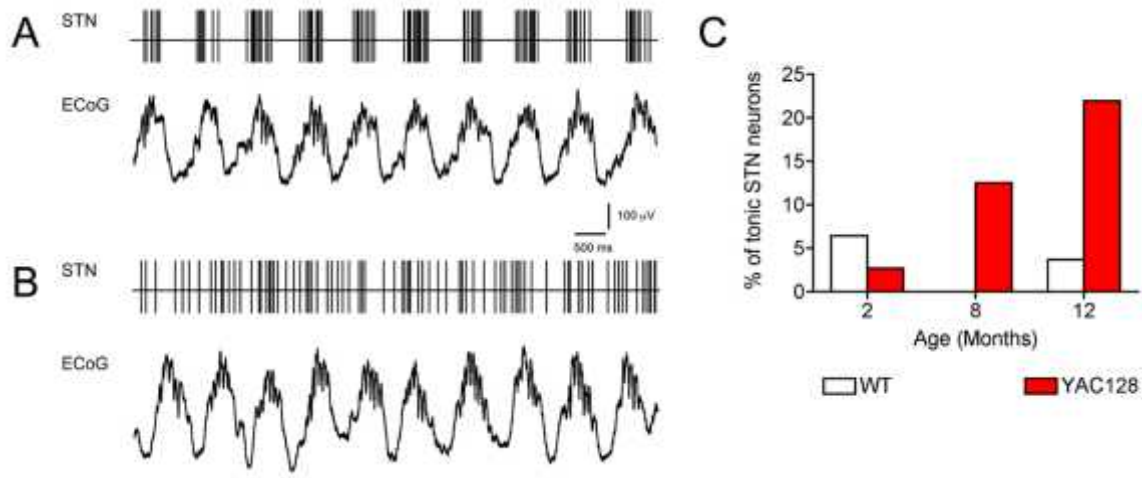

Figure 4: Oscillatory entrainment of STN neuronal activity during synchronized ECoG epochs in WT and YAC128 mice. (*A*) LFO STN neuron (firing rate = 9.5 Hz; CV = 1.68; lomb frequency = 1.04 Hz) recorded from 12-month-old YAC128 mouse during synchronized ECoG epoch (total power = 1235.09 µV; 0.5-4 Hz power = 1166.19 µV; 4-7 Hz power = 20.54 µV; 7-13 Hz power = 23.83 µV; 13-30 Hz power = 21.61 µV; and 30-100 Hz power = 2.91 µV; dominant frequency = 0.97 Hz). (*B*) Tonic STN neuron (firing rate = 7.33 Hz; CV = 0.71; lomb frequency = N/A Hz) recorded from 12-month-old YAC128 mouse during synchronized ECoG epoch (total power = 1553.30 µV; 0.5-4 Hz power = 1492.23 µV; 4-7 Hz power = 19.75 µV; 7-13 Hz power = 11.96 µV; 13-30 Hz power = 25.32 µV; and 30-100 Hz power = 4.04 µV; dominant frequency = 0.97 Hz). (*C*) Proportion of tonic STN neurons in WT and YAC128 mice as a function of age. All data are mean ± SEM.

Spectral composition of ECoG in the synchronized state. There was no significant difference in the dominant frequency of the ECoG during recording epochs of LFO neurons in 2-month-old YAC128 mice (1.05 ± 0.04 Hz) compared to those collected from LFO neurons in age-matched WT mice (1.12 ± 0.04 Hz) [$t(63) = 1.31$; $p = 0.10$]. In 2-month-old YAC128 mice, the total power of the ECoG within the lowest frequency bandwidth (0.5-4 Hz) was significantly greater during recording epochs in LFO neurons compared to those collected from LFO neurons in age-matched WT mice [$t(63) = 1.67$; $p < 0.05$] (Figure 5A). In addition, at 2 months of age, there was a significant genotype x bandwidth interaction for the total power of the ECoG within higher frequencies (4-100

Hz) [F (6, 63) = 3.29; $p < 0.01$]. Planned comparisons indicated that the power within 7-13 Hz was greater during recording epochs in LFO neurons in 2-month-old YAC128 mice relative to those collected from LFO neurons in age-matched WT mice (Fig. 5A). In 8-month-old YAC128 mice, there was no significant difference in the dominant frequency of the ECoG during recording epochs of LFO neurons (1.05 ± 0.03 Hz) or tonic neurons (1.05 ± 0.18 Hz) in comparison to those collected from LFO neurons in age-matched WT mice (1.03 ± 0.05 Hz) [H = 1.40, d.f.= 2, $p = 0.50$]. Likewise, at 8 months of age, there was no significant difference in the total power of the ECoG within the lowest frequency bandwidth (0.5-4 Hz) [F (2, 71) = 2.87; $p = 0.06$] or within higher frequencies (4-100 Hz) [F (2, 71) = 2.68; $p = 0.08$] during recording epochs of STN neurons as a function of genotype (Fig. 5B). In 12-month-old YAC128 mice, there was no significant difference in the dominant frequency of the ECoG during recording epochs of LFO neurons (1.12 ± 0.05 Hz) or tonic neurons (0.89 ± 0. 0.06 Hz) in comparison to those collected from LFO neurons in age-matched WT mice (1.06 ± 0.05 Hz) [F (2, 64) = 2.73; $p = 0.07$]. At 12 months of age, there was no significant difference in the total power of the ECoG within the lowest frequency bandwidth (0.5-4 Hz) [F (2, 64) = 0.16; $p = 0.85$] (Fig. 5C). However, there was a significant genotype x bandwidth interaction for the total power of the ECoG within higher frequencies (4-100 Hz) in 12-month-old YAC128 and WT mice [F (6, 64) = 3.44; $p < 0.01$]. Planned comparisons indicated that the power within 4-7 Hz was diminished during recording epochs in both LFO and tonic neurons in 12-month-old YAC128 mice relative to those collected from LFO neurons in age-matched WT mice (Fig. 5C).

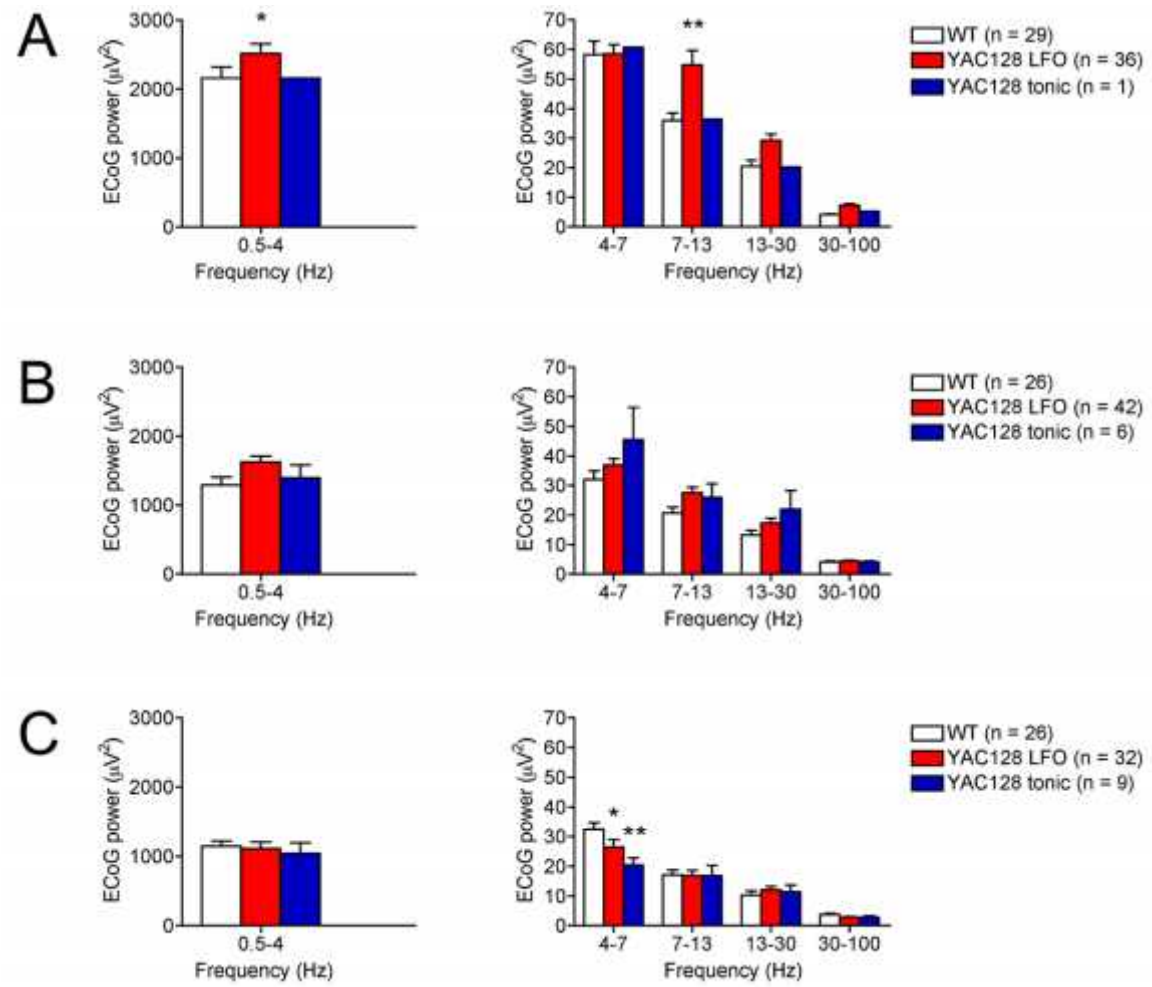

Figure 5: ECoG spectral power acquired in synchronized epochs concomitant to the recording of WT STN neurons, YAC128 LFO STN neurons and YAC128 tonic STN neurons as a function of age. (*A*) Total power spectral density of ECoG within (*left*) low frequency components and (*right*) higher frequency components in 2-month-old WT and YAC128 mice. (*B*) Total power spectral density of ECoG within (*left*) low frequency components and (*right*) higher frequency components in 8-month-old WT and YAC128 mice. (*C*) Total power spectral density of ECoG within (*left*) low frequency components and (*right*) higher frequency components in 12-month-old WT and YAC128 mice. All data are mean ± SEM. * indicates significantly different from WT, $p < 0.05$; ** indicates significantly different from WT, $p < 0.01$.

Coherence between STN activity and ECoG in the synchronized state. At 2 months of age, there was no significant difference in the magnitude of the coherence between LFO unit spiking and ECoG within the lowest frequency bandwidth (0.5-4 Hz) in YAC128 mice (0.84 ± 0.02) compared to that of age-matched WT mice (0.87 ± 0.01) [U (63) =

471.0; p = 0.25]. In 8-month-old YAC128 mice, the magnitude of the coherence between tonic unit spiking and ECoG specifically within the lowest frequency bandwidth (0.5-4 Hz) was significantly less (0.66 ± 0.04) than that of LFO neurons recorded from both age-matched YAC128 (0.86 ± 0.02) and WT mice (0.88 ± 0.01) [F (2, 71) = 12.84; p < 0.01]. Likewise, in 12-month-old YAC128 mice, the magnitude of the coherence between tonic unit spiking and ECoG specifically within the lowest frequency bandwidth (0.5-4 Hz) was significantly less (0.70 ± 0.05) than that of LFO neurons recorded from both age-matched YAC128 (0.86 ± 0.02) and WT mice (0.88 ± 0.01) [H = 11.64, d.f.= 2, p < 0.01]. There was no significant difference in magnitude of the coherence between STN LFP activity and ECoG within the lowest frequency bandwidth at 2 months of age [t (7) = 1.46; p = 0.09; n = 5 WT, n = 4 YAC128], 8 months of age [t (9) = 0.62; p = 0.27; n = 6 WT, n = 5 YAC128] or 12 months of age [t (6) = 0.26; p = 0.40; n = 4 WT, n = 4 YAC128] as a function of genotype.

STN excitatory activity evoked by cortical stimulation. For the YAC128 group, in contrast to WT mice, the proportion of STN neurons that exhibited a fast excitatory response evoked by focal cortical stimulation decreased linearly as a function of age (Fig. 6B). The response latency of STN neurons to focal cortical stimulation was significantly slower in 8-month-old YAC128 mice (2.57 ± 0.17 ms) in contrast to age-matched WT mice (1.81 ± 0.11 ms) [t (31) = 3.81; p < 0.01]. In addition, the duration of the fast excitatory response recorded from STN neurons was significantly reduced in 12-month-old YAC128 mice (1.20 ± 0.25 ms) in contrast to age-matched WT controls (1.97 ± 0.20 ms) [t (26) = 2.28; p < 0.05].

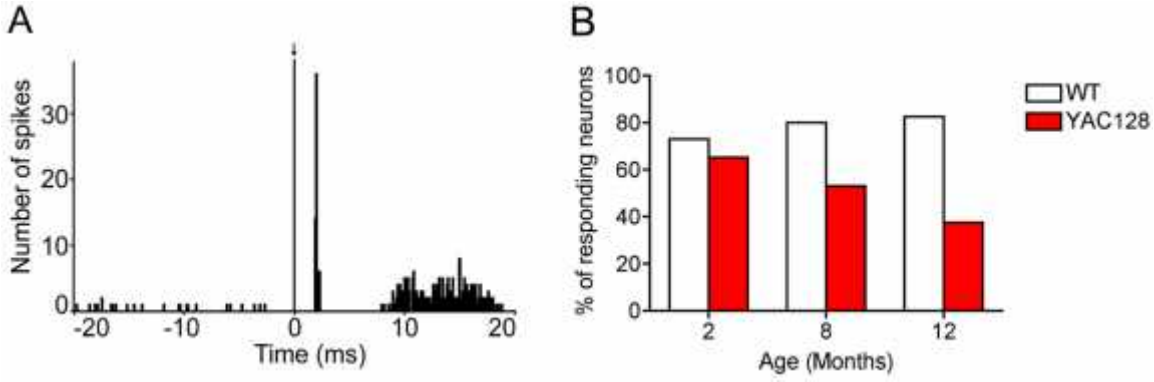

Figure 6: Excitatory response evoked by cortical stimulation in the STN of WT and YAC128 mice. (*A*) Peristimulus time histogram (PSTH) from a spike train recorded from a STN neuron responding to cortical stimulation in a 2-month-old WT mouse. Arrow indicates the time of stimulation (0 ms). (*B*) Proportion of STN neurons that exhibit short latency excitation (< 4 ms) evoked by cortical stimulation in WT and YAC128 mice as a function of age.

Table 2. Characteristics of the excitatory response in STN neurons evoked by cortical stimulation.

	Genotype	2 Month	8 Month	12 Month
Number of cells	WT	26	20	23
	YAC128	23	32	24
% Responding cells	WT	73.08	80.00	82.61
	YAC128	65.22	53.13	37.50
Latency (ms)	WT	2.29 ± 0.24	1.81 ± 0.11	1.94 ± 0.13
	YAC128	2.74 ± 0.31	2.57 ± 0.17**	2.02 ± 0.32
Duration (ms)	WT	1.87 ± 0.23	1.58 ± 0.22	1.97 ± 0.20
	YAC128	2.57 ± 0.38	1.73 ± 0.24	1.20 ± 0.25 *

Table 2: All data are mean ± SEM. * indicates significantly different from WT, $p < 0.05$; ** indicates significantly different from WT, $p < 0.01$.

STN spike train activity in the desynchronized ECoG state in YAC128 mice.

At 2 months of age, there was no significant difference in the firing rate of STN neurons between YAC128 (14.95 ± 1.95 Hz) and WT (12.47 ± 0.93 Hz) mice [U (53) = 361.0; p

= 0.40] (Table 3). However, in 2-month-old YAC128 mice, the CV of STN neurons (0.96 ± 0.08) was significantly larger than that of STN neurons recorded from age-matched WT mice (0.74 ± 0.04) [U (53) = 261.0; $p < 0.05$] (Table 3). In 8-month-old YAC128 mice, neurons recorded from the STN (10.28 ± 0.73 Hz) discharged with significantly slower firing rates compared to STN units recorded from age-matched WT mice (13.65 ± 1.15 Hz) [t (61) = 2.60; $p < 0.01$] (Table 3). There was no significant difference between the CV of STN neurons recorded from 8-month-old YAC128 mice (0.69 ± 0.04) compared to age-matched WT mice (0.63 ± 0.04) [U (53) = 434.0; $p = 0.28$] (Table 3). In 12-month-old YAC128 mice, neurons recorded from the STN (8.27 ± 0.79 Hz) discharged with significantly slower firing rates compared to STN units recorded from age-matched WT mice (12.67 ± 1.19 Hz) [t (50) = 3.13; $p < 0.01$] (Table 3). There was no significant difference between the CV of STN neurons recorded from 12-month-old YAC128 mice (0.80 ± 0.05) in comparison to age-matched WT mice (0.68 ± 0.04) [U (50) = 265.0; $p = 0.09$] (Table 3). Furthermore, the firing rate of STN neurons was significantly reduced in 12-month-old YAC128 mice (8.27 ± 0.79 Hz) compared to 2-month-old YAC128 mice (14.95 ± 1.95 Hz) [H = 8.08, d.f.= 2, $p < 0.01$] (Table 3). In addition, the CV of STN neurons recorded in 8-month-old YAC128 mice (0.69 ± 0.04) was significantly smaller than that of STN neurons recorded from 2-month-old YAC128 mice (0.96 ± 0.08) [F (2, 90) = 0.11; $p < 0.01$] (Table 3).

Table 2. Firing properties of STN neurons during desynchronized ECoG epochs.

	Genotype	2 Month	8 Month	12 Month
Number of cells	WT	29	25	25
	YAC128	26	38	27
Firing rate (Hz)	WT	12.47 ± 0.93	13.65 ± 1.15	12.67 ± 1.19
	YAC128	14.95 ± 1.95	10.28 ± 0.73 **	8.27 ± 0.79 ** #
CV	WT	0.74 ± 0.04	0.63 ± 0.04	0.68 ± 0.04
	YAC128	0.96 ± 0.08 **	0.69 ± 0.04 ##	0.80 ± 0.05

Table 3: All data are mean ± SEM. ** indicates significantly different from WT, $p < 0.01$; # indicates significantly different from YAC128 LFO, $p < 0.05$; ## indicates significantly different from YAC128 LFO, $p < 0.01$.

Spectral composition of ECoG in the desynchronized state. At 2 months of age, there was no significant difference in the total power of the ECoG within the lowest frequency bandwidth (0.5-4 Hz) between genotypes [t (53) = 0.39; p = 0.35] (Figure 7A). However, at 2 months of age, there was a significant genotype x bandwidth interaction for the total power of the ECoG within higher frequencies (4-100 Hz) [F (3, 53) = 2.83; p < 0.05]. Planned comparisons indicated that the power within 7-13 Hz was higher during recording epochs in STN neurons in YAC128 mice in comparison to those collected from STN neurons in WT mice (Fig. 7A). At 8 months of age, there was no significant difference in the total power of the ECoG within the lowest frequency bandwidth (0.5-4 Hz) [t (61) = 0.48; p = 0.32] or in the total power of the ECoG within higher frequencies (4-100 Hz) [F (1, 61) = 0.20; p = 0.66] during recording epochs of STN neurons as a function of genotype (Fig. 7B). At 12 months of age, there was no significant difference between genotypes in the total power of the ECoG within the lowest frequency bandwidth (0.5-4 Hz) [t (50) = 0.26; p = 0.40] (Fig. 7C). However, at 12 months of age, there was a significant genotype x bandwidth interaction for the total power of the ECoG

within higher frequencies (4-100 Hz) [F (3, 50) = 15.87; $p < 0.01$]. Planned comparisons indicated that the power within 4-7 Hz was diminished during recording epochs in STN neurons of 12-month-old YAC128 mice relative to those collected from STN neurons in age-matched WT mice (Fig. 7C).

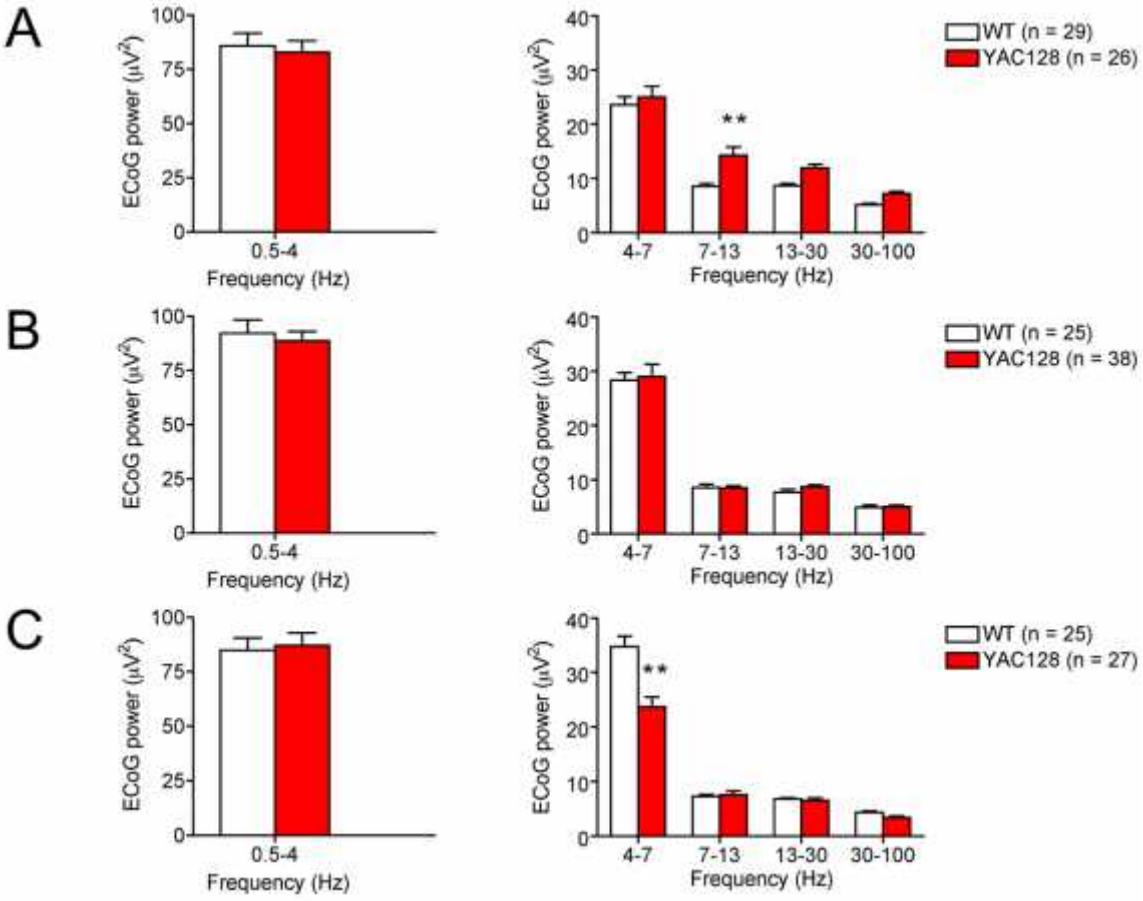

Figure 7: ECoG spectral power acquired in desynchronized epochs concomitant to the recording of WT and YAC128 as a function of age. (*A*) Total power spectral density of ECoG within (*left*) low frequency components and (*right*) higher frequency components in 2-month-old WT and YAC128 mice. (*B*) Total power spectral density of ECoG within (*left*) low frequency components and (*right*) higher frequency components in 8-month-old WT and YAC128 mice. (*C*) Total power spectral density of ECoG within (*left*) low frequency components and (*right*) higher frequency components in 12-month-old WT and YAC128 mice. All data are mean ± SEM. ** indicates significantly different from WT, $p < 0.01$.

3.5 DISCUSSION

The present study was undertaken to investigate the relationship between neuronal activity in the cortex and STN as a function of disease progression in the YAC128 transgenic mouse model of HD. Our results demonstrate dynamic age-dependent alterations in STN discharge patterns in YAC128 mice with progressive reductions in cortical entrainment and cortically evoked responses. Such patterns of activity in the STN are mediated through the hyperdirect pathway and implicate corticosubthalamic synaptic disconnection in symptomatic YAC128 mice.

Under urethane anesthesia cortical activity alternates between two primary patterns, synchronized and desynchronized states, which have differential effects on shaping the neuronal activity in the STN (Magill et al., 2000, 2001; Mallet et al., 2008). During synchronized conditions, cortical ECoG is dominated by large amplitude oscillations in the low-frequency (~1 Hz) range (Steriade, 2001). This pattern of high voltage LFO activity in the ECoG reflects synchronous fluctuations of cortical pyramidal neurons between depolarized up states and hyperpolarized down states (Steriade et al., 1993). Such rhythmic cortical activity exerts a powerful phasic excitatory drive that can entrain activity patterns in the STN and results in phase-locked LFO discharge of STN units to cortical up states (Magill et al., 2000, 2001; Bevan et al., 2002). Hence, the urethane-anesthetized animal enables control over ECoG organization and serves as an effective model for assessing the functional connectivity between the cortex and the STN (Magill et al., 2000, 2001; Mallet et al., 2008). In contrast to epochs of cortical synchronization, desynchronization is characterized by a persistently depolarized state

and the ECoG is dominated less by of high voltage LFO activity (Steriade, 2001). As a result, the powerful synchronizing drive of the cortex on the STN is diminished. During desynchronized ECoG conditions, STN neurons discharge with more tonic regularity and this autonomous activity is largely a result of intrinsic mechanisms, such as persistent sodium currents (Bevan and Wilson, 1999).

YAC128 mice exhibit progressive phenotypic abnormalities and similar to previous longitudinal studies, we observed significant impairments on the rotarod task and reduced locomotor activity as a function of age (Slow et al., 2003; Van Raamsdonk et al., 2005). In 2-month-old YAC128 mice, prior to the emergence of overt motor phenotype dysfunction, STN neurons displayed patterns of hyperexcitability. During synchronized ECoG conditions, while approximately all STN neurons (~97%) recorded from 2-month-old YAC128 mice discharged with significant LFO activity, their spike trains exhibited excessive burst firing compared to WT mice as characterized by larger CV values, a higher percentage of spikes per burst and longer burst durations. Similarly, during desynchronized ECoG conditions, the mean CV of STN discharge was significantly larger in 2-month-old YAC128 mice compared to WT mice. The firing rates of STN neurons in 2-month-old YAC128 mice were also slightly elevated in comparison to WT mice during both synchronized and desynchronized ECoG conditions, although neither was significant. Previous groups have demonstrated increased glutamate transmission at corticostriatal terminals in presymptomatic YAC128 mice (Joshi et al., 2009; Andre et al., 2011a) and similar early alterations at corticosubthalamic terminals could promote neuronal hyperexcitability in the STN. Interestingly, neuronal activity in the STN in a transgenic rat model of HD is increased at ~12 month of age

(Vlamings et al., 2012) suggesting that these models may share similar pathophysiological characteristics, albeit at contrasting ages.

Early hyperexcitability in cortical networks has been reported in multiple transgenic mouse models of HD (Cepeda et al., 2003; Walker et al., 2008; Cummings et al., 2009). In 2-month-old YAC128 mice, during synchronized ECoG conditions, the density of power concentrated in low frequencies was increased. Optical stimulation experiments have suggested that the locus of the LFO genesis originates from the synchronization of excitatory pyramidal neurons in deep cortical layers (mainly layer V) (Hughes and Crunelli, 2013; Kuki et al., 2013) and increased cortical excitation could lead to excessive synchrony and increased glutamate transmission. In addition, during both synchronized and desynchronized ECoG conditions, the spectral power specifically within the 7-13 Hz bandwidth was increased in 2-month-old YAC128 mice. Oscillations in the ECoG within the 7-13 Hz frequency range can be driven by rhythmic excitatory input from the thalamus (Steriade and Llinas, 1988; McCormick and Bal, 1997). These oscillations are present during cortical up states and STN burst firing is strengthened by such oscillatory activity (Magill et al., 2000). While less is known about thalamic contributions to HD pathogenesis, regional elevations in metabolic activity in the thalamus are evident in presymptomatic HD patients (Feigin et al., 2006). Greater synchrony within thalamocortical circuits could lead to increased excitatory drive within basal ganglia targets and such activity will need to be further investigated in future studies.

In the present study, motor impairments emerged in YAC128 mice at 8 months and worsened as a function of age. In 8-month-old YAC128 mice, during synchronized

ECoG conditions, ~13% of STN neurons failed to discharge with LFO activity. In 12-month-old YAC128 mice, the proportion of STN neurons recorded during synchronized ECoG conditions that did not exhibit LFO activity in their spike trains increased to ~22%. In contrast, approximately all STN neurons recorded from WT mice discharged with significant LFO activity during synchronized ECoG conditions and this pattern was stable across ages. Thus, cortically entrained STN neuronal discharge is dynamically disrupted over time in YAC128 mice. We have previously reported analogous deficits in R6/2 mice in which ~20% of STN neurons failed to fire with expected LFO discharge during synchronized ECoG conditions (Callahan and Abercrombie, 2013, *submitted*). Collectively, these results indicate that the flow of information between the cortex and STN is disrupted as a function of the mutant Huntingtin protein.

In 8-month-old and 12-month-old YAC128 mice, during synchronized states, there were no significant differences in the spectral power within low frequencies or the 7-13 Hz band compared to age-matched WT mice. This is in agreement with previous reports indicating that cortical hyperexcitability is only present during early stages of the disease (Joshi et al., 2009; Andre et al., 2011a). As such LFO activity in the ECoG seems to be expressed normally in symptomatic YAC128 mice and presumably drives the normal patterns of neuronal discharge that we observed in LFO STN neurons. Moreover, this indicates that spectral changes in cortical networks cannot account for the progressive loss of STN entrainment in symptomatic YAC128 mice. The density of power concentrated within the 4-7 Hz band was reduced during both synchronized and desynchronized epochs in 8-month-old and 12-month-old YAC128 mice. While less is known about the relationship between these oscillations and STN activity, we cannot rule

out the possibility that reductions in power within the 4-7 Hz range could contribute to the reported alterations in STN neuronal firing.

During synchronized ECoG conditions, cortical entrainment of LFO activity in STN neurons is mediated through monosynaptic glutamatergic afferents in the hyperdirect pathway (Magill et al., 2001; Kita and Kita, 2012). These projections are thought to arise from long range pyramidal tract neurons (PT) in layer V of the cortex (Kita and Kita, 2012). Disconnection of corticostriatal synapses has been reported in HD (Cepeda et al., 2007) and our results indicate the presence of similar interruptions in the hyperdirect pathway. In order to directly assess the integrity of the hyperdirect pathway in YAC128 mice we examined the effects of focal cortical stimulation on STN discharge. Stimulation of the ipsilateral frontal cortex leads to multiphasic activity patterns in STN neurons distinguished by an initial short latency excitatory response that is generated by excitation of monosynaptic terminals in the hyperdirect pathway (Kitai and Deniau, 1981; Fujimoto and Kita, 1993; Nambu et al., 2000; Magill et al., 2004). While the proportion of STN neurons that responded to cortical stimulation with short latency excitatory responses was relatively stable across ages in WT mice, there was a striking reduction in the ratio of responsive STN neurons in YAC128 mice as a function of age. Additionally, the latency of cortically evoked responses in STN units was increased in 8-month-old YAC128 mice and the duration of responses was decreased in 12-month-old YAC128 mice. Cortical degeneration and reductions in glutamate release have been reported in symptomatic humans and animal models of HD and could contribute to the failure in hyperdirect pathway activation (Macdonald and Halliday, 2002; Joshi et al., 2009). To

our knowledge this is the first report to demonstrate the progressive disconnection of the hyperdirect pathway in an experimental model of HD.

Interestingly, we observed no significant changes in the firing rate of STN neurons during synchronized conditions and it seems that the impact of hyperdirect circuit dysfunction may contribute more to the spatiotemporal coding of STN neuronal activity than absolute spike rate in YAC128 mice. In contrast, during desynchronized ECoG conditions, the firing rates of STN neurons recorded from YAC128 mice diminished progressively as a function of age. We found a similar reduction in the firing rate of STN neurons during desynchronized ECoG conditions in R6/2 mice (Callahan and Abercrombie, 2013, *submitted*). As striatal degeneration is a cardinal pathology in HD, disinhibition of neurons in the globus pallidus (GPe) could exert an augmented GABAergic tone in the STN in HD. In addition, alterations in the intrinsic membrane properties of STN neurons could lead to reduced spiking. Future studies will need to investigate the mechanisms that drive the progressive firing rate changes of STN neurons in transgenic mouse models of HD.

These results have valuable clinical implications for HD. The STN plays an important role in the synaptic integration of functionally diverse cortical information and is the fastest channel in which the cortex can modulate basal ganglia output (Bosch et al., 2012). In particular, hyperdirect pathway activation is thought to act a stop signal and mediate action suppression (Frank, 2006). Remote STN lesions (~4-20% total volume) result in hyperkinetic movement disorders that mimic the chorea seen in HD (Whittier and Mettler, 1949; Hamada and DeLong, 1992). Our results suggest progressive

disconnection in the hyperdirect pathway which could lead to impairments in the output capabilities of the basal ganglia and disordered motor control in HD.

3.6 ACKNOWLEDGEMENTS

This research was supported by NIH grant NS059921 (EDA) and Rutgers, the State University of New Jersey. The authors wish to thank Anna Chavez and Nupur Jain for technical assistance. We thank Dr. Michael Hayden for the contribution of mice. We thank Dr. Andrew Farrar, Dr. James Tepper and Dr. Peter Magill for their helpful discussions. We declare no competing financial interests.

CHAPTER 4: IN VIVO DOPAMINE EFFLUX IS DECREASED IN STRIATUM OF BOTH FRAGMENT (R6/2) AND FULL-LENGTH (YAC128) TRANSGENIC MOUSE MODELS OF HUNTINGTON'S DISEASE

Authors: Joshua W. Callahan and Elizabeth D. Abercrombie

Journal: Frontiers in Systems Neuroscience (Published)

4.1 ABSTRACT

Huntington's disease (HD) is characterized by alterations within the corticostriatal circuitry. The striatum is innervated by a dense array of dopaminergic (DA) terminals and these DA synapses are critical to the proper execution of motor functions. As motor disturbances are prevalent in HD we examined DA neurotransmission in the striatum in transgenic (tg) murine models of HD. We used in vivo microdialysis to compare extracellular concentrations of striatal DA in both a fragment (R6/2) model, which displays a rapid and severe phenotype, and a full-length (YAC128) model that expresses a more progressive phenotype. Extracellular striatal DA concentrations were significantly reduced in R6/2 mice and decreased concomitantly with age-dependent increasing motor impairments on the rotarod task (7, 9, and 11 weeks). In a sample of 11-week-old R6/2 mice, we also measured tissue concentrations of striatal DA and found that total levels of DA were significantly depleted. However, the loss of total DA content (<50%) was insufficient to account for the full extent of DA depletion in the extracellular fluid (ECF) (~75%). We also observed a significant reduction in extracellular DA concentrations in the striatum of 7-month-old YAC128 mice. In a separate set of experiments, we applied d-amphetamine (AMPH) (10 μm) locally into the striatum to stimulate the release of intracellular DA into the ECF. The AMPH-induced increase in extracellular DA levels was significantly blunted in 9-week-old R6/2 mice. There also was a decrease in AMPH-stimulated DA efflux in 7-month-old YAC128 mice in comparison to WT controls, although the effect was milder. In the same cohort of 7-month-old YAC128 mice we observed a significant reduction in the total locomotor activity in response to systemic

AMPH (2 mg/kg). Our data demonstrate that extracellular DA release is attenuated in both a fragment and full-length tg mouse model of HD and support the concept of DA involvement in aspects of the syndrome.

4.2 INTRODUCTION

Huntington's disease (HD) is a genetically inherited neurodegenerative disorder that results in motor, cognitive and psychiatric disturbances. One out of every 10,000 people is affected with the disorder and an even greater proportion remains at risk. HD is caused by a polyglutamine (CAG) trinucleotide repeat expansion in the IT-15 (*HTT*) gene, located on the short arm of chromosome 4 (The Huntington's Disease Collaborative Research Group, 1993). The mutation is autosomal dominant and onset occurs between 30-50 years of age, although in a rare juvenile variant of the disease, symptoms can emerge as early as 5 years old. The severity of symptoms progressively worsens as a function of age and the illness is ultimately fatal (Walker, 2007). No cure exists for HD, however, therapeutics that target the dopamine system have shown promise for managing the motor syndromes that are involved with the disorder (Bonelli and Wenning, 2006; Bonelli and Hofmann, 2007)

Since the discovery of the mutation in the *HTT* gene, several transgenic mouse models expressing the CAG repeat expansion have been developed which recapitulate characteristics of the disorder, including reductions in total brain volume, mutant huntingtin (mHtt) protein aggregation, transcriptional dysregulation and neurotransmitter receptor alterations (Davies et al., 1997; Cha et al., 1998; Luthi-Carter et al., 2000; Stack

et al., 2005). Critically, these pathological changes are accompanied by progressive motor and cognitive deficits (Menalled and Chesselet, 2002; Levine et al., 2004) that closely mimic the human condition. Transgenic mouse models of HD can be sorted into two broad categories depending on whether they possess a fragment (e.g. exon 1) of the *HTT* gene or the full-length composition. Mouse strains from fragment models express only a truncated mHtt protein fraction and *in vitro* studies have demonstrated that this abbreviated fragment may be more toxic than the full-length protein (Hackam et al., 1998; Lunkes and Mandel, 1998). As such, fragment models typically exhibit an accelerated phenotype in comparison to full-length models that includes motor deficits, altered gait, hypoactivity and weight loss (Carter et al., 1999). While fragment models display an HD-like phenotype, the obvious weakness is that they lack the natural genomic and protein context of the polyglutamine expansion. This raises the potential for alterations in protein dynamics and therefore necessitates the use of full-length models to investigate any resulting changes in disease features.

R6 transgenic mice are the most widely used strain derived from the fragment models and were the first established transgenic line in HD research. The most extensively characterized variant of this transgenic strain is the R6/2 line, which express the first of 67 exons and carry a ~160 CAG repeat expansion (Mangiarini et al., 1996). These mice develop an aggressive HD-like phenotype that advances rapidly until the occurrence of spontaneous morbidity by 14-16 weeks of age (Carter et al., 1999). In contrast to the R6 models, the YAC128 transgenic mouse model incorporates the entire HD gene, using a yeast artificial chromosome (YAC) vector system to express the full-length human *HTT* gene with a 128 CAG repeat expansion (Slow et al., 2003). The

lifespan, as well as the progression of the HD-like phenotype in YAC128 mice is more prolonged than in R6/2 mice, with neuropathological and behavioral abnormalities manifesting at later ages (Slow et al., 2003; Van Raamsdonk et al., 2007).

Evidence implicates abnormal nigrostriatal dopaminergic neurotransmission in HD. In both human cases and animal models, early reductions in the striatal expression of dopamine receptors, attenuated receptor binding, and loss of the dopamine- and cAMP-regulated phosphoprotein (DARPP-32) have been reported (Joyce et al., 1988; Sedvall et al., 1994; Cha et al., 1998; Bibb et al., 2000; Miller and Bezprozvanny, 2010). Reduced dopamine concentrations in striatal tissue and the degeneration of nigrostriatal terminals emerge in late stages of the disorder in both human cases and transgenic models of HD (Kish et al., 1987; Reynolds et al., 1999; Suzuki et al., 2001; Petersen et al., 2002). Additionally, studies utilizing striatal slice preparations have demonstrated that electrically evoked dopamine efflux is reduced in both R6/1 and R6/2 mice (Johnson et al., 2007; Ortiz et al., 2011), suggesting that dopamine release may be compromised in these models. As of yet, the synaptic release of dopamine has not been studied during awake, behaving conditions in transgenic mouse models of HD.

The goal of the present study was to examine, and compare where possible, nigrostriatal dopamine release dynamics in the fragment R6/2 and the full-length YAC128 mouse models of HD, using *in vivo* microdialysis. Both R6/2 and YAC128 mice develop deficits on the rotarod treadmill task and we measured the levels of striatal dopamine during these periods of motor dysfunction. As analogous neurophysiological abnormalities have been shown to exist across fragment and full-length transgenic models (Cummings et al., 2010), we speculated that neurochemical abnormalities may

also be a common feature of such models. Specifically, we hypothesized that extracellular striatal dopamine release would be attenuated in R6/2 and YAC128 mice in awake, behaving conditions concomitant with motor decline and as a function of age. *In vitro* studies have indicated that the intracellular storage of dopamine in nerve terminals may be compromised in HD as well and such a deficiency could contribute to deficits in extracellular dopamine release (Ortiz et al., 2011). In a separate set of experiments, we therefore measured the effects of amphetamine, a dopamine-releasing agent, on local striatal neurochemistry and on locomotor activity in order to investigate the integrity of intracellular dopamine stores in R6/2 and YAC128 mice.

4.3 EXPERIMENTAL PROCEDURES

Animals. Transgenic male mice expressing a truncated human *HTT* gene with a 160 ± 10 CAG repeat expansion (R6/2) or a full-length human *HTT* gene with a 128 CAG repeat expansion (YAC128) in exon 1 and their respective wild-type controls were obtained from Jackson Laboratories (Bar Harbor, ME). Animals were housed individually in plastic microisolator cages with food and water available *ad libitum*. Animals were kept under conditions of constant temperature (21°C) and humidity (40%) and maintained on a 12 hour light/dark cycle (lights on from 7:00 am - 7:00 pm). All efforts were made to minimize animal suffering and to limit the number of animals utilized for these experiments. Animal procedures were conducted in accordance with the National Institutes of Health *Guide for the Care and Use of Laboratory Animals* and were approved by Rutgers University Institutional Animal Care and Use Committee.

Motor Phenotype. Motor coordination was assessed using an Economex rotarod apparatus (Columbus Instruments, Columbus, OH). R6/2 mice and wild-type controls were trained on the rotarod treadmill task at 10 rpm for three consecutive trials (60 second maximum duration) one day prior to testing. The following day, mice were tested at five fixed speeds (5, 10, 15, 20, 25 rpm) for two separate trials. Fall latency (s) at each speed was averaged across trials and used for statistical comparison. Testing was carried out at 7, 9 and 11 weeks in separate groups of R6/2 mice and 7 months in YAC128 mice and their respective wild-type controls.

Microdialysis Procedure. Microdialysis probes were of a vertical, concentric design, similar to that previously described in our laboratory (Cobb and Abercrombie, 2002). Probes were constructed such that the probe inlet consisted of a piece of PE-10 tubing (Clay Adams, Parsippany, NJ, USA) and a piece of fused silica capillary tubing (I.D. 75 μm and O.D. 150 μm; Polymicro Technologies, Phoenix, AZ, USA) served as the outlet. A semi-permeable microdialysis membrane (molecular weight cut-off = 13 kD; o.d. = 216 μm; Spectrum Laboratories, Rancho Dominguez, CA, USA) was placed over the end of the exposed silica tubing, glued to the PE-10 tubing and coated with a thin epoxy layer, leaving a 2 mm long active exchange area at the end of the probe. Probes were continuously perfused with artificial cerebrospinal fluid (aCSF; NaCl 147mM, KCl 2.5 mM, $CaCl_2$ 1.3 mM, $MgCl_2$ 0.9 mM, pH 7.4) using a microliter infusion pump (Harvard Apparatus, Holliston, MA, USA) at a flow rate of 1.5 μl/min. Prior to implantation, probes were calibrated *in vitro* to determine their relative recovery rates. Only probes with recovery rates between 10 and 15 % were used.

R6/2 mice and their wild-type controls were anesthetized with 40-50 mg/kg pentobarbital and 250 mg/kg chloral hydrate (i.p.). YAC128 mice and their wild-type controls were anesthetized with 80-100 mg/kg ketamine and 10 mg/kg xylazine (i.p.). The mice were placed into a stereotaxic frame (David Kopf Instruments, Tujunga, CA) and onto a heating pad to prevent hypothermia. With the skull flat, the microdialysis probe was implanted into the striatum at the following coordinates: AP: +0.5 mm, ML: ± 1.95 mm relative to bregma and DV: -4.0 mm from dura (Paxinos and Franklin, 2001). Probes were anchored to the skull by two small screws (Small Parts, Miami Lakes, FL) and dental cement. The probe inlet and outlet lines were then fed through a metal tether that attached to the head-post at one end, and to a single-channel fluid swivel (Instech Laboratories, Plymouth Meeting, PA) at the other end. The mice were allowed to recover for at least 18 hours before experiments began. Post-operative care consisted of administering lactated Ringer's solution (1.0-2.0 ml/30g body weight, s.c.) and placing the animal under a heat lamp for 1-3 hours after surgery. All microdialysis experiments were conducted during the light portion of the diurnal cycle.

Dopamine Quantification. Microdialysis experiments were conducted in round plastic test chambers (14 cm x 20 cm) equipped with a counter-balanced arm and a swivel assembly (Instech, Plymouth Meeting, PA). The HPLC-EC system consisted of an injector (Rheodyne, Cotati, CA), a VeloSep RP-18 column (100 x 3.2 mm; PerkinElmer, Waltham, MA) and a Shimadzu LC-10AD VP solvent delivery pump (Shimadzu Scientific Instruments, Inc., Columbia, MD), that delivered the mobile phase at a flow rate of 0.7 ml/min. The mobile phase was composed of 0.1 M sodium acetate buffer (pH

4.2), 0.1 mM EDTA, 1.2mM sodium octyl sulfate and 8% (v/v) methanol. An electrochemical detector (Coulochem II; ESA Inc., Chelmsford, MA) with a flow cell electrode set at an applied potential of +260mV was used. The detector output was connected to a computerized data acquisition system (PowerChrom, Denistone East, NSW). Dopamine and 3,4-dihydroxyphenylacetic acid (DOPAC) were identified by retention time and quantified based on peak height relative to the peak height of a 10 nM standard prepared in 0.1 M perchloric acid that was made up fresh daily.

A separate cohort of 11-week-old R6/2 mice and their wild-type controls were sacrificed by decapitation and the striata were rapidly dissected on ice, wrapped in aluminum foil, labeled and frozen at -80°C until analysis. The weight of each striatum was measured and then tissue was homogenized in 0.1 M perchloric acid containing 100 µM EDTA (20 µl/mg wet tissue weight). Homogenates were centrifuged at 29,200 g for 25 minutes at 2-8°C. The amount of dopamine in 20 µl samples of the resulting supernatant was quantified by HPLC-EC using the protocol described above for the analysis of dopamine in dialysate samples.

Experimental Procedures. Prior to pharmacological manipulations, baseline dialysate samples were assayed for dopamine until three consecutive samples differed by less than 15%. In experiments involving the local application of d-amphetamine into the striatum via reverse microdialysis, a glass syringe containing a 10 µM solution of amphetamine dissolved in aCSF was connected to the inlet of the probe following the initial baseline determination. Collection of dialysate samples resumed 15 minutes later to allow for the fluid to flow through the probe and equilibrate to the drug solution. Samples were

collected every 10 minutes for a 60 minute duration. The effect of local amphetamine on extracellular dopamine was investigated in 9-week-old R6/2 mice, 7-month-old YAC128 mice and their respective wild-type controls. All experiments involving the local application of amphetamine were conducted 48 hours after probe implantation.

In experiments involving systemic administration of d-amphetamine (2 mg/kg, i.p.), the drug was dissolved in sterile 0.9% saline vehicle. The effect of systemic amphetamine on locomotor activity was investigated in 7-month-old YAC128 mice and their wild-type controls. Prior to testing, mice were untethered and the polyethylene tubing emanating from the probes was clipped so that only the acrylic head cap remained. Mice were allowed to habituate in their home cages with this new arrangement for at least one week preceding amphetamine treatment. Based on qualitative observations, animals showed no signs of impairment due to either the surgery or the presence of head caps. One day prior to amphetamine administration, mice were habituated to plastic open field chambers (51 cm x 32 cm x 20 cm) overnight. Following habituation, mice were administered drug and spontaneous locomotor activity was monitored for 60 minutes via automated activity chambers equipped with infrared photobeams (Flexfield, San Diego Instruments, Inc., San Diego, CA).

Data Analysis. Data are presented as mean ± S.E.M. Dialysate values represent picograms per 20 µl microdialysis sample. Factorial ANOVA was used to assess main effect in each data set examined. Data then were subdivided according to the interactions found in the global test and separate lower order analyses carried out. Where appropriate,

the Bonferroni post-hoc test was used for multiple comparisons. Differences were considered statistically significant when $p < 0.05$.

Histology. Upon completion of each experiment, animals were administered a lethal dose of sodium pentobarbital and were perfused intracardially with 0.9% saline followed by 10% formaldehyde. Brains were extracted and post-fixed in fresh fixative overnight at 4°C and transferred to 30% sucrose in phosphate buffer solution overnight at 4°C for cryoprotection. Coronal sections of 50 μm thickness were obtained from striata and stained with Cresyl Violet to verify probe placement in the striatum. A representative histological section showing a microdialysis probe track in the mouse striatum is shown in Figure 1.

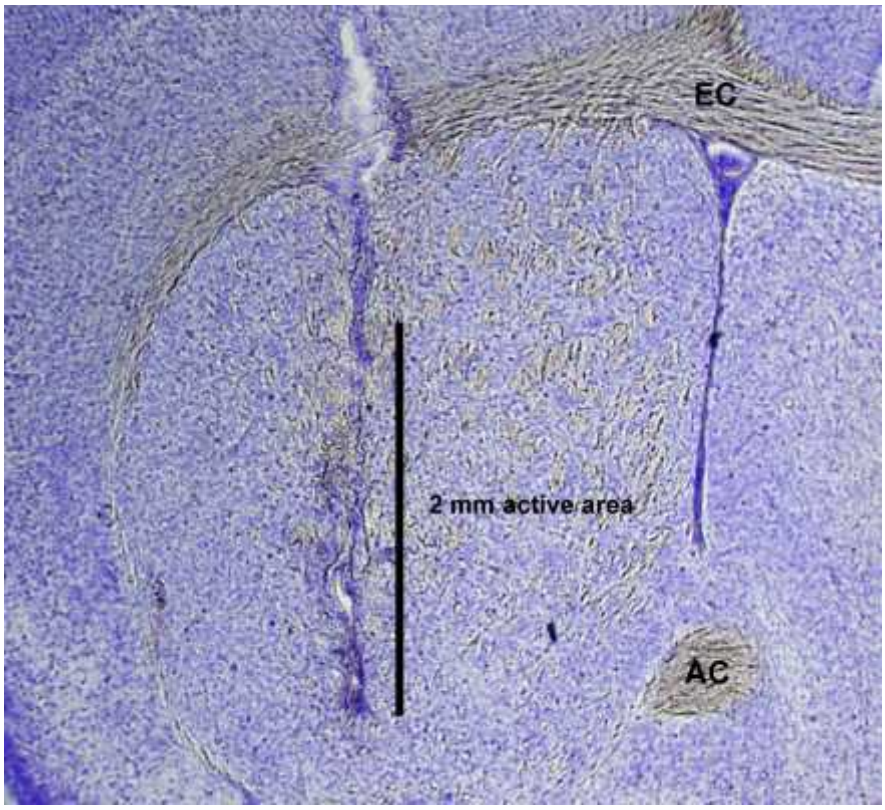

Figure 1: Photomicrograph of Nissl-stained histological section demonstrating representative microdialysis probe placement with a 2 mm active area in mouse striatum. (AC = Anterior commissure; EC = External capsule).

Materials. Ketamine was purchased from Phoenix Pharmaceutical Inc. (St. Joseph, MO). Xylazine, chloral hydrate, sodium pentobarbital and d-amphetamine were purchased from Sigma (St. Louis, MO). All other reagents and chemicals were of the highest purity commercially available (Fisher Scientific, Suwanee, GA).

4.4 RESULTS

Rotarod assessment in R6/2 and YAC128 mice.

Performance on a fixed speed rotarod paradigm was assessed in R6/2, YAC128 mice and their respective wild-type controls (Fig. 2A). Mice were placed on an elevated,

rotating platform for a maximum of 60 seconds and the latency that it took for each to fall off was measured at 5, 10, 15, 20 and 25 rpm. The latency to stay on the rotating platform was significantly reduced as a function of genotype in 7-week-old [F (1, 172) = 18.78; $p < 0.0001$), 9-week-old [F (1, 104) = 50.84; $p < 0.0001$] and 11-week-old [F (1, 72) = 98.22; $p < 0.0001$] R6/2 mice compared to wild-type controls. Post-hoc tests revealed that R6/2 mice fell off the rotarod at significantly shorter latencies than wild-type controls at every speed across all ages tested. One-way ANOVA tests showed that the latency to remain on the rotating platform significantly decreased as a function of age in R6/2 mice [F (2, 39) = 8.074; $p < 0.01$] but not in wild-type controls [F (2, 48) = 2.013; n.s.]. The latency to stay on the rotating platform also was significantly diminished as a function of genotype in 7-month-old YAC128 mice compared to age-matched wild-type controls [F (1, 56) = 11.88; $p < 0.01$] (Fig. 2B). Post-hoc tests indicated that 7-month-old YAC128 mice fell at significantly shorter latencies than wild-type controls at every speed faster than 5 rpm. Data are only presented in graphical form for 10 and 20 rpm as these speeds are most representative of overall performance in both genotypes.

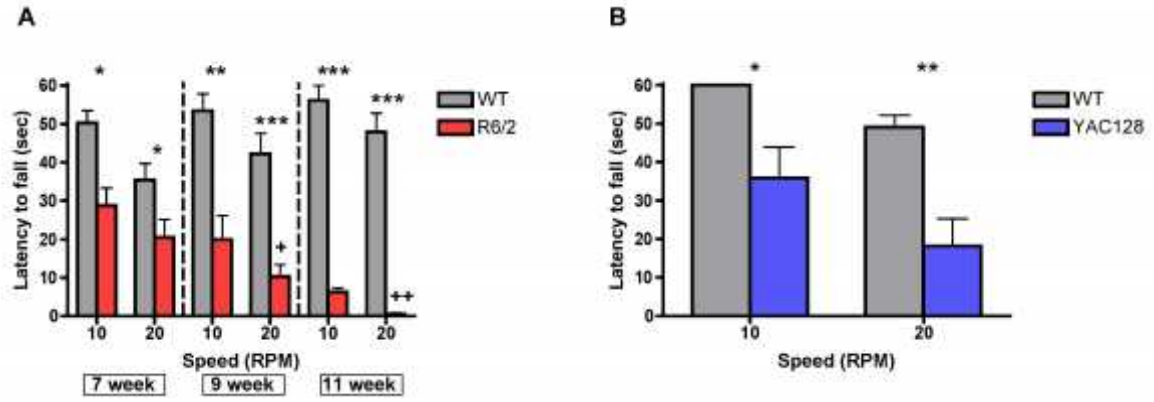

Figure 2: Rotarod performance in (A) R6/2 transgenic mice (7 weeks, n = 22 WT, 23 R6/2; 9 weeks, n = 15 WT, 13 R6/2; 11 weeks, n = 14 WT, 6 R6/2) and (B) 7-month-old YAC128 transgenic mice (n = 7 WT, 9 YAC128). All data are mean ± SEM. * indicates significantly different from WT, $p < 0.05$; ** indicates $p < 0.01$; *** indicates $p < 0.005$; +, ++ R6/2 week 7 vs. weeks 9 and 11 ($p < 0.05$, 0.01, respectively).

Extracellular striatal dopamine and DOPAC concentrations.

R6/2 mice. Extracellular striatal dopamine was significantly attenuated as a function of genotype [F (1, 34) = 46.96; $p < 0.0001$] (Fig.3A). Post-hoc tests revealed that there was a significant reduction in extracellular dopamine in R6/2 mice and levels were diminished at 7 weeks (WT: 8.4 ± 0.9 pg/20 µl; R6/2: 5.6 ± 0.6 pg/20 µl), 9 weeks (WT: 8.1 ± 1.4 pg/20 µl; R6/2: 3.3 ± 0.7 pg/20 µl) and 11 weeks of age (WT: 11.4 ± 1.2 pg/20 µl; R6/2: 2.7 ± 0.5 pg/20 µl). One-way ANOVA indicated that extracellular levels of striatal dopamine significantly decreased in R6/2 mice as a function of age [F (2, 17) = 6.812; $p < 0.01$]. Specifically, post-hoc tests demonstrated that extracellular dopamine was significantly reduced in 9- and 11-week old R6/2 mice in comparison to 7-week-old R6/2 mice. There was no change in striatal extracellular dopamine concentrations as a function of age in wild-type controls [F (2, 17) = 2.303; n.s.]. Extracellular striatal DOPAC was significantly attenuated as a function of genotype [F (1, 34) = 50.96; $p < 0.0001$] (Fig. 3B). Post hoc tests indicated that although extracellular concentrations of

striatal DOPAC were not significantly different at 7 weeks (WT: 1569 ± 137 pg/20 µl; R6/2: 1191 ± 114 pg/20 µl) they were significantly reduced by 9 weeks (WT: 1589 ± 127 pg/20 µl; R6/2: 647 ± 122 pg/20 µl) and 11 weeks of age (WT: 1544 ± 191 pg/20 µl; R6/2: 503 ± 453 pg/20 µl) in R6/2 mice in comparison to wild-type controls. A one-way ANOVA revealed that extracellular DOPAC significantly decreased in R6/2 mice as a function of age [F (2, 17) = 15.32; $p < 0.001$]. There was no change in extracellular DOPAC amounts as a function of age in wild-type controls [F (2, 17) = 0.20; n.s.].

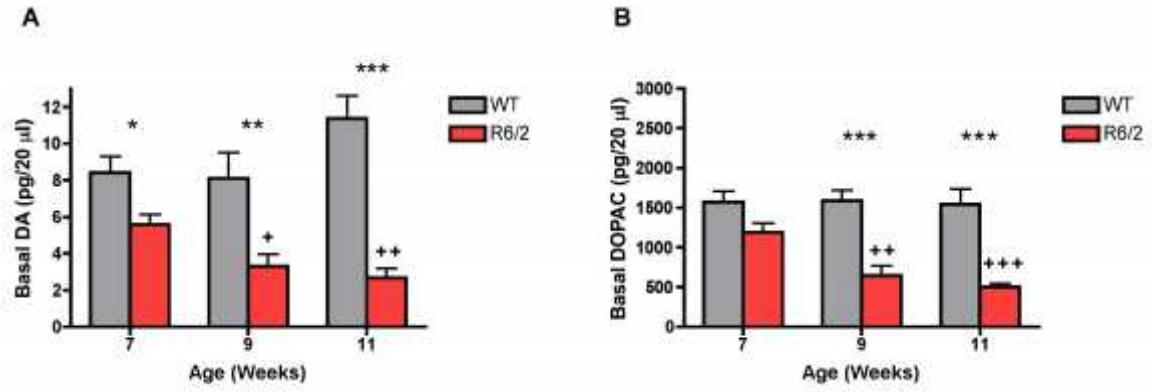

Figure 3: In vivo microdialysis measurements of basal levels of extracellular (A) dopamine and (B) DOPAC in striatum of R6/2 transgenic mice (7 weeks, n = 6 WT, 6 R6/2; 9 weeks, n = 6 WT, 6 R6/2; 11 weeks, n = 8 WT, 8 R6/2). Data are picograms per 20 µl sample. All data are mean ± SEM. * indicates significantly different from WT, $p < 0.05$; ** indicates $p < 0.01$; *** indicates $p < 0.005$; +, ++ R6/2 week 7 vs. weeks 9 and 11 ($p < 0.05$, 0.01, respectively).

In the 11-week-old cohort, striatal tissue concentrations of dopamine were measured in R6/2 mice and wild-type controls (Fig. 4A). R6/2 mice exhibited a significant abatement in striatal tissue dopamine content (5478 ± 487 pg/20 µl) in comparison to wild-type controls (10680 ± 833 pg/20 µl) [t (10) = 5.39; $p < 0.001$]. The reduction in striatal tissue content of dopamine (47%) was not as dramatic as the

reduction in striatal extracellular concentrations of dopamine (76%) in 11-week-old R6/2 mice (Fig. 4B).

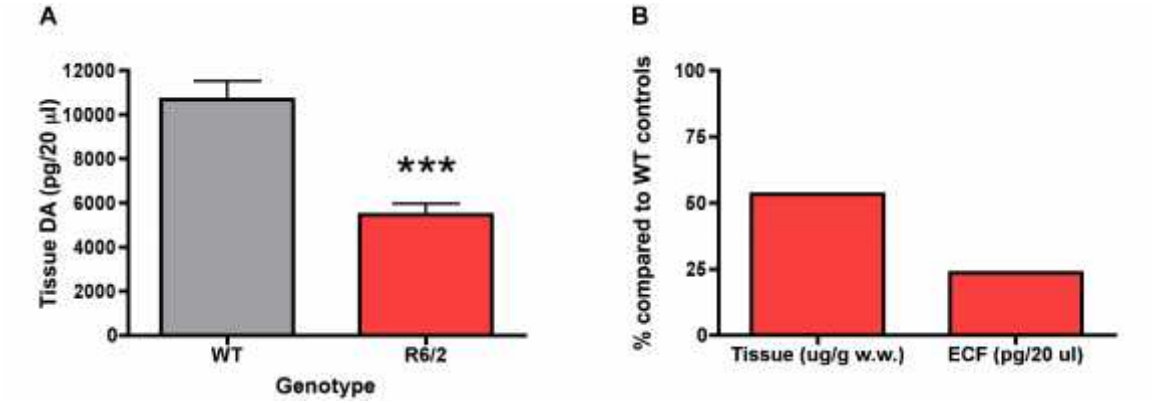

Figure 4: Dopamine content in (A) striatal tissue of 11-week-old R6/2 transgenic mice (n = 6 WT, 6 R6/2) and (B) comparison of the percentage of dopamine levels in relation to WT mice in tissue and the extracellular fluid (ECF). Striatal tissue dopamine content data are µg/g wet weight of tissue and striatal ECF dopamine data are picograms per 20 µl sample of dialysate. All data are mean ± SEM. *** indicates significantly different from WT, $P < 0.005$.

YAC128 mice. Extracellular dopamine concentrations in 7-month-old YAC128 mice were significantly reduced (5.0 ± 1.4 pg/20 µl) in comparison to wild-type controls (10.5 ± 1.9 pg/20 µl) [t (14) = 2.39; $p < 0.05$] (Fig. 5A). Although extracellular DOPAC levels were slightly lower in 7-month-old YAC128 mice (1834 ± 245 pg/20 µl), there was no significant difference between wild-type controls (2358 ± 299 pg/20 µl) [t (14) = 1.37; n.s.] (Fig. 5B).

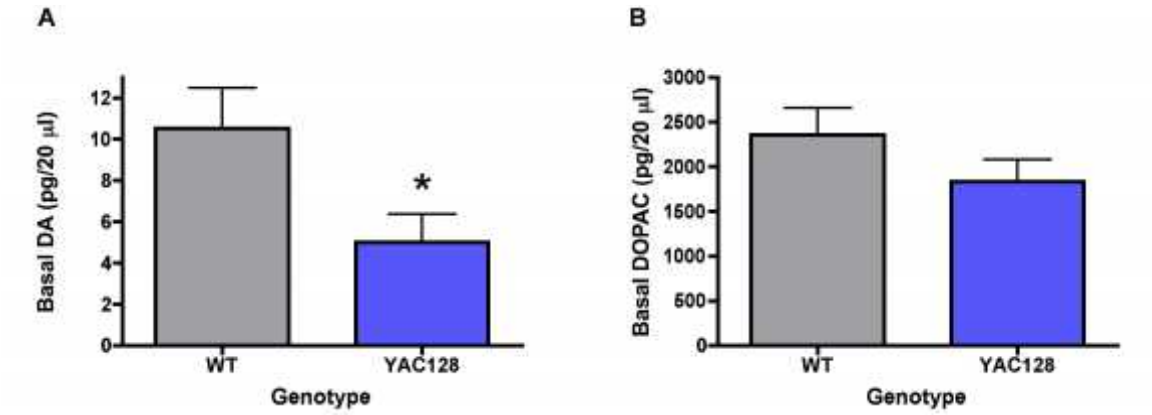

Figure 5: In vivo microdialysis measurements of basal levels of extracellular (A) dopamine and (B) DOPAC in striatum of 7-month-old YAC128 mice (n = 7 WT, 9 YAC128). Data are picograms per 20 µl sample. All data are mean ± SEM. * indicates significantly different from WT, $p < 0.05$.

Effect of local striatal amphetamine (10uM) application on extracellular dopamine concentrations.

R6/2 mice. Local amphetamine induced a significant increase in extracellular dopamine levels across time [F (6, 24) = 75.42; $p < 0.0001$]. The amphetamine induced increase in dopamine efflux was significantly attenuated as a function of genotype [F (1,24) = 42.25; $p < 0.01$] (Fig. 6A). Post hoc tests indicated that amphetamine induced dopamine release was significantly diminished in 9-week-old R6/2 mice in comparison to wild-type controls at all time intervals measured. The maximum peak response in amphetamine induced dopamine efflux was significantly diminished in 9-week-old R6/2 mice (38.9 ± 7.4 pg/20 µl) versus wild-type controls (114.4 ± 10.7 pg/20 µl) [t (4) = 5.82; $p < 0.01$] (Fig. 6B).

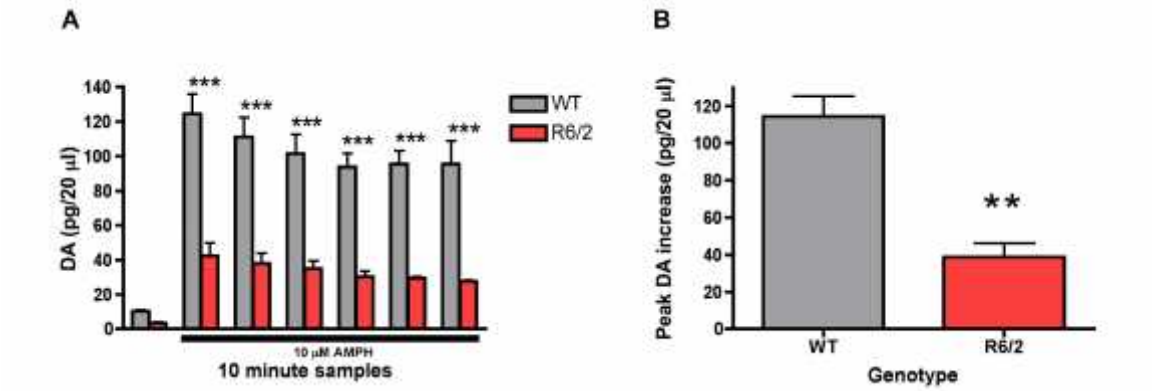

Figure 6: Effect of intrastriatal application of amphetamine (10 µM) on striatal (A) dopamine release and the (B) maximum peak increase in dopamine efflux in 9-week-old R6/2 transgenic mice (n = 3 WT, 3 R6/2). Presence of amphetamine in perfusate is indicated by black bar. Data are picograms per 20 µl sample. All data are mean ± SEM. * indicates significantly different from WT, $P < 0.05$; ** indicates $P < 0.01$; *** indicates $P < 0.005$.

YAC128 mice. Local amphetamine induced a significant increase in extracellular dopamine across time [F (6, 72) = 23.04; $p < 0.0001$] (Fig. 7A). Although amphetamine induced dopamine efflux was diminished in 7-month-old YAC128 mice in comparison to wild-type controls, there was no significant effect of genotype [F (1, 72) = 1.93, n.s.]. Similarly, while the maximum peak response in amphetamine induced dopamine release was diminished in 7-month-old YAC128 mice (31.8 ± 9.6 pg/20 µl) versus wild-type controls (50.2 ± 12.0 pg/20 µl) the effect was not significant [t (12) = 1.18; n.s.] (Fig. 7B).

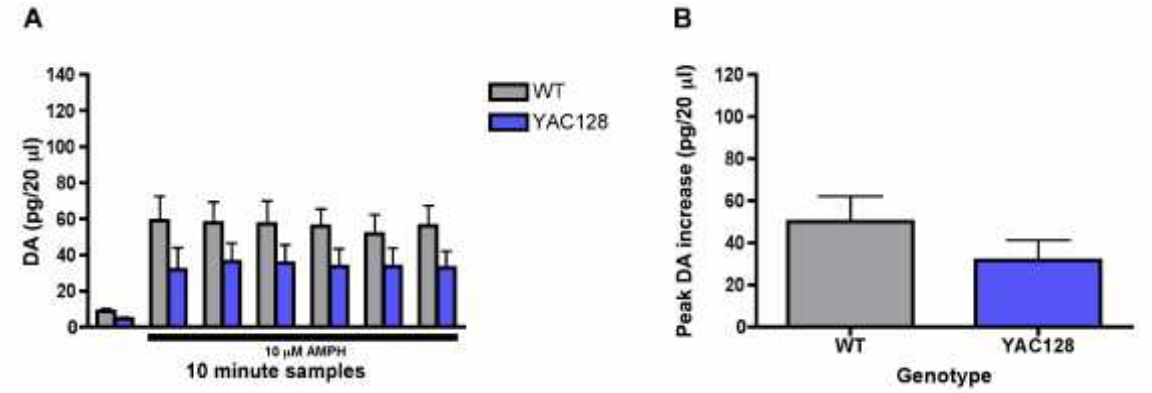

Figure 7: Effect of intrastriatal application of amphetamine (10 µM) on striatal (A) dopamine release and the (B) maximum peak increase in dopamine efflux in 7-month-old YAC128 transgenic mice (n = 5 WT, 9 YAC128). Presence of amphetamine in perfusate is indicated by black bar. Data are picograms per 20 µl sample. All data are mean ± SEM. * indicates significantly different from WT, $P < 0.05$; ** indicates $P < 0.01$; *** indicates $P < 0.005$.

In 7-month-old YAC128 mice, the effect of systemic amphetamine (2 mg/kg, i.p.) on spontaneous locomotor activity was investigated. There was no significant difference in the basal activity counts between genotypes in 7-month-old YAC128 mice and wild-type controls [t (9) = 0.39; n.s.] (Fig. 8A). Amphetamine induced a significant increase in locomotor activity across time [F (6, 54) = 0.96; $p < 0.05$]. Although amphetamine induced locomotor activity was diminished in 7-month-old YAC128 mice in comparison to wild-type controls, there was no significant effect of genotype [F (1, 54) = 3.80, n.s.]. Collapsing the locomotor counts across all time bins revealed that the total activity in response to amphetamine over 60 minutes post-drug was significantly attenuated in 7-month-old YAC128 mice versus wild-type controls [t (9) = 1.88; $p < 0.05$] (Fig. 8B).

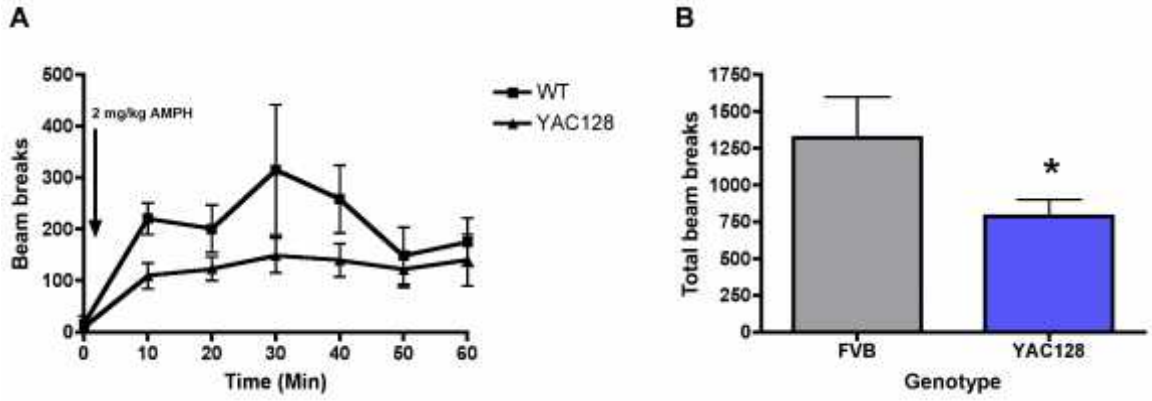

Figure 8: Effect of systemic injection of amphetamine (2 mg/kg; injection indicated by arrow) on (A) 10 minute bins of locomotor activity and (B) the total beam break counts during a 60 minute period in 7-month-old YAC128 transgenic mice (n = 5 WT, 6 YAC128). * indicates significantly different from WT, $P < 0.05$.

4.5 DISCUSSION

The present studies utilized *in vivo* microdialysis to assess striatal dopamine release dynamics in two transgenic mouse models of HD. We report that the concentrations of extracellular striatal dopamine are reduced in R6/2 and YAC128 transgenic mice relative to their respective wild-type controls. These data are consistent with previous studies demonstrating alterations in nigrostriatal function in both animal models and human cases of HD (Kish et al., 1987; Petersen et al., 2002; Johnson et al., 2007; Ortiz et al., 2011). Importantly, the present studies extend these findings and represent the first demonstration of attenuated striatal dopamine release across transgenic mouse models of HD constructed using different genetic approaches.

Performance deficits on the rotarod treadmill task are reliably documented across multiple HD transgenic strains, including R6/2 and YAC128 mice (Carter et al., 1999; Menalled and Chesselet, 2002; Slow et al., 2003). In the present studies, significant

impairments in the rotarod assay were apparent in R6/2 and YAC128 mice, with rotarod performance being roughly comparable at 7 weeks and 7 months of age, respectively. In both R6/2 and YAC128 mice, decline in motor function were associated with a significant reduction in the levels of extracellular striatal dopamine. Interestingly, while the 7-month age point in YAC128 mice is characterized by motor disturbances, blunt neurodegeneration does not emerge until older ages (Slow et al., 2003) suggesting the presence of alternative pathological alterations. Motor performance and striatal dopamine release were further assessed in R6/2 mice at 9 and 11 weeks of age, with both measures progressively diminishing as a function of group time point. Pentobarbital can attenuate dopamine release (Masuzawa et al., 2003). and while we used this compound as a general anesthetic during surgical procedures, all experiments took place at least 18 hours subsequent to surgery making it unlikely that there was an interaction between anesthesia and extracellular dopamine at the time experiments were conducted. Taken together, these findings lend support to the notion that alterations in synaptic function, including reduced levels of extracellular dopamine, may contribute to the disease phenotype across different transgenic mouse models of HD. Indeed, a wide range of dopamine related abnormalities have been reported, including dopamine receptor sensitization, attenuated striatal dopamine-dependent plasticity and altered dopamine-dependent modulation of corticostriatal currents, that may reflect the attenuated extracellular dopamine concentrations presently reported (Pineda et al., 2005; Cummings et al., 2007; Kung et al., 2007; Andre et al., 2011b).

In addition to extracellular dopamine concentrations, dopamine content in striatal tissue was assessed in 11-week old R6/2 mice. In agreement with previous reports

(Reynolds et al., 1999; Mochel et al., 2011), it was found that striatal tissue levels of dopamine were reduced by roughly half, relative to wild-type control animals. Importantly, reductions in tissue concentrations of dopamine were not as severe as the reductions observed in the extracellular fluid (45% vs. 75% reduction, respectively), suggesting the presence of an available intracellular pool of dopamine that is not being adequately utilized under spontaneous *in vivo* conditions. This finding is particularly intriguing when viewed in the context of animal models of Parkinson's disease (PD) in which the opposite pattern emerges. In PD models, tissue levels of dopamine must be depleted by greater than 80% in order for deficits in extracellular dopamine release to emerge (Abercrombie et al., 1990). The loss of tissue dopamine content and reductions in the density of postsynaptic dopamine receptors has been reported extensively in HD, however, this finding accentuates the need to account for presynaptic release deficits in HD pathogenesis as well.

There are multiple factors that could contribute to exocytotic release dysfunctions in HD. Several synaptic proteins that are involved in exocytotic processes, including complexin II, snare complex, synaptobrevin 2 and rab3a, have been shown to be abnormal in both transgenic mouse models and human cases of HD (Morton and Edwardson, 2001; Freeman and Morton, 2004; Glynn et al., 2007). In line with our results, there is a progressive decline in complexin II from 7 weeks onward in R6/2 mice (Morton and Edwardson, 2001). Another potential mechanism may involve alterations in calcium homeostasis and signaling, which could lead to changes in vesicular release probabilities (Bibb et al., 2000; Hansson et al., 2001). Moreover, the mHtt protein also disrupts vesicular transport and such an abnormality could alter vesicular pool sizes

(Velier et al., 1998). Indeed, Ortiz et al. (2010) demonstrated that storage vesicles in acute nigrostriatal slices are significantly diminished in R6/2 mice.

Intriguingly, the concentrations of extracellular striatal DOPAC (the main catabolite of dopamine) were significantly decreased in R6/2 mice and showed a tendency to be decreased in YAC128 mice, although this effect was not significant. Extracellular DOPAC derives from, and reflects the metabolism of, newly synthesized dopamine in the cytosol (Zetterstrom et al., 1988; Yadid et al., 2000). In the present studies, the observation of diminished amounts of striatal DOPAC coupled to the finding that tissue levels of striatal dopamine are reduced lends support to the possibility that cytosolic dopamine pools are depleted as well in transgenic mouse models of HD.

In order to more directly quantify cytosolic dopamine concentrations, we examined the effect of intrastiatal application of amphetamine on striatal dopamine efflux via reverse microdialysis. Amphetamine is a psychostimulant that promotes the release of newly synthesized dopamine from cytosolic pools into the extracellular fluid via an impulse-independent, exchange diffusion method and selective inhibition of the dopamine transporter (Fisher and Cho 1979). Previous work has confirmed the mechanism of action of amphetamine by demonstrating that its stimulant properties are abolished (except at very high doses) with the pretreatment of alpha-methyl-para-tyrosine (AMPT), a compound that inhibits the synthesis of dopamine in the cytosol, but not by reserpine, which depletes dopamine stored in vesicles (Chiueh and Moore, 1974; Niddam et al., 1985; Callaway et al., 1989; Heeringa and Abercrombie, 1995). Alterations in the levels and/or kinetics of the dopamine transporter could obscure the comparisons between genotypes, however, Petersen et al. (2002) demonstrated that the expression

patterns of striatal dopamine transporters were comparable and correspondingly Johnson et al. (2006) exhibited that uptake through the dopamine transporter was similar between R6/2 and wild-type controls.

The local application of amphetamine into the striatum produced an increase in extracellular dopamine release in both 9-week-old R6/2 mice and 7-month-old YAC128 mice, as well as in their respective wild-type controls. However, overall dopamine efflux was significantly attenuated across all time points in R6/2 mice and considerably reduced in 7-month-old YAC128 mice, although this effect fell short of significance. Similarly, the maximal effect of amphetamine on dopamine release was attenuated in both R6/2 and YAC128 mice (66% and 37% reductions, respectively). It should be noted that amphetamine-stimulated dopamine levels were considerably lower in the wild-type controls for the YAC128 mice, compared to those for the R6/2 mice. It is plausible that the different background strains and/or the divergent ages of the respective wild-type mice (7 months vs. 9 weeks) may account for the differences in amphetamine-stimulated dopamine release. Alternatively, it is possible that cytosolic pools of dopamine in 7-month-old YAC128 mice are not as depleted as in 9-week-old R6/2 mice. In any case, further experimentation at different age points, both younger and older, is necessary to fully delineate the progression of changes in dopamine release dynamics in the extended phenotype YAC128 mice.

In addition to the effect of local amphetamine on striatal dopamine release, the effect of systemic amphetamine on locomotor activity was assessed in the same cohort of 7-month-old YAC128 mice after a one-week drug washout period. Phenotype progression is too rapid to challenge the same cohort of R6/2 mice to systemic

amphetamine after an extended washout period and as such these experiments were only performed in YAC128 mice. Overall, there was a significant effect of genotype on locomotion, with YAC128 mice showing significantly reduced amphetamine-induced locomotion. This finding is consistent with decreased amphetamine-stimulated dopamine release and parallels a study in which amphetamine-induced locomotor activity was reduced in R6/2 mice (Hickey et al., 2002). These data lend support to the notion that cytosolic dopamine is attenuated in R6/2 and YAC128 mice and may contribute to the deficits in extracellular dopamine concentrations that we report.

Reductions in cytosolic dopamine levels could be caused by either deficits in the production of newly synthesized dopamine or the loss of nigrostriatal terminals. In light of the fact that tyrosine hydroxylase (TH) is the rate-limiting enzyme in the biosynthetic pathway for the production of dopamine, studies have demonstrated a significant reduction in TH activity in the striatum of 12 week-old-R6/2 mice (Yohrling et al., 2003), raising the possibility that deficits in dopamine synthesis may underlie depleted cytosolic concentrations. Alternatively, accumulating evidence indicates that the depletion of dopamine may be the result of nigrostriatal degeneration that manifests in an age-dependent manner. In 16-week-old R6/1 mice there is no difference in the number of nigrostriatal projections or the number of dopamine neurons within the substantia nigra pars compacta (Petersen et al., 2002). By 30 weeks, however, nigrostriatal projections are decreased and the total number of cells within the SNc is reduced (Pineda et al., 2005; Rubio et al., 2009). Interestingly, neurons within the SNc of 16-week-old R6/1 mice were diminished in size and exhibited mHtt aggregate bodies, suggesting that these pathological abnormalities may precede blunt degeneration within this area (Petersen et

al., 2002). Similarly, studies have demonstrated that there was a late stage reduction of nigrostriatal terminals in 11-12 week old R6/2 mice (Ariano et al., 2002). Studies in human cases also indicate that there is a reduction in nigrostriatal terminals and decreased striatal dopamine content in late stages of the disease (Kish et al., 1987; Ginovart et al., 1997; Bohnen et al., 2000)

This is the first report comparing extracellular striatal dopamine release dynamics in a fragment and full-length HD transgenic mouse model under awake behaving conditions and distinctively reveals that extracellular dopamine concentrations are attenuated across models. We speculate that the dysfunctions in dopamine release stems from a multifactorial set of presynaptic abnormalities that include both impairments in the synaptic machinery required to release dopamine as well as deficits in dopamine production and perhaps dopamine storage. Future research will need to determine with more specificity the nature of such alterations, when they emerge and the extent each contributes to HD symptomology.

4.6 ACKNOWLEDGEMENTS

The authors would like to thank Dr. Andrew Farrar for his contributions to the manuscript and Anna Chavez her technical assistance. This research was supported by United States Public Health Service grant NS059921 and the Hereditary Disease Foundation.

CHAPTER 5: DISCUSSION

5.1 CORTICAL NETWORK ALTERATIONS IN HD TRANSGENIC MICE

Global brain states can be monitored by voltage fluctuations in ECoG/EEG recordings and each brain state has a characteristic frequency spectrum (Steriade, 1997; Herculano-Houzel et al., 1999). During both synchronized and desynchronized states, we found ECoG alterations across ages in R6/2 and YAC128 transgenic HD mice. In presymptomatic YAC128 mice, ECoG spectral changes suggested early patterns of cortical network hyperexcitability. In accordance, imaging studies have demonstrated hyperactivity in the prefrontal cortex in presymptomatic human HD patients (Feigin et al., 2006). Evidence indicates that cortical pyramidal neurons are more excitable at early ages in HD transgenic mice which could lead to widespread network alterations (Walker et al., 2008; Cummings et al., 2009; Andre et al., 2011a). Early hyperexcitability in cortical pyramidal neurons in HD transgenic mice has been attributed to several changes including reductions in GABAergic inhibitory input, alterations in intrinsic membrane properties and increased glutamate release (Gu et al., 2005; Cummings et al., 2009; Joshi et al., 2009; Andre et al., 2011a). Interestingly, oscillations in the ECoG within frequency ranges that can be driven by rhythmic thalamic inputs were also augmented in young YAC128 mice (Steriade and Llinas, 1988; McCormick and Bal, 1997). Significant elevations in thalamic metabolic activity have been reported in presymptomatic HD patients (Feigin et al., 2007). Greater synchrony within thalamocortical circuits early in HD disease progression could lead to increased excitatory drive within the cortex or alternative thalamic targets.

At older ages, symptomatic R6/2 and YAC128 mice exhibited contrasting spectral changes in the ECoG signal. Likewise, EEG patterns vary widely in symptomatic HD patients (Bylsma et al., 1994). In R6/2 mice, the density of spectral power in low frequencies was reduced while the density of spectral power in higher frequencies was augmented. A shift in spectral density towards higher frequencies has also been demonstrated in R6/2 mice during awake, behaving conditions and confirms that the patterns we report are not merely an artifact of anesthesia (Hong et al., 2012). During synchronized conditions, high voltage cortical LFO activity is believed to be generated by cortical pyramidal neurons (Steriade et al., 2001). In vivo intracellular recordings demonstrate that the membrane potential of cortical pyramidal neurons shows rhythmic depolarizing and hyperpolarizing shifts that are strongly correlated with ECoG/EEG LFO activity (Amzica and Steriade, 1995; Destexhe et al., 1999; Steriade et al., 2001). As ECoG reflects cortical electrical activity, neuronal loss in the cortex should be expected to result in reductions in the power of cortical LFO activity, during synchronized states, by reducing the substrate necessary for network summation. Indeed, cortical atrophy generally yields diminished EEG amplitude (Wiegand et al., 1991). In contrast to YAC128 mice, neuronal loss in the cortex is absent in R6/2 mice. Thus, it is surprising that ECoG LFO power during synchronized states was diminished in R6/2 mice and unchanged in YAC128 mice.

While neuronal loss in the cortex has not been reported in R6/2 mice, reductions in cortical volume are apparent. Cortical volume reduction has been to linked to morphological alterations of pyramidal neurons which include reductions in somatic size, decrease density of dendrites and loss of dendritic spines (Turmaine et al., 2000;

Klapstein et al., 2001; Laforet et al., 2001; Stack et al., 2005). These characteristics are similar to dendritic changes reported in pyramidal cells of HD postmortem brains (Sotrel et al., 1993; Vonsattel and DiFiglia, 1998). Network summations of oscillations are only apparent when neurons oscillate coherently and such structural alterations could lead to reductions in the strength of connectivity and diminished correlated activity between cells. In accordance, correlated firing is reduced in cortical neurons recorded from R6/2 mice during awake, behaving conditions (Walker et al., 2008). Reduced cortical plasticity has also been shown in both R6/2 mice and human HD patients and could contribute to the diminished capacity to generate high voltage LFO activity in the cortex (Kung et al., 2007; Crupi et al., 2008; Dallerac et al., 2011).

In symptomatic YAC128 mice, the only change in ECoG power that we observed was a reduction within the 4-7 Hz bandwidth. In accordance, diminishment of spectral power within the 4-7 Hz range has been shown in symptomatic HD patients (Bylsma et al., 1994). Oscillations in the ECoG within the 4-7 Hz frequency range can be generated from the hippocampus (Steriade et al., 2001) and will need to be further investigated in future studies.

5.2 LOSS OF CORTICAL ENTRAINMENT OF STN NEURONS IN HD TRANSGENIC MICE

Network synchronization between the cortex and basal ganglia is critical for proper neuronal processing (Magill et al., 2000, 2001; Brown, 2003; Courtemanche et al., 2003; Berke et al., 2004; Sharott et al., 2005; Mallet et al., 2008; Litvak et al., 2011)).

During synchronized conditions, neuronal discharge in the cortex is highly synchronized in a low-frequency range across widespread regions (Amzica and Steriade, 1995; Contreras and Steriade, 1997; Destexhe et al., 1999; Steriade, 2001). During up states, cortical neurons discharge synchronized bursts of action potentials that exert a powerful driving force on the STN (Amzica and Steriade, 1998; Steriade, 2001). In turn, this causes phase-locked firing of STN neurons which become entrained to cortical LFOs. LFO activity in the STN is thought to be driven specifically through the hyperdirect pathway, as GPe neurons show relatively little entrainment and cortical ablation abolishes such patterns in the STN (Magill et al., 2000, 2001; Bevan et al., 2002). During synchronized conditions, in symptomatic HD transgenic mice, ~20% of STN neurons failed to fire with LFO discharge. These neurons instead exhibited firing patterns that resembled the autonomous tonic discharge normally seen in the absence of cortical input. Hence, this population appears to represent a segment of STN neurons that has been functionally disconnected from cortical input. This has important clinical implications as lesions that affect only 4-20% of the structure can result in hyperkinetic movement abnormalities that resemble the HD phenotype (Whittier and Mettler, 1949; Carpenter et al., 1950).

Corticosubthalamic projections originate from PT neurons in layer V of the cortex (Kita and Kita, 2012). While the hyperdirect pathway circuit has not been investigated in HD, Rosas et al. (2006) demonstrated using diffusion tensor imaging that white matter alterations in PT axons occurred early in HD and were independent of neuronal atrophy. Pyramidal neurons in layers III, V, and VI of the cortex also demonstrate subcellular pathological changes that include mHtt aggregation, inclusion bodies and dystrophic

neurites (Vonsattel et al., 1985; DiFiglia et al., 1997; Vonsattel and DiFiglia, 1998). Thus, corticosubthalamic projections may be vulnerable in HD. In order to directly assess the integrity of the hyperdirect pathway, we examined the effects of focal cortical stimulation on STN neuronal discharge in YAC128 mice. Stimulation of the ipsilateral frontal cortex leads to activity patterns in STN neurons distinguished by an initial short latency excitatory response that is generated by excitation of monosynaptic terminals in the hyperdirect pathway (Kitai and Deniau, 1981; Fujimoto and Kita, 1993; Nambu et al., 2000; Magill et al., 2004). While the proportion of STN neurons that responded to cortical stimulation with short latency excitation was relatively stable across ages in WT mice, there was a striking reduction in the ratio of responsive STN neurons in YAC128 mice as a function of age. This indicates that electrical signals are conducted through the hyperdirect pathway with less effectiveness as a function of the mutant Htt protein and could account for the loss of functional connectivity that we report in symptomatic HD mice.

At symptomatic age points, both strains of transgenic HD mice demonstrated an analogous reduction in the proportion of STN neurons that exhibited entrainment. However, in contrast to LFO STN neurons recorded from YAC128 mice, LFO STN neurons recorded from R6/2 mice were less phase-locked to cortical input. There are several factors that could explain this difference. Reductions in the density of ECoG power in low frequencies, during synchronized states, was only observed in R6/2 mice and suggests that cortical synchrony is more disrupted in symptomatic R6/2 mice than YAC128 mice. This could lead to reductions in the excitatory cortical drive in the STN, as a group of neurons are more effective in recruiting their postsynaptic targets if they

discharge in synchrony than if they fire asynchronously. An increase in the dominant frequency of the ECoG during synchronized states was also only observed in R6/2 mice. Pyramidal cortical neurons recorded from R6/2 mice demonstrate more shorter duration down states and could lead to recruitment errors (Stern, 2011). Alterations in the activity patterns of GPe neurons between R6/2 and YAC128 mice could also contribute to such changes as well. GABAergic GPe afferents can act as a gating mechanism for STN activity and increased GPe discharge could effectively decrease the sensitivity of STN neurons to cortical inputs (Urbain et al., 2002). Different populations of GPe neurons have been described that have divergent firing patterns during synchronized states (Paz et al., 2005). "Early discharging" neurons discharge with single spikes or short bursts of activity that are correlated with cortical up states. "Pausing" neurons discharge with bursts of spikes that are correlated with cortical down states, which are thought to contribute to the reduction in STN neuronal activity during these periods. Alterations in the expression or firing pattern of these neurons during synchronized states could contribute to the disruptions in phase-locked firing in LFO STN neurons in R6/2 mice. In addition, changes in the intrinsic membrane properties of STN neurons in R6/2 mice could contribute as well. For instance, increased expression of silent plateaus could diminish spiking to excitatory cortical drive.

5.3 DIMINISHED FIRING RATES OF STN NEURONS IN HD TRANSGENIC MICE

During desynchronized conditions, high voltage LFO activity in the cortex is abolished and the powerful synchronizing drive on basal ganglia targets is reduced (Magill et al., 2001). Hence, the firing rate and patterns of STN neurons during desynchronized conditions is more generally a product of GPe synaptic input and intrinsic mechanisms. In symptomatic transgenic HD mice, during desynchronized conditions, we found that the spontaneous firing rate of STN neurons was reduced. Degeneration of MSNs in the striatum is a pathological hallmark of HD and degeneration of indirect pathway MSNs occurs earliest in disease progression. Loss of MSNs has been reported in symptomatic YAC128 mice. While MSN loss has not been reported in R6/2 mice, there is a decrease in PENK/ENK mRNA expression in striatal MSNs and a reduction in ENK-immunoreactive fiber intensity in the GPe (Menalled et al., 2000; Sun et al., 2002), suggestive of neuronal injury in the indirect pathway. Activation of MSNs in the indirect pathway inhibits neurons in the GPe and leads to net excitation of STN neurons via a disinhibitory mechanism (Fujimoto and Kita, 1993). Loss of MSNs in the striatum, specifically in the indirect pathway, would lead to reduced inhibition on the GPe and an increase of GABAergic tone in the STN. Such alterations could account for the reduced firing rates of STN neurons in symptomatic transgenic HD mice. Interestingly, while the reductions in firing rates were similar between symptomatic transgenic HD mice, the firing patterns of STN neurons diverged between strains. STN neurons recorded from symptomatic R6/2 mice displayed less tonic regularity while there were no significant alterations in the regularity of discharge in STN neurons recorded from symptomatic YAC128 mice. Interestingly, similar to 9-week-old R6/2 mice, STN neurons recorded from 2-month-old YAC128 mice also exhibited less regular patterns of

discharge. Studies have demonstrated that the MSN activity is increased in both 9-week-old R6/2 mice and 2-month-old YAC128 mice and such hyperexcitability in the striatum could contribute, through the GPe, to abnormal patterning of STN discharge. Future research will need to examine whether changes in GPe activity exist in transgenic mouse models of HD.

5.4 REDUCED EXTRACELLULAR DOPAMINE RELEASE IN HD MICE

We found reductions in extracellular dopamine release in the striatum of symptomatic HD mice. Our lab has also shown similar reductions in DA release in the prefrontal cortex of R6/2 mice (*unpublished*). There are multiple factors that could contribute to presynaptic release dysfunction in HD. The mHtt protein interferes with synaptic proteins that are involved in exocytotic processes, including complexin II, snare complex, synaptobrevin 2 and rab3a, in both transgenic mouse models and human cases of HD (Morton and Edwardson, 2001; Morton et al., 2001; Freeman and Morton, 2004; Glynn et al., 2007). In addition, the reductions in spontaneous firing rates of STN neurons that we report could lead to downstream effects in the SNc. STN lesions leads to reduced burst firing of DA neurons and could cause diminished extracellular release (Smith and Grace, 1992).

The effects of DA depletion could have profound effects across the cortico-basal ganglia network. Following DA depletion, neurons in the motor and dorsal insular cortex projecting to the STN are hypoactive (Orieux et al., 2002). These changes could contribute to the reductions in cortical drive that we report in STN neurons in

symptomatic HD mice. In addition, chronic depletion of DA can increase the power of cortical oscillations in higher frequency ranges, specifically in the 13-30 Hz range (Brown, 2003). This shift is likely to be a consequence of plasticity induced by long-term progressive dopamine depletion (Nambu et al., 2002; Brown, 2003). Deficits in DA transmission were larger in symptomatic R6/2 mice compared to 7-month-old YAC128 mice and could contribute to the increase in ECoG power in higher frequency ranges in R6/2 mice that was not observed in YAC128 mice. In accordance, computational models suggest that exaggerated power in higher frequency oscillations only emerges following extensive dopamine depletion and moderate dopamine depletion is insufficient to induce such changes (Leblois et al., 2006). Interestingly, the expression of postsynaptic DA receptors is also reduced in R6/2 mice, while normal in YAC128 mice, (Benn et al., 2007) and could also contribute to the differences in cortical ECoG patterns that we report between strains.

Impaired DAergic transmission could also contribute to the changes that we report in the firing rates and pattern of STN neurons in transgenic HD mice. DA release excites STN neurons through postsynaptic D1 receptors and loss of DAergic tone could lead to reduced firing rates that we report in symptomatic transgenic HD mice (Kreiss et al., 1996; Kreiss et al., 1997). In addition, activation of presynaptic D2 receptors on GPe terminals increases the frequency of autonomous firing of STN neurons (Shen and Johnson, 2000; Cragg et al., 2004) and reductions in DAergic tone could contribute to the diminishments in the regularity of firing that we observed in R6/2 mice. Reduced DA transmission could lead to reductions in the tonic regularity of discharge that we report in R6/2 mice. To specifically address such questions, future work will need to investigate

whether DA release is as reduced in the STN as that which we report in the striatum and cortex.

5.5 LIMITATIONS AND FUTURE DIRECTIONS

A major limitation in the present research is the lack of specificity regarding factors that differentiate the population of tonic STN neurons not entrained to cortical signals in HD mice. Our data suggest that these tonic neurons arise from disconnection in the corticosubthalamic hyperdirect pathway, however, these studies cannot delineate whether this occurs through presynaptic or postsynaptic changes. Excitatory terminals can be marked within the STN at the electron microscopic level as their synaptic vesicles contain the vesicular glutamate transporter, VGLUT1. Future studies could assay the proportions of VGLUT1-labeled terminals in HD mice to investigate whether the loss of cortical terminals emerge as a function of HD progression. Loss of postsynaptic NMDA receptors has been demonstrated in human HD patients (Young et al., 1988) and such loss of NMDA receptors in STN neurons could lead to reductions in the sensitivity of these neurons to cortical inputs. Future studies could examine whether differences in STN NMDA receptor expression and binding sensitivity exist in symptomatic HD mice. Interestingly, heterogeneity also exists among STN neurons based upon their specific projection targets (Sato et al., 2000). Single-cell juxtacellular techniques make it possible to label recorded units and could be used to reconstruct the axonal branching patterns of tonic neurons in symptomatic HD mice to investigate whether specific STN targets are more widely affected.

5.6 IMPLICATIONS FOR HD

Evidence suggests that the corticosubthalamic hyperdirect pathway activation plays a pivotal role in action suppression (Hamada and DeLong, 1992; Baunez et al., 1995; Baunez and Robbins, 1997; Dybdal and Gale, 2000; Aron and Poldrack, 2006; Schmidt et al., 2013). Glutamatergic neurons of the STN act as a powerful driving force for promoting neuronal activity in the output structures of the basal ganglia and thus inhibiting unintended commands (Nambu et al., 2002). STN blockade or lesion causes a decrease in both the spontaneous activity and cortically evoked excitatory responses in neurons of the basal ganglia output nuclei (Whittier and Mettler, 1949; Carpenter et al., 1950; Crossman, 1989; Hamada and DeLong, 1992; Nambu et al., 2002). This leads to hyperkinetic movement syndromes that resemble the HD phenotype. Our results demonstrate impairments in the fidelity of information flow through the hyperdirect pathway as a function of disease progression. This could lead to reduced control of basal ganglia output structures and disordered motor control.

CHAPTER 6: REFERENCES

Abercrombie ED, Bonatz AE, Zigmond MJ (1990) Effects of L-dopa on extracellular dopamine in striatum of normal and 6-hydroxydopamine-treated rats. Brain Res 525:36-44.

Adam OR, Jankovic J (2008) Symptomatic treatment of Huntington disease. Neurotherapeutics 5:181-197.

Afsharpour S (1985) Topographical projections of the cerebral cortex to the subthalamic nucleus. J Comp Neurol 236:14-28.

Albin RL, Young AB, Penney JB (1989) The functional anatomy of basal ganglia disorders. Trends Neurosci 12:366-375.

Albin RL, Reiner A, Anderson KD, Penney JB, Young AB (1990) Striatal and nigral neuron subpopulations in rigid Huntington's disease: implications for the functional anatomy of chorea and rigidity-akinesia. Ann Neurol 27:357-365.

Alexander GE, Crutcher MD (1990) Functional architecture of basal ganglia circuits: neural substrates of parallel processing. Trends Neurosci 13:266-271.

Alexander GE, Crutcher MD, DeLong MR (1990) Basal ganglia-thalamocortical circuits: parallel substrates for motor, oculomotor, "prefrontal" and "limbic" functions. Prog Brain Res 85:119-146.

Amzica F, Steriade M (1995) Short- and long-range neuronal synchronization of the slow (< 1 Hz) cortical oscillation. J Neurophysiol 73:20-38.

Amzica F, Steriade M (1998) Electrophysiological correlates of sleep delta waves. Electroencephalogr Clin Neurophysiol 107:69-83.

Andre VM, Fisher YE, Levine MS (2011a) Altered Balance of Activity in the Striatal Direct and Indirect Pathways in Mouse Models of Huntington's Disease. Front Syst Neurosci 5:46.

Andre VM, Cepeda C, Venegas A, Gomez Y, Levine MS (2006) Altered cortical glutamate receptor function in the R6/2 model of Huntington's disease. J Neurophysiol 95:2108-2119.

Andre VM, Cepeda C, Fisher YE, Huynh M, Bardakjian N, Singh S, Yang XW, Levine MS (2011b) Differential electrophysiological changes in striatal output neurons in Huntington's disease. J Neurosci 31:1170-1182.

Ariano MA, Aronin N, Difiglia M, Tagle DA, Sibley DR, Leavitt BR, Hayden MR, Levine MS (2002) Striatal neurochemical changes in transgenic models of Huntington's disease. J Neurosci Res 68:716-729.

Aron AR, Poldrack RA (2006) Cortical and subcortical contributions to Stop signal response inhibition: role of the subthalamic nucleus. J Neurosci 26:2424-2433.

Atherton JF, Menard A, Urbain N, Bevan MD (2013) Short-term depression of external globus pallidus-subthalamic nucleus synaptic transmission and implications for patterning subthalamic activity. J Neurosci 33:7130-7144.

Aylward EH, Anderson NB, Bylsma FW, Wagster MV, Barta PE, Sherr M, Feeney J, Davis A, Rosenblatt A, Pearlson GD, Ross CA (1998) Frontal lobe volume in patients with Huntington's disease. Neurology 50:252-258.

Barnes TD, Kubota Y, Hu D, Jin DZ, Graybiel AM (2005) Activity of striatal neurons reflects dynamic encoding and recoding of procedural memories. Nature 437:1158-1161.

Baunez C, Robbins TW (1997) Bilateral lesions of the subthalamic nucleus induce multiple deficits in an attentional task in rats. Eur J Neurosci 9:2086-2099.

Baunez C, Nieoullon A, Amalric M (1995) In a rat model of parkinsonism, lesions of the subthalamic nucleus reverse increases of reaction time but induce a dramatic premature responding deficit. J Neurosci 15:6531-6541.

Becher MW, Kotzuk JA, Sharp AH, Davies SW, Bates GP, Price DL, Ross CA (1998) Intranuclear neuronal inclusions in Huntington's disease and dentatorubral and pallidoluysian atrophy: correlation between the density of inclusions and IT15 CAG triplet repeat length. Neurobiol Dis 4:387-397.

Beckstead RM (1983) A reciprocal axonal connection between the subthalamic nucleus and the neostriatum in the cat. Brain Res 275: 137-142.

Benn CL, Slow EJ, Farrell LA, Graham R, Deng Y, Hayden MR, Cha JH (2007) Glutamate receptor abnormalities in the YAC128 transgenic mouse model of Huntington's disease. Neuroscience 147:354-372.

Berardelli A, Noth J, Thompson PD, Bollen EL, Curra A, Deuschl G, van Dijk JG, Topper R, Schwarz M, Roos RA (1999) Pathophysiology of chorea and bradykinesia in Huntington's disease. Mov Disord 14:398-403.

Berke JD, Okatan M, Skurski J, Eichenbaum HB (2004) Oscillatory entrainment of striatal neurons in freely moving rats. Neuron 43:883-896.

Beurrier C, Bioulac B, Hammond C (2000) Slowly inactivating sodium current (I(NaP)) underlies single-spike activity in rat subthalamic neurons. J Neurophysiol 83:1951-1957.

Beurrier C, Congar P, Bioulac B, Hammond C (1999) Subthalamic nucleus neurons switch from single-spike activity to burst-firing mode. J Neurosci 19:599-609.

Bevan MD, Wilson CJ (1999) Mechanisms underlying spontaneous oscillation and rhythmic firing in rat subthalamic neurons. J Neurosci 19:7617-7628.

Bevan MD, Francis CM, Bolam JP (1995) The glutamate-enriched cortical and thalamic input to neurons in the subthalamic nucleus of the rat: convergence with GABA-positive terminals. J Comp Neurol 361:491-511.

Bevan MD, Clarke NP, Bolam JP (1997) Synaptic integration of functionally diverse pallidal information in the entopeduncular nucleus and subthalamic nucleus in the rat. J Neurosci 17:308-324.

Bevan MD, Hallworth NE, Baufreton J (2007) GABAergic control of the subthalamic nucleus. Prog Brain Res 160:173-188.

Bevan MD, Wilson CJ, Bolam JP, Magill PJ (2000) Equilibrium potential of GABA(A) current and implications for rebound burst firing in rat subthalamic neurons in vitro. J Neurophysiol 83:3169-3172.

Bevan MD, Magill PJ, Terman D, Bolam JP, Wilson CJ (2002) Move to the rhythm: oscillations in the subthalamic nucleus-external globus pallidus network. Trends Neurosci 25:525-531.

Bibb JA, Yan Z, Svenningsson P, Snyder GL, Pieribone VA, Horiuchi A, Nairn AC, Messer A, Greengard P (2000) Severe deficiencies in dopamine signaling in presymptomatic Huntington's disease mice. Proc Natl Acad Sci U S A 97:6809-6814.

Bilney B, Morris ME, Churchyard A, Chiu E, Georgiou-Karistianis N (2005) Evidence for a disorder of locomotor timing in Huntington's disease. Mov Disord 20:51-57.

Bohnen NI, Koeppe RA, Meyer P, Ficaro E, Wernette K, Kilbourn MR, Kuhl DE, Frey KA, Albin RL (2000) Decreased striatal monoaminergic terminals in Huntington disease. Neurology 54:1753-1759.

Bokil H, Andrews P, Kulkarni JE, Mehta S, Mitra PP (2010) Chronux: a platform for analyzing neural signals. J Neurosci Methods 192:146-151.

Bonelli RM, Wenning GK (2006) Pharmacological management of Huntington's disease: an evidence-based review. Curr Pharm Des 12:2701-2720.

Bonelli RM, Hofmann P (2007) A systematic review of the treatment studies in Huntington's disease since 1990. Expert Opin Pharmacother 8:141-153.

Brackenridge CJ (1980) Factors influencing dementia and epilepsy in Huntington's disease of early onset. Acta Neurol Scand 62:305-311.

Bradbury AJ, Costall B, Kelly ME, Naylor RJ, Smith JA (1985) Biochemical correlates of motor changes caused by the manipulation of dopamine function in the substantia nigra of the mouse. Neuropharmacology 24:1155-1161.

Brenner RP (1985) The electroencephalogram in altered states of consciousness. Neurol Clin 3:615-631.

Bronfeld M, Bar-Gad I (2011) Loss of specificity in Basal Ganglia related movement disorders. Front Syst Neurosci 5:38.

Brooks SP, Dunnett SB (2013) Cognitive deficits in animal models of basal ganglia disorders. Brain Res Bull 92:29-40.

Brown LL, Markman MH, Wolfson LI, Dvorkin B, Warner C, Katzman R (1979) A direct role of dopamine in the rat subthalamic nucleus and an adjacent intrapeduncular area. Science 206:1416-1418.

Brown P (2003) Oscillatory nature of human basal ganglia activity: relationship to the pathophysiology of Parkinson's disease. Mov Disord 18:357-363.

Bylsma FW, Peyser CE, Folstein SE, Folstein MF, Ross C, Brandt J (1994) EEG power spectra in Huntington's disease: clinical and neuropsychological correlates. Neuropsychologia 32:137-150.

Callaway CW, Kuczenski R, Segal DS (1989) Reserpine enhances amphetamine stereotypies without increasing amphetamine-induced changes in striatal dialysate dopamine. Brain Res 505:83-90.

Canteras NS, Shammah-Lagnado SJ, Silva BA, Ricardo JA (1988) Somatosensory inputs to the subthalamic nucleus: a combined retrograde and anterograde horseradish peroxidase study in the rat. Brain Res 458:53-64.

Canteras NS, Shammah-Lagnado SJ, Silva BA, Ricardo JA (1990) Afferent connections of the subthalamic nucleus: a combined retrograde and anterograde horseradish peroxidase study in the rat. Brain Res 513:43-59.

Carpenter MB, Whittier JR, Mettler FA (1950) Analysis of choreoid hyperkinesia in the Rhesus monkey; surgical and pharmacological analysis of hyperkinesia resulting from lesions in the subthalamic nucleus of Luys. J Comp Neurol 92:293-331.

Carter RJ, Lione LA, Humby T, Mangiarini L, Mahal A, Bates GP, Dunnett SB, Morton AJ (1999) Characterization of progressive motor deficits in mice transgenic for the human Huntington's disease mutation. J Neurosci 19:3248-3257.

Cepeda C, Wu N, Andre VM, Cummings DM, Levine MS (2007) The corticostriatal pathway in Huntington's disease. Prog Neurobiol 81:253-271.

Cepeda C, Hurst RS, Calvert CR, Hernandez-Echeagaray E, Nguyen OK, Jocoy E, Christian LJ, Ariano MA, Levine MS (2003) Transient and progressive electrophysiological alterations in the corticostriatal pathway in a mouse model of Huntington's disease. J Neurosci 23:961-969.

Cha JH, Kosinski CM, Kerner JA, Alsdorf SA, Mangiarini L, Davies SW, Penney JB, Bates GP, Young AB (1998) Altered brain neurotransmitter receptors in transgenic mice expressing a portion of an abnormal human huntington disease gene. Proc Natl Acad Sci U S A 95:6480-6485.

Chergui K, Akaoka H, Charlety PJ, Saunier CF, Buda M, Chouvet G (1994) Subthalamic nucleus modulates burst firing of nigral dopamine neurones via NMDA receptors. Neuroreport 5:1185-1188.

Chiueh CC, Moore KE (1974) Effects of alpha-methyltyrosine on d-amphetamine-induced release of endogenously synthesized and exogenously administered catecholamines from the cat brain in vivo. J Pharmacol Exp Ther 190:100-108.

Clarke NP, Bolam JP (1998) Distribution of glutamate receptor subunits at neurochemically characterized synapses in the entopeduncular nucleus and subthalamic nucleus of the rat. J Comp Neurol 397:403-420.

Cobb WS, Abercrombie ED (2002) Distinct roles for nigral GABA and glutamate receptors in the regulation of dendritic dopamine release under normal conditions and in response to systemic haloperidol. J Neurosci 22:1407-1413.

Contreras D, Steriade M (1997) Synchronization of low-frequency rhythms in corticothalamic networks. Neuroscience 76:11-24.

Cossette M, Levesque M, Parent A (1999) Extrastriatal dopaminergic innervation of human basal ganglia. Neurosci Res 34:51-54.

Courtemanche R, Fujii N, Graybiel AM (2003) Synchronous, focally modulated beta-band oscillations characterize local field potential activity in the striatum of awake behaving monkeys. J Neurosci 23:11741-11752.

Cowan RL, Wilson CJ (1994) Spontaneous firing patterns and axonal projections of single corticostriatal neurons in the rat medial agranular cortex. J Neurophysiol 71:17-32.

Coyle JT, Schwarcz R (1976) Lesion of striatal neurones with kainic acid provides a model for Huntington's chorea. Nature 263:244-246.

Coyle JT, Schwarcz R, Bennett JP, Campochiaro P (1977) Clinical, neuropathologic and pharmacologic aspects of Huntington's disease: correlates with a new animal model. Prog Neuropsychopharmacol 1:13-30.

Cragg SJ, Baufreton J, Xue Y, Bolam JP, Bevan MD (2004) Synaptic release of dopamine in the subthalamic nucleus. Eur J Neurosci 20:1788-1802.

Crossman AR (1989) Neural mechanisms in disorders of movement. Comp Biochem Physiol A Comp Physiol 93:141-149.

Crupi D, Ghilardi MF, Mosiello C, Di Rocco A, Quartarone A, Battaglia F (2008) Cortical and brainstem LTP-like plasticity in Huntington's disease. Brain Res Bull 75:107-114.

Cummings DM, Cepeda C, Levine MS (2010) Alterations in striatal synaptic transmission are consistent across genetic mouse models of Huntington's disease. ASN Neuro 2:e00036.

Cummings DM, Milnerwood AJ, Dallerac GM, Vatsavayai SC, Hirst MC, Murphy KP (2007) Abnormal cortical synaptic plasticity in a mouse model of Huntington's disease. Brain Res Bull 72:103-107.

Cummings DM, Andre VM, Uzgil BO, Gee SM, Fisher YE, Cepeda C, Levine MS (2009) Alterations in cortical excitation and inhibition in genetic mouse models of Huntington's disease. J Neurosci 29:10371-10386.

Dallerac GM, Vatsavayai SC, Cummings DM, Milnerwood AJ, Peddie CJ, Evans KA, Walters SW, Rezaie P, Hirst MC, Murphy KP (2011) Impaired long-term potentiation in the prefrontal cortex of Huntington's disease mouse models: rescue by D1 dopamine receptor activation. Neurodegener Dis 8:230-239.

Davies SW, Turmaine M, Cozens BA, Raza AS, Mahal A, Mangiarini L, Bates GP (1999) From neuronal inclusions to neurodegeneration: neuropathological investigation of a transgenic mouse model of Huntington's disease. Philos Trans R Soc Lond B Biol Sci 354:981-989.

Davies SW, Turmaine M, Cozens BA, DiFiglia M, Sharp AH, Ross CA, Scherzinger E, Wanker EE, Mangiarini L, Bates GP (1997) Formation of neuronal intranuclear inclusions underlies the neurological dysfunction in mice transgenic for the HD mutation. Cell 90:537-548.

Degos B, Deniau JM, Le Cam J, Mailly P, Maurice N (2008) Evidence for a direct subthalamo-cortical loop circuit in the rat. Eur J Neurosci 27:2559-2610.

DeLong MR (1990) Primate models of movement disorders of basal ganglia origin. Trends Neurosci 13:281-285.

Destexhe A, Contreras D, Steriade M (1999) Spatiotemporal analysis of local field potentials and unit discharges in cat cerebral cortex during natural wake and sleep states. J Neurosci 19:4595-4608.

Difiglia M, Pasik P, Pasik T (1982) A Golgi and ultrastructural study of the monkey globus pallidus. J Comp Neurol 212:53-75.

DiFiglia M, Sapp E, Chase KO, Davies SW, Bates GP, Vonsattel JP, Aronin N (1997) Aggregation of huntingtin in neuronal intranuclear inclusions and dystrophic neurites in brain. Science 277:1990-1993.

Djousse L, Knowlton B, Cupples LA, Marder K, Shoulson I, Myers RH (2002) Weight loss in early stage of Huntington's disease. Neurology 59:1325-1330.

Do MT, Bean BP (2003) Subthreshold sodium currents and pacemaking of subthalamic neurons: modulation by slow inactivation. Neuron 39:109-120.

Dumas EM, van den Bogaard SJ, Middelkoop HA, Roos RA (2013) A review of cognition in Huntington's disease. Front Biosci (Schol Ed) 5:1-18.

Dunah AW, Jeong H, Griffin A, Kim YM, Standaert DG, Hersch SM, Mouradian MM, Young AB, Tanese N, Krainc D (2002) Sp1 and TAFII130 transcriptional activity disrupted in early Huntington's disease. Science 296:2238-2243.

Duyao MP, Auerbach AB, Ryan A, Persichetti F, Barnes GT, McNeil SM, Ge P, Vonsattel JP, Gusella JF, Joyner AL, et al. (1995) Inactivation of the mouse Huntington's disease gene homolog Hdh. Science 269:407-410.

Dybdal D, Gale K (2000) Postural and anticonvulsant effects of inhibition of the rat subthalamic nucleus. J Neurosci 20:6728-6733.

Feger J, Bevan M, Crossman AR (1994) The projections from the parafascicular thalamic nucleus to the subthalamic nucleus and the striatum arise from separate neuronal populations: a comparison with the corticostriatal and corticosubthalamic efferents in a retrograde fluorescent double-labelling study. Neuroscience 60:125-132.

Feigin A, Ghilardi MF, Huang C, Ma Y, Carbon M, Guttman M, Paulsen JS, Ghez CP, Eidelberg D (2006) Preclinical Huntington's disease: compensatory brain responses during learning. Ann Neurol 59:53-59.

Feigin A, Tang C, Ma Y, Mattis P, Zgaljardic D, Guttman M, Paulsen JS, Dhawan V, Eidelberg D (2007) Thalamic metabolism and symptom onset in preclinical Huntington's disease. Brain 130:2858-2867.

Ferrante RJ, Andreassen OA, Jenkins BG, Dedeoglu A, Kuemmerle S, Kubilus JK, Kaddurah-Daouk R, Hersch SM, Beal MF (2000) Neuroprotective effects of creatine in a transgenic mouse model of Huntington's disease. J Neurosci 20:4389-4397.

Ferron JF, Kroeger D, Chever O, Amzica F (2009) Cortical inhibition during burst suppression induced with isoflurane anesthesia. J Neurosci 29:9850-9860.

Fiorillo CD, Tobler PN, Schultz W (2003) Discrete coding of reward probability and uncertainty by dopamine neurons. Science 299:1898-1902.

Fisher SP, Black SW, Schwartz MD, Wilk AJ, Chen TM, Lincoln WU, Liu HW, Kilduff TS, Morairty SR (2013) Longitudinal analysis of the electroencephalogram and sleep phenotype in the R6/2 mouse model of Huntington's disease. Brain 136:2159-2172.

Foroud T, Siemers E, Kleindorfer D, Bill DJ, Hodes ME, Norton JA, Conneally PM, Christian JC (1995) Cognitive scores in carriers of Huntington's disease gene compared to noncarriers. Ann Neurol 37:657-664.

Francois C, Percheron G, Yelnik J, Heyner S (1984) A Golgi analysis of the primate globus pallidus. I. Inconstant processes of large neurons, other neuronal types, and afferent axons. J Comp Neurol 227:182-199.

Francois C, Savy C, Jan C, Tande D, Hirsch EC, Yelnik J (2000) Dopaminergic innervation of the subthalamic nucleus in the normal state, in MPTP-treated monkeys, and in Parkinson's disease patients. J Comp Neurol 425:121-129.

Frank MJ (2006) Hold your horses: a dynamic computational role for the subthalamic nucleus in decision making. Neural Netw 19:1120-1136.

Freeman W, Morton AJ (2004) Regional and progressive changes in brain expression of complexin II in a mouse transgenic for the Huntington's disease mutation. Brain Res Bull 63:45-55.

Fujimoto K, Kita H (1993) Response characteristics of subthalamic neurons to the stimulation of the sensorimotor cortex in the rat. Brain Res 609:185-192.

Fusco FR, Chen Q, Lamoreaux WJ, Figueredo-Cardenas G, Jiao Y, Coffman JA, Surmeier DJ, Honig MG, Carlock LR, Reiner A (1999) Cellular localization of huntingtin in striatal and cortical neurons in rats: lack of correlation with neuronal vulnerability in Huntington's disease. J Neurosci 19:1189-1202.

Gerfen CR (1992) The neostriatal mosaic: multiple levels of compartmental organization. J Neural Transm Suppl 36:43-59.

Ghiglieri V, Bagetta V, Calabresi P, Picconi B (2012) Functional interactions within striatal microcircuit in animal models of Huntington's disease. Neuroscience 211:165-184.

Ginovart N, Lundin A, Farde L, Halldin C, Backman L, Swahn CG, Pauli S, Sedvall G (1997) PET study of the pre- and post-synaptic dopaminergic markers for the neurodegenerative process in Huntington's disease. Brain 120 (Pt 3):503-514.

Glynn D, Reim K, Brose N, Morton AJ (2007) Depletion of Complexin II does not affect disease progression in a mouse model of Huntington's disease (HD); support for role for complexin II in behavioural pathology in a mouse model of HD. Brain Res Bull 72:108-120.

Gomez-Tortosa E, MacDonald ME, Friend JC, Taylor SA, Weiler LJ, Cupples LA, Srinidhi J, Gusella JF, Bird ED, Vonsattel JP, Myers RH (2001) Quantitative neuropathological changes in presymptomatic Huntington's disease. Ann Neurol 49:29-34.

Gordon AM, Quinn L, Reilmann R, Marder K (2000) Coordination of prehensile forces during precision grip in Huntington's disease. Exp Neurol 163:136-148.

Gourfinkel-An I, Cancel G, Duyckaerts C, Faucheux B, Hauw JJ, Trottier Y, Brice A, Agid Y, Hirsch EC (1998) Neuronal distribution of intranuclear inclusions in Huntington's disease with adult onset. Neuroreport 9:1823-1826.

Graham RK, Pouladi MA, Joshi P, Lu G, Deng Y, Wu NP, Figueroa BE, Metzler M, Andre VM, Slow EJ, Raymond L, Friedlander R, Levine MS, Leavitt BR, Hayden MR (2009) Differential susceptibility to excitotoxic stress in YAC128 mouse models of Huntington disease between initiation and progression of disease. J Neurosci 29:2193-2204.

Gu X, Li C, Wei W, Lo V, Gong S, Li SH, Iwasato T, Itohara S, Li XJ, Mody I, Heintz N, Yang XW (2005) Pathological cell-cell interactions elicited by a neuropathogenic form of mutant Huntingtin contribute to cortical pathogenesis in HD mice. Neuron 46:433-444.

Gunawardena S, Her LS, Brusch RG, Laymon RA, Niesman IR, Gordesky-Gold B, Sintasath L, Bonini NM, Goldstein LS (2003) Disruption of axonal transport by loss of huntingtin or expression of pathogenic polyQ proteins in Drosophila. Neuron 40:25-40.

Hackam AS, Singaraja R, Wellington CL, Metzler M, McCutcheon K, Zhang T, Kalchman M, Hayden MR (1998) The influence of huntingtin protein size on nuclear localization and cellular toxicity. J Cell Biol 141:1097-1105.

Halliday GM, McRitchie DA, Macdonald V, Double KL, Trent RJ, McCusker E (1998) Regional specificity of brain atrophy in Huntington's disease. Exp Neurol 154:663-672.

Hallworth NE, Wilson CJ, Bevan MD (2003) Apamin-sensitive small conductance calcium-activated potassium channels, through their selective coupling to voltage-gated calcium channels, are critical determinants of the precision, pace, and pattern of action potential generation in rat subthalamic nucleus neurons in vitro. J Neurosci 23:7525-7542.

Hamada I, DeLong MR (1992) Excitotoxic acid lesions of the primate subthalamic nucleus result in transient dyskinesias of the contralateral limbs. J Neurophysiol 68:1850-1858.

Hansson O, Guatteo E, Mercuri NB, Bernardi G, Li XJ, Castilho RF, Brundin P (2001) Resistance to NMDA toxicity correlates with appearance of nuclear inclusions, behavioural deficits and changes in calcium homeostasis in mice transgenic for exon 1 of the huntington gene. Eur J Neurosci 14:1492-1504.

Hassani OK, Francois C, Yelnik J, Feger J (1997) Evidence for a dopaminergic innervation of the subthalamic nucleus in the rat. Brain Res 749:88-94.

Haynes WI, Haber SN (2013) The organization of prefrontal-subthalamic inputs in primates provides an anatomical substrate for both functional specificity and integration: implications for Basal Ganglia models and deep brain stimulation. J Neurosci 33:4804-4814.

Hazrati LN, Parent A (1992a) Convergence of subthalamic and striatal efferents at pallidal level in primates: an anterograde double-labeling study with biocytin and PHA-L. Brain Res 569:336-340.

Hazrati LN, Parent A (1992b) Differential patterns of arborization of striatal and subthalamic fibers in the two pallidal segments in primates. Brain Res 598:311-315.

Hedreen JC (1999) Tyrosine hydroxylase-immunoreactive elements in the human globus pallidus and subthalamic nucleus. J Comp Neurol 409:400-410.

Hedreen JC, Folstein SE (1995) Early loss of neostriatal striosome neurons in Huntington's disease. J Neuropathol Exp Neurol 54:105-120.

Heeringa MJ, Abercrombie ED (1995) Biochemistry of somatodendritic dopamine release in substantia nigra: an in vivo comparison with striatal dopamine release. J Neurochem 65:192-200.

Herculano-Houzel S, Munk MH, Neuenschwander S, Singer W (1999) Precisely synchronized oscillatory firing patterns require electroencephalographic activation. J Neurosci 19:3992-4010.

Hickey MA, Reynolds GP, Morton AJ (2002) The role of dopamine in motor symptoms in the R6/2 transgenic mouse model of Huntington's disease. J Neurochem 81:46-59.

Higgins DS, Hoyt KR, Baic C, Vensel J, Sulka M (1999) Metabolic and glutamatergic disturbances in the Huntington's disease transgenic mouse. Ann N Y Acad Sci 893:298-300.

Hollerman JR, Schultz W (1998) Dopamine neurons report an error in the temporal prediction of reward during learning. Nat Neurosci 1:304-309.

Hong SL, Cossyleon D, Hussain WA, Walker LJ, Barton SJ, Rebec GV (2012) Dysfunctional behavioral modulation of corticostriatal communication in the R6/2 mouse model of Huntington's disease. PLoS One 7:e47026.

Hughes S, Crunelli V (2013) UP states rise from the depths. Nat Neurosci 16:115-117.

Huntington's Disease Collaborative Group (1993) A novel gen containing a trinucleotide repeat that is expanded and unstable on Huntington's disease chromosomes. Cell 72: 971-983.

Jackson A, Crossman AR (1983) Nucleus tegmenti pedunculopontinus: efferent connections with special reference to the basal ganglia, studied in the rat by anterograde and retrograde transport of horseradish peroxidase. Neuroscience 10:725-765.

Jahfari S, Waldorp L, van den Wildenberg WP, Scholte HS, Ridderinkhof KR, Forstmann BU (2011) Effective connectivity reveals important roles for both the hyperdirect (fronto-subthalamic) and the indirect (fronto-striatal-pallidal) fronto-basal ganglia pathways during response inhibition. J Neurosci 31:6891-6899.

Jernigan TL, Salmon DP, Butters N, Hesselink JR (1991) Cerebral structure on MRI, Part II: Specific changes in Alzheimer's and Huntington's diseases. Biol Psychiatry 29:68-81.

Jinnai K, Matsuda Y (1979) Neurons of the motor cortex projecting commonly on the caudate nucleus and the lower brain stem in the cat. Neurosci Lett 13:121-126.

Johnson AE, Coirini H, Kallstrom L, Wiesel FA (1994) Characterization of dopamine receptor binding sites in the subthalamic nucleus. Neuroreport 5:1836-1838.

Johnson MA, Villanueva M, Haynes CL, Seipel AT, Buhler LA, Wightman RM (2007) Catecholamine exocytosis is diminished in R6/2 Huntington's disease model mice. J Neurochem 103:2102-2110.

Joshi PR, Wu NP, Andre VM, Cummings DM, Cepeda C, Joyce JA, Carroll JB, Leavitt BR, Hayden MR, Levine MS, Bamford NS (2009) Age-dependent alterations of corticostriatal activity in the YAC128 mouse model of Huntington disease. J Neurosci 29:2414-2427.

Joshua M, Adler A, Prut Y, Vaadia E, Wickens JR, Bergman H (2009) Synchronization of midbrain dopaminergic neurons is enhanced by rewarding events. Neuron 62:695-704.

Joyce JN, Lexow N, Bird E, Winokur A (1988) Organization of dopamine D1 and D2 receptors in human striatum: receptor autoradiographic studies in Huntington's disease and schizophrenia. Synapse 2:546-557.

Kaneoke Y, Vitek JL (1996) Burst and oscillation as disparate neuronal properties. J Neurosci Methods 68:211-223.

Kantor S, Szabo L, Varga J, Cuesta M, Morton AJ (2013) Progressive sleep and electroencephalogram changes in mice carrying the Huntington's disease mutation. Brain 136:2147-2158.

Karachi C, Yelnik J, Tande D, Tremblay L, Hirsch EC, Francois C (2005) The pallidosubthalamic projection: an anatomical substrate for nonmotor functions of the subthalamic nucleus in primates. Mov Disord 20:172-180.

Kass JI, Mintz IM (2006) Silent plateau potentials, rhythmic bursts, and pacemaker firing: three patterns of activity that coexist in quadristable subthalamic neurons. Proc Natl Acad Sci U S A 103:183-188.

Kassubek J, Gaus W, Landwehrmeyer GB (2004) Evidence for more widespread cerebral pathology in early HD: an MRI-based morphometric analysis. Neurology 62:523-524; author reply 524.

Kemp JM, Powell TP (1970) The cortico-striate projection in the monkey. Brain 93:525-546.

Kincaid AE, Zheng T, Wilson CJ (1998) Connectivity and convergence of single corticostriatal axons. J Neurosci 18:4722-4731.

Kish SJ, Shannak K, Hornykiewicz O (1987) Elevated serotonin and reduced dopamine in subregionally divided Huntington's disease striatum. Ann Neurol 22:386-389.

Kita T, Kita H (2012) The subthalamic nucleus is one of multiple innervation sites for long-range corticofugal axons: a single-axon tracing study in the rat. J Neurosci 32:5990-5999.

Kita H, Kitai S (1987) Efferent projections of the subthalamic nucleus in the rat: light and electron microscopic analysis with the PHA-L method. J Comp Neurol 260:435-452.

Kitai ST, Deniau JM (1981) Cortical inputs to the subthalamus: intracellular analysis. Brain Res 214:411-415.

Kitai ST, Kocsis JD, Wood J (1976) Origin and characteristics of the cortico-caudate afferents: an anatomical and electrophysiological study. Brain Res 118:137-141.

Klapstein GJ, Fisher RS, Zanjani H, Cepeda C, Jokel ES, Chesselet MF, Levine MS (2001) Electrophysiological and morphological changes in striatal spiny neurons in R6/2 Huntington's disease transgenic mice. J Neurophysiol 86:2667-2677.

Kolomiets BP, Deniau JM, Mailly P, Menetrey A, Glowinski J, Thierry AM (2001) Segregation and convergence of information flow through the cortico-subthalamic pathways. J Neurosci 21:5764-5772.

Kreiss DS, Anderson LA, Walters JR (1996) Apomorphine and dopamine D(1) receptor agonists increase the firing rates of subthalamic nucleus neurons. Neuroscience 72:863-876.

Kreiss DS, Mastropietro CW, Rawji SS, Walters JR (1997) The response of subthalamic nucleus neurons to dopamine receptor stimulation in a rodent model of Parkinson's disease. J Neurosci 17:6807-6819.

Kremer B, Goldberg P, Andrew SE, Theilmann J, Telenius H, Zeisler J, Squitieri F, Lin B, Bassett A, Almqvist E, et al. (1994) A worldwide study of the Huntington's disease mutation. The sensitivity and specificity of measuring CAG repeats. N Engl J Med 330:1401-1406.

Kuki T, Ohshiro T, Ito S, Ji ZG, Fukazawa Y, Matsuzaka Y, Yawo H, Mushiake H (2013) Frequency-dependent entrainment of neocortical slow oscillation to repeated optogenetic stimulation in the anesthetized rat. Neurosci Res 75:35-45.

Kung VW, Hassam R, Morton AJ, Jones S (2007) Dopamine-dependent long term potentiation in the dorsal striatum is reduced in the R6/2 mouse model of Huntington's disease. Neuroscience 146:1571-1580.

Kuwajima M, Hall RA, Aiba A, Smith Y (2004) Subcellular and subsynaptic localization of group I metabotropic glutamate receptors in the monkey subthalamic nucleus. J Comp Neurol 474:589-602.

Laforet GA, Sapp E, Chase K, McIntyre C, Boyce FM, Campbell M, Cadigan BA, Warzecki L, Tagle DA, Reddy PH, Cepeda C, Calvert CR, Jokel ES, Klapstein GJ, Ariano MA, Levine MS, DiFiglia M, Aronin N (2001) Changes in cortical and striatal neurons predict behavioral and electrophysiological abnormalities in a transgenic murine model of Huntington's disease. J Neurosci 21:9112-9123.

Landry P, Wilson CJ, Kitai ST (1984) Morphological and electrophysiological characteristics of pyramidal tract neurons in the rat. Exp Brain Res 57:177-190.

Lange KW, Sahakian BJ, Quinn NP, Marsden CD, Robbins TW (1995) Comparison of executive and visuospatial memory function in Huntington's disease and dementia of Alzheimer type matched for degree of dementia. J Neurol Neurosurg Psychiatry 58:598-606.

Lavoie B, Parent A (1990) Immunohistochemical study of the serotoninergic innervation of the basal ganglia in the squirrel monkey. J Comp Neurol 299:1-16.

Lavoie B, Parent A (1994) Pedunculopontine nucleus in the squirrel monkey: projections to the basal ganglia as revealed by anterograde tract-tracing methods. J Comp Neurol 344:210-231.

Lavoie B, Smith Y, Parent A (1989) Dopaminergic innervation of the basal ganglia in the squirrel monkey as revealed by tyrosine hydroxylase immunohistochemistry. J Comp Neurol 289:36-52.

Leblois A, Boraud T, Meissner W, Bergman H, Hansel D (2006) Competition between feedback loops underlies normal and pathological dynamics in the basal ganglia. J Neurosci 26:3567-3583.

Lee CR, Tepper JM (2009) Basal ganglia control of substantia nigra dopaminergic neurons. J Neural Transm Suppl:71-90.

Levesque M, Parent A (1998) Axonal arborization of corticostriatal and corticothalamic fibers arising from prelimbic cortex in the rat. Cereb Cortex 8:602-613.

Levesque M, Charara A, Gagnon S, Parent A, Deschenes M (1996) Corticostriatal projections from layer V cells in rat are collaterals of long-range corticofugal axons. Brain Res 709:311-315.

Levine MS, Cepeda C, Hickey MA, Fleming SM, Chesselet MF (2004) Genetic mouse models of Huntington's and Parkinson's diseases: illuminating but imperfect. Trends Neurosci 27:691-697.

Levy G, Nobre ME, Cimini VT, Raskin S, Engelhardt E (1999) Juvenile Huntington's disease confirmed by genetic examination in twins. Arq Neuropsiquiatr 57:867-869.

Lione LA, Carter RJ, Hunt MJ, Bates GP, Morton AJ, Dunnett SB (1999) Selective discrimination learning impairments in mice expressing the human Huntington's disease mutation. J Neurosci 19:10428-10437.

Litvak V, Jha A, Eusebio A, Oostenveld R, Foltynie T, Limousin P, Zrinzo L, Hariz MI, Friston K, Brown P (2011) Resting oscillatory cortico-subthalamic connectivity in patients with Parkinson's disease. Brain 134:359-374.

Lunkes A, Mandel JL (1998) A cellular model that recapitulates major pathogenic steps of Huntington's disease. Hum Mol Genet 7:1355-1361.

Luthi-Carter R, Apostol BL, Dunah AW, DeJohn MM, Farrell LA, Bates GP, Young AB, Standaert DG, Thompson LM, Cha JH (2003) Complex alteration of NMDA receptors in transgenic Huntington's disease mouse brain: analysis of mRNA and protein expression, plasma membrane association, interacting proteins, and phosphorylation. Neurobiol Dis 14:624-636.

Luthi-Carter R, Strand A, Peters NL, Solano SM, Hollingsworth ZR, Menon AS, Frey AS, Spektor BS, Penney EB, Schilling G, Ross CA, Borchelt DR, Tapscott SJ, Young AB, Cha JH, Olson JM (2000) Decreased expression of striatal signaling genes in a mouse model of Huntington's disease. Hum Mol Genet 9:1259-1271.

Macdonald V, Halliday G (2002) Pyramidal cell loss in motor cortices in Huntington's disease. Neurobiol Dis 10:378-386.

Magill PJ, Bolam JP, Bevan MD (2000) Relationship of activity in the subthalamic nucleus-globus pallidus network to cortical electroencephalogram. J Neurosci 20:820-833.

Magill PJ, Bolam JP, Bevan MD (2001) Dopamine regulates the impact of the cerebral cortex on the subthalamic nucleus-globus pallidus network. Neuroscience 106:313-330.

Magill PJ, Sharott A, Bevan MD, Brown P, Bolam JP (2004) Synchronous unit activity and local field potentials evoked in the subthalamic nucleus by cortical stimulation. J Neurophysiol 92:700-714.

Mahant N, McCusker EA, Byth K, Graham S (2003) Huntington's disease: clinical correlates of disability and progression. Neurology 61:1085-1092.

Mallet N, Pogosyan A, Sharott A, Csicsvari J, Bolam JP, Brown P, Magill PJ (2008) Disrupted dopamine transmission and the emergence of exaggerated beta oscillations in subthalamic nucleus and cerebral cortex. J Neurosci 28:4795-4806.

Mangiarini L, Sathasivam K, Seller M, Cozens B, Harper A, Hetherington C, Lawton M, Trottier Y, Lehrach H, Davies SW, Bates GP (1996) Exon 1 of the HD gene with an expanded CAG repeat is sufficient to cause a progressive neurological phenotype in transgenic mice. Cell 87:493-506.

Masuzawa M, Nakao S, Miyamoto E, Yamada M, Murao K, Nishi K, Shingu K (2003) Pentobarbital inhibits ketamine-induced dopamine release in the rat nucleus accumbens: a microdialysis study. Anesth Analg 96:148-152, table of contents.

Mathai A, Smith Y (2011) The corticostriatal and corticosubthalamic pathways: two entries, one target. So what? Front Syst Neurosci 5:64.

Maurice N, Deniau JM, Glowinski J, Thierry AM (1998) Relationships between the prefrontal cortex and the basal ganglia in the rat: physiology of the corticosubthalamic circuits. J Neurosci 18:9539-9546.

McCormick DA, Bal T (1997) Sleep and arousal: thalamocortical mechanisms. Annu Rev Neurosci 20:185-215.

McGeorge AJ, Faull RL (1989) The organization of the projection from the cerebral cortex to the striatum in the rat. Neuroscience 29:503-537.

Menalled L, Zanjani H, MacKenzie L, Koppel A, Carpenter E, Zeitlin S, Chesselet MF (2000) Decrease in striatal enkephalin mRNA in mouse models of Huntington's disease. Exp Neurol 162:328-342.

Menalled LB, Chesselet MF (2002) Mouse models of Huntington's disease. Trends Pharmacol Sci 23:32-39.

Miller BR, Bezprozvanny I (2010) Corticostriatal circuit dysfunction in Huntington's disease: intersection of glutamate, dopamine and calcium. Future Neurol 5:735-756.

Miller BR, Walker AG, Barton SJ, Rebec GV (2011) Dysregulated Neuronal Activity Patterns Implicate Corticostriatal Circuit Dysfunction in Multiple Rodent Models of Huntington's Disease. Front Syst Neurosci 5:26.

Milnerwood AJ, Raymond LA (2007) Corticostriatal synaptic function in mouse models of Huntington's disease: early effects of huntingtin repeat length and protein load. J Physiol 585:817-831.

Mink JW (1996) The basal ganglia: focused selection and inhibition of competing motor programs. Prog Neurobiol 50:381-425.

Missale C, Nash SR, Robinson SW, Jaber M, Caron MG (1998) Dopamine receptors: from structure to function. Physiol Rev 78:189-225.

Mochel F, Durant B, Durr A, Schiffmann R (2011) Altered dopamine and serotonin metabolism in motorically asymptomatic R6/2 mice. PLoS One 6:e18336.

Mohr E, Brouwers P, Claus JJ, Mann UM, Fedio P, Chase TN (1991) Visuospatial cognition in Huntington's disease. Mov Disord 6:127-132.

Monakow KH, Akert K, Kunzle H (1978) Projections of the precentral motor cortex and other cortical areas of the frontal lobe to the subthalamic nucleus in the monkey. Exp Brain Res 33:395-403.

Mori S, Takino T, Yamada H, Sano Y (1985) Immunohistochemical demonstration of serotonin nerve fibers in the subthalamic nucleus of the rat, cat and monkey. Neurosci Lett 62:305-309.

Moriizumi T, Hattori T (1992) Separate neuronal populations of the rat globus pallidus projecting to the subthalamic nucleus, auditory cortex and pedunculopontine tegmental area. Neuroscience 46:701-710.

Morton AJ (2013) Circadian and sleep disorder in Huntington's disease. Exp Neurol 243:34-44.

Morton AJ, Edwardson JM (2001) Progressive depletion of complexin II in a transgenic mouse model of Huntington's disease. J Neurochem 76:166-172.

Morton AJ, Faull RL, Edwardson JM (2001) Abnormalities in the synaptic vesicle fusion machinery in Huntington's disease. Brain Res Bull 56:111-117.

Morton AJ, Lagan MA, Skepper JN, Dunnett SB (2000) Progressive formation of inclusions in the striatum and hippocampus of mice transgenic for the human Huntington's disease mutation. J Neurocytol 29:679-702.

Mouroux M, Hassani OK, Feger J (1995) Electrophysiological study of the excitatory parafascicular projection to the subthalamic nucleus and evidence for ipsi- and contralateral controls. Neuroscience 67:399-407.

Myers RH, Vonsattel JP, Stevens TJ, Cupples LA, Richardson EP, Martin JB, Bird ED (1988) Clinical and neuropathologic assessment of severity in Huntington's disease. Neurology 38:341-347.

Nakanishi H, Kita H, Kitai ST (1987) Electrical membrane properties of rat subthalamic neurons in an in vitro slice preparation. Brain Res 437:35-44.

Nambu A (2011) Somatotopic organization of the primate Basal Ganglia. Front Neuroanat 5:26.

Nambu A, Tokuno H, Takada M (2002) Functional significance of the cortico-subthalamo-pallidal 'hyperdirect' pathway. Neurosci Res 43:111-117.

Nambu A, Takada M, Inase M, Tokuno H (1996) Dual somatotopical representations in the primate subthalamic nucleus: evidence for ordered but reversed body-map transformations from the primary motor cortex and the supplementary motor area. J Neurosci 16:2671-2683.

Nambu A, Tokuno H, Hamada I, Kita H, Imanishi M, Akazawa T, Ikeuchi Y, Hasegawa N (2000) Excitatory cortical inputs to pallidal neurons via the subthalamic nucleus in the monkey. J Neurophysiol 84:289-300.

Nauta HJ, Cole M (1978) Efferent Projections of the subthalamic nucleus: an autoradiographic study in monkey and cat. J Comp Neurol 180:1-16.

Nguyen L, Bradshaw JL, Stout JC, Croft RJ, Georgiou-Karistianis N (2010) Electrophysiological measures as potential biomarkers in Huntington's disease: review and future directions. Brain Res Rev 64:177-194.

Ni Z, Gao D, Bouali-Benazzouz R, Benabid AL, Benazzouz A (2001a) Effect of microiontophoretic application of dopamine on subthalamic nucleus neuronal activity in normal rats and in rats with unilateral lesion of the nigrostriatal pathway. Eur J Neurosci 14:373-381.

Ni Z, Bouali-Benazzouz R, Gao D, Benabid AL, Benazzouz A (2001b) Intrasubthalamic injection of 6-hydroxydopamine induces changes in the firing rate and pattern of subthalamic nucleus neurons in the rat. Synapse 40:145-153.

Niddam R, Arbilla S, Scatton B, Dennis T, Langer SZ (1985) Amphetamine induced release of endogenous dopamine in vitro is not reduced following pretreatment with reserpine. Naunyn Schmiedebergs Arch Pharmacol 329:123-127.

Oka H (1980) Organization of the cortico-caudate projections. A horseradish peroxidase study in the cat. Exp Brain Res 40:203-208.

Orieux G, Francois C, Feger J, Hirsch EC (2002) Consequences of dopaminergic denervation on the metabolic activity of the cortical neurons projecting to the subthalamic nucleus in the rat. J Neurosci 22:8762-8770.

Ortiz AN, Kurth BJ, Osterhaus GL, Johnson MA (2011) Impaired dopamine release and uptake in R6/1 Huntington's disease model mice. Neurosci Lett 492:11-14.

Overton PG, Greenfield SA (1995) Determinants of neuronal firing pattern in the guinea-pig subthalamic nucleus: an in vivo and in vitro comparison. J Neural Transm Park Dis Dement Sect 10:41-54.

Pallier PN, Drew CJ, Morton AJ (2009) The detection and measurement of locomotor deficits in a transgenic mouse model of Huntington's disease are task- and protocol-dependent: influence of non-motor factors on locomotor function. Brain Res Bull 78:347-355.

Panov AV, Gutekunst CA, Leavitt BR, Hayden MR, Burke JR, Strittmatter WJ, Greenamyre JT (2002) Early mitochondrial calcium defects in Huntington's disease are a direct effect of polyglutamines. Nat Neurosci 5:731-736.

Parent A, Hazrati LN (1995) Functional anatomy of the basal ganglia. II. The place of subthalamic nucleus and external pallidum in basal ganglia circuitry. Brain Res Brain Res Rev 20:128-154.

Parent A, Smith Y (1987) Organization of efferent projections of the subthalamic nucleus in the squirrel monkey as revealed by retrograde labeling methods. Brain Res 436: 296-310.

Paulsen JS (2011) Cognitive impairment in Huntington disease: diagnosis and treatment. Curr Neurol Neurosci Rep 11:474-483.

Paz JT, Deniau JM, Charpier S (2005) Rhythmic bursting in the cortico-subthalamo-pallidal network during spontaneous genetically determined spike and wave discharges. J Neurosci 25:2092-2101.

Pazo JH, Hocht C, Barcelo AC, Fillipini B, Lomastro MJ (2010) Effect of electrical and chemical stimulation of the subthalamic nucleus on the release of striatal dopamine. Synapse 64:905-915.

Petersen A, Puschban Z, Lotharius J, NicNiocaill B, Wiekop P, O'Connor WT, Brundin P (2002) Evidence for dysfunction of the nigrostriatal pathway in the R6/1 line of transgenic Huntington's disease mice. Neurobiol Dis 11:134-146.

Pineda JR, Canals JM, Bosch M, Adell A, Mengod G, Artigas F, Ernfors P, Alberch J (2005) Brain-derived neurotrophic factor modulates dopaminergic deficits in a transgenic mouse model of Huntington's disease. J Neurochem 93:1057-1068.

Plenz D, Kital ST (1999) A basal ganglia pacemaker formed by the subthalamic nucleus and external globus pallidus. Nature 400:677-682.

Pringsheim T, Wiltshire K, Day L, Dykeman J, Steeves T, Jette N (2012) The incidence and prevalence of Huntington's disease: a systematic review and meta-analysis. Mov Disord 27:1083-1091.

Raymond LA, Andre VM, Cepeda C, Gladding CM, Milnerwood AJ, Levine MS (2011) Pathophysiology of Huntington's disease: time-dependent alterations in synaptic and receptor function. Neuroscience 198:252-273.

Reiner A, Jiao Y, Del Mar N, Laverghetta AV, Lei WL (2003) Differential morphology of pyramidal tract-type and intratelencephalically projecting-type corticostriatal neurons and their intrastriatal terminals in rats. J Comp Neurol 457:420-440.

Reynolds GP, Garrett NJ (1986) Striatal dopamine and homovanillic acid in Huntington's disease. J Neural Transm 65:151-155.

Reynolds GP, Dalton CF, Tillery CL, Mangiarini L, Davies SW, Bates GP (1999) Brain neurotransmitter deficits in mice transgenic for the Huntington's disease mutation. J Neurochem 72:1773-1776.

Richfield EK, Herkenham M (1994) Selective vulnerability in Huntington's disease: preferential loss of cannabinoid receptors in lateral globus pallidus. Ann Neurol 36:577-584.

Richfield EK, O'Brien CF, Eskin T, Shoulson I (1991) Heterogeneous dopamine receptor changes in early and late Huntington's disease. Neurosci Lett 132:121-126.

Robitaille Y, Lopes-Cendes I, Becher M, Rouleau G, Clark AW (1997) The neuropathology of CAG repeat diseases: review and update of genetic and molecular features. Brain Pathol 7:901-926.

Rosas HD, Salat DH, Lee SY, Zaleta AK, Hevelone N, Hersch SM (2008a) Complexity and heterogeneity: what drives the ever-changing brain in Huntington's disease? Ann N Y Acad Sci 1147:196-205.

Rosas HD, Tuch DS, Hevelone ND, Zaleta AK, Vangel M, Hersch SM, Salat DH (2006) Diffusion tensor imaging in presymptomatic and early Huntington's disease: Selective white matter pathology and its relationship to clinical measures. Mov Disord 21:1317-1325.

Rosas HD, Salat DH, Lee SY, Zaleta AK, Pappu V, Fischl B, Greve D, Hevelone N, Hersch SM (2008b) Cerebral cortex and the clinical expression of Huntington's disease: complexity and heterogeneity. Brain 131:1057-1068.

Rosas HD, Reuter M, Doros G, Lee SY, Triggs T, Malarick K, Fischl B, Salat DH, Hersch SM (2011) A tale of two factors: what determines the rate of progression in Huntington's disease? A longitudinal MRI study. Mov Disord 26:1691-1697.

Rosas HD, Liu AK, Hersch S, Glessner M, Ferrante RJ, Salat DH, van der Kouwe A, Jenkins BG, Dale AM, Fischl B (2002) Regional and progressive thinning of the cortical ribbon in Huntington's disease. Neurology 58:695-701.

Rouzaire-Dubois B, Scarnati E (1985) Bilateral corticosubthalamic nucleus projections: an electrophysiological study in rats with chronic cerebral lesions. Neuroscience 15:69-79.

Royce GJ (1982) Laminar origin of cortical neurons which project upon the caudate nucleus: a horseradish peroxidase investigation in the cat. J Comp Neurol 205:8-29.

Rubio I, Rodriguez-Navarro JA, Tomas-Zapico C, Ruiz C, Casarejos MJ, Perucho J, Gomez A, Rodal I, Lucas JJ, Mena MA, de Yebenes JG (2009) Effects of partial suppression of parkin on huntingtin mutant R6/1 mice. Brain Res 1281:91-100.

Rudy B, McBain CJ (2001) Kv3 channels: voltage-gated K+ channels designed for high-frequency repetitive firing. Trends Neurosci 24:517-526.

Sapp E, Penney J, Young A, Aronin N, Vonsattel JP, DiFiglia M (1999) Axonal transport of N-terminal huntingtin suggests early pathology of corticostriatal projections in Huntington disease. J Neuropathol Exp Neurol 58:165-173.

Sapp E, Ge P, Aizawa H, Bird E, Penney J, Young AB, Vonsattel JP, DiFiglia M (1995) Evidence for a preferential loss of enkephalin immunoreactivity in the external globus pallidus in low grade Huntington's disease using high resolution image analysis. Neuroscience 64:397-404.

Sato F, Parent M, Levesque M, Parent A (2000) Axonal branching pattern of neurons of the subthalamic nucleus in primates. J Comp Neurol 424:142-152.

Schmidt R, Leventhal DK, Mallet N, Chen F, Berke JD (2013) Canceling actions involves a race between basal ganglia pathways. Nat Neurosci 16:1118-1124.

Schultz W (1998a) The phasic reward signal of primate dopamine neurons. Adv Pharmacol 42:686-690.

Schultz W (1998b) Predictive reward signal of dopamine neurons. J Neurophysiol 80:1-27.

Schultz W (2007) Behavioral dopamine signals. Trends Neurosci 30:203-210.

Sedvall G, Karlsson P, Lundin A, Anvret M, Suhara T, Halldin C, Farde L (1994) Dopamine D1 receptor number--a sensitive PET marker for early brain

degeneration in Huntington's disease. Eur Arch Psychiatry Clin Neurosci 243:249-255.

Selemon LD, Rajkowska G, Goldman-Rakic PS (2004) Evidence for progression in frontal cortical pathology in late-stage Huntington's disease. J Comp Neurol 468:190-204.

Sharott A, Magill PJ, Bolam JP, Brown P (2005) Directional analysis of coherent oscillatory field potentials in the cerebral cortex and basal ganglia of the rat. J Physiol 562:951-963.

Shen KZ, Johnson SW (2000) Presynaptic dopamine D2 and muscarine M3 receptors inhibit excitatory and inhibitory transmission to rat subthalamic neurones in vitro. J Physiol 525 Pt 2:331-341.

Shimo Y, Wichmann T (2009) Neuronal activity in the subthalamic nucleus modulates the release of dopamine in the monkey striatum. Eur J Neurosci 29:104-113.

Shink E, Smith Y (1995) Differential synaptic innervation of neurons in the internal and external segments of the globus pallidus by the GABA- and glutamate-containing terminals in the squirrel monkey. J Comp Neurol 358:119-141.

Shink E, Bevan MD, Bolam JP, Smith Y (1996) The subthalamic nucleus and the external pallidum: two tightly interconnected structures that control the output of the basal ganglia in the monkey. Neuroscience 73:335-357.

Slow EJ, van Raamsdonk J, Rogers D, Coleman SH, Graham RK, Deng Y, Oh R, Bissada N, Hossain SM, Yang YZ, Li XJ, Simpson EM, Gutekunst CA, Leavitt BR, Hayden MR (2003) Selective striatal neuronal loss in a YAC128 mouse model of Huntington disease. Hum Mol Genet 12:1555-1567.

Smith ID, Grace AA (1992) Role of the subthalamic nucleus in the regulation of nigral dopamine neuron activity. Synapse 12:287-303.

Smith Y, Parent A (1988) Neurons of the subthalamic nucleus in primates display glutamate but not GABA immunoreactivity. Brain Res 453:353-356.

Smith Y, Bolam JP, Von Krosigk M (1990) Topographical and Synaptic Organization of the GABA-Containing Pallidosubthalamic Projection in the Rat. Eur J Neurosci 2:500-511.

Song WJ, Baba Y, Otsuka T, Murakami F (2000) Characterization of Ca(2+) channels in rat subthalamic nucleus neurons. J Neurophysiol 84:2630-2637.

Sotrel A, Williams RS, Kaufmann WE, Myers RH (1993) Evidence for neuronal degeneration and dendritic plasticity in cortical pyramidal neurons of Huntington's disease: a quantitative Golgi study. Neurology 43:2088-2096.

Spokes EG (1980) Neurochemical alterations in Huntington's chorea: a study of post-mortem brain tissue. Brain 103:179-210.

Stack EC, Kubilus JK, Smith K, Cormier K, Del Signore SJ, Guelin E, Ryu H, Hersch SM, Ferrante RJ (2005) Chronology of behavioral symptoms and neuropathological sequela in R6/2 Huntington's disease transgenic mice. J Comp Neurol 490:354-370.

Steffan JS, Agrawal N, Pallos J, Rockabrand E, Trotman LC, Slepko N, Illes K, Lukacsovich T, Zhu YZ, Cattaneo E, Pandolfi PP, Thompson LM, Marsh JL (2004) SUMO modification of Huntingtin and Huntington's disease pathology. Science 304:100-104.

Steriade M (1997) Synchronized activities of coupled oscillators in the cerebral cortex and thalamus at different levels of vigilance. Cereb Cortex 7:583-604.

Steriade M (2001) Impact of network activities on neuronal properties in corticothalamic systems. J Neurophysiol 86:1-39.

Steriade M, Llinas RR (1988) The functional states of the thalamus and the associated neuronal interplay. Physiol Rev 68:649-742.

Steriade M, Nunez A, Amzica F (1993) A novel slow (< 1 Hz) oscillation of neocortical neurons in vivo: depolarizing and hyperpolarizing components. J Neurosci 13:3252-3265.

Steriade M, Timofeev I, Grenier F (2001) Natural waking and sleep states: a view from inside neocortical neurons. J Neurophysiol 85:1969-1985.

Stern EA (2011) Functional Changes in Neocortical Activity in Huntington's Disease Model Mice: An in vivo Intracellular Study. Front Syst Neurosci 5:47.

Sugimoto T, Hattori T, Mizuno N, Itoh K, Sato M (1983) Direct projections from the centre median-parafascicular complex to the subthalamic nucleus in the cat and rat. J Comp Neurol 214:209-216.

Sun Z, Del Mar N, Meade C, Goldowitz D, Reiner A (2002) Differential changes in striatal projection neurons in R6/2 transgenic mice for Huntington's disease. Neurobiol Dis 11:369-385.

Suzuki M, Desmond TJ, Albin RL, Frey KA (2001) Vesicular neurotransmitter transporters in Huntington's disease: initial observations and comparison with traditional synaptic markers. Synapse 41:329-336.

Terman D, Rubin JE, Yew AC, Wilson CJ (2002) Activity patterns in a model for the subthalamopallidal network of the basal ganglia. J Neurosci 22:2963-2976.

Thompson PD, Berardelli A, Rothwell JC, Day BL, Dick JP, Benecke R, Marsden CD (1988) The coexistence of bradykinesia and chorea in Huntington's disease and its implications for theories of basal ganglia control of movement. Brain 111 (Pt 2):223-244.

Tian J, Herdman SJ, Zee DS, Folstein SE (1992) Postural stability in patients with Huntington's disease. Neurology 42:1232-1238.

Turmaine M, Raza A, Mahal A, Mangiarini L, Bates GP, Davies SW (2000) Nonapoptotic neurodegeneration in a transgenic mouse model of Huntington's disease. Proc Natl Acad Sci U S A 97:8093-8097.

Unschuld PG, Joel SE, Liu X, Shanahan M, Margolis RL, Biglan KM, Bassett SS, Schretlen DJ, Redgrave GW, van Zijl PC, Pekar JJ, Ross CA (2012) Impaired cortico-striatal functional connectivity in prodromal Huntington's Disease. Neurosci Lett 514:204-209.

Urbain N, Rentero N, Gervasoni D, Renaud B, Chouvet G (2002) The switch of subthalamic neurons from an irregular to a bursting pattern does not solely depend on their GABAergic inputs in the anesthetic-free rat. J Neurosci 22:8665-8675.

Van der Kooy D, Kolb B (1985) Non-cholinergic globus pallidus cells that project to the cortex but not to the subthalamic nucleus in rat. Neurosci Lett 57:113-118.

Van Raamsdonk JM, Pearson J, Slow EJ, Hossain SM, Leavitt BR, Hayden MR (2005) Cognitive dysfunction precedes neuropathology and motor abnormalities in the YAC128 mouse model of Huntington's disease. J Neurosci 25:4169-4180.

Van Raamsdonk JM, Metzler M, Slow E, Pearson J, Schwab C, Carroll J, Graham RK, Leavitt BR, Hayden MR (2007) Phenotypic abnormalities in the YAC128 mouse model of Huntington disease are penetrant on multiple genetic backgrounds and modulated by strain. Neurobiol Dis 26:189-200.

Velier J, Kim M, Schwarz C, Kim TW, Sapp E, Chase K, Aronin N, DiFiglia M (1998) Wild-type and mutant huntingtins function in vesicle trafficking in the secretory and endocytic pathways. Exp Neurol 152:34-40.

Vlamings R, Benazzouz A, Chetrit J, Janssen ML, Kozan R, Visser-Vandewalle V, Steinbusch HW, von Horsten S, Temel Y (2012) Metabolic and

electrophysiological changes in the basal ganglia of transgenic Huntington's disease rats. Neurobiol Dis 48:488-494.

Vonsattel JP (2008) Huntington disease models and human neuropathology: similarities and differences. Acta Neuropathol 115:55-69.

Vonsattel JP, DiFiglia M (1998) Huntington disease. J Neuropathol Exp Neurol 57:369-384.

Vonsattel JP, Myers RH, Stevens TJ, Ferrante RJ, Bird ED, Richardson EP, Jr. (1985) Neuropathological classification of Huntington's disease. J Neuropathol Exp Neurol 44:559-577.

Walker AG, Miller BR, Fritsch JN, Barton SJ, Rebec GV (2008) Altered information processing in the prefrontal cortex of Huntington's disease mouse models. J Neurosci 28:8973-8982.

Walker FO (2007) Huntington's disease. Lancet 369:218-228.

Whelan G, Flecknell PA (1992) The assessment of depth of anaesthesia in animals and man. Lab Anim 26:153-162.

Whittier JR, Mettler FA (1949) Studies on the subthalamus of the rhesus monkey; hyperkinesia and other physiologic effects of subthalamic lesions; with special reference to the subthalamic nucleus of Luys. J Comp Neurol 90:319-372.

Wiegand M, Moller AA, Schreiber W, Lauer C, Krieg JC (1991) Brain morphology and sleep EEG in patients with Huntington's disease. Eur Arch Psychiatry Clin Neurosci 240:148-152.

Wilson CJ (1987) Morphology and synaptic connections of crossed corticostriatal neurons in the rat. J Comp Neurol 263:567-580.

Wright AK, Ramanathan S, Arbuthnott GW (2001) Identification of the source of the bilateral projection system from cortex to somatosensory neostriatum and an exploration of its physiological actions. Neuroscience 103:87-96.

Wright AK, Norrie L, Ingham CA, Hutton EA, Arbuthnott GW (1999) Double anterograde tracing of outputs from adjacent "barrel columns" of rat somatosensory cortex. Neostriatal projection patterns and terminal ultrastructure. Neuroscience 88:119-133.

Xiang Z, Wang L, Kitai ST (2005) Modulation of spontaneous firing in rat subthalamic neurons by 5-HT receptor subtypes. J Neurophysiol 93:1145-1157.

Yadid G, Harvey-White JD, Kopin IJ, Goldstein DS (2000) Estimation of striatal dopamine spillover and metabolism in vivo. Neuroreport 11:3367-3373.

Yohrling GJt, Jiang GC, DeJohn MM, Miller DW, Young AB, Vrana KE, Cha JH (2003) Analysis of cellular, transgenic and human models of Huntington's disease reveals tyrosine hydroxylase alterations and substantia nigra neuropathology. Brain Res Mol Brain Res 119:28-36.

Young AB, Greenamyre JT, Hollingsworth Z, Albin R, D'Amato C, Shoulson I, Penney JB (1988) NMDA receptor losses in putamen from patients with Huntington's disease. Science 241: 981-983.

Zeron MM, Hansson O, Chen N, Wellington CL, Leavitt BR, Brundin P, Hayden MR, Raymond LA (2002) Increased sensitivity to N-methyl-D-aspartate receptor-mediated excitotoxicity in a mouse model of Huntington's disease. Neuron 33:849-860.

Zetterstrom T, Sharp T, Collin AK, Ungerstedt U (1988) In vivo measurement of extracellular dopamine and DOPAC in rat striatum after various dopamine-releasing drugs; implications for the origin of extracellular DOPAC. Eur J Pharmacol 148:327-334.

Zheng T, Wilson CJ (2002) Corticostriatal combinatorics: the implications of corticostriatal axonal arborizations. J Neurophysiol 87:1007-1017.

Zoghbi HY, Orr HT (2000) Glutamine repeats and neurodegeneration. Annu Rev Neurosci 23:217-247.

Zuccato C, Ciammola A, Rigamonti D, Leavitt BR, Goffredo D, Conti L, MacDonald ME, Friedlander RM, Silani V, Hayden MR, Timmusk T, Sipione S, Cattaneo E (2001) Loss of huntingtin-mediated BDNF gene transcription in Huntington's disease. Science 293:493-498.

CHAPTER 7: VITA

Joshua W. Callahan

1982	Born July 18, 1982 in Seattle, WA.
2000	Graduated Roosevelt High School, Seattle, WA.
2000-2005	Attended Western Washington University, Seattle, WA. Major: Biological Psychology.
2005	Bachelor of Arts degree, Western Washington University.
2005-2007	Research Associate, MDS Pharma Services.
2007-2013	Graduate Assistantship, Behavioral and Neural Sciences Program, Rutgers University, Newark, NJ.
2011	Article: Callahan JW, & Abercrombie ED "In vivo dopamine efflux is decreased in striatum of both fragment (R6/2) and full-length (YAC128) transgenic mouse models of Huntington's disease. *Front Sys Neurosci.*
2013	Article: Callahan JW, & Abercrombie ED "Relationship between subthalamic nucleus (STN) neuronal activity and electrocorticogram (ECoG) is altered in the R6/2 mouse model of Huntington's disease." *J. Neuroscience.* (*submitted*)
2013	Article: Callahan JW, & Abercrombie ED "Contribution of hyperdirect pathway alterations to subthalamic nucleus dysfunction in the YAC128 mouse model of Huntington's disease." *J. Neuroscience.* (*submitted*)